

University of Windsor

Scholarship at UWindor

Electronic Theses and Dissertations

Theses, Dissertations, and Major Papers

2000

Aging characteristics of solid polymeric materials used for electrical insulation.

Hui. Zhang
University of Windsor

Follow this and additional works at: <https://scholar.uwindsor.ca/etd>

Recommended Citation

Zhang, Hui., "Aging characteristics of solid polymeric materials used for electrical insulation." (2000).
Electronic Theses and Dissertations. 918.
<https://scholar.uwindsor.ca/etd/918>

This online database contains the full-text of PhD dissertations and Masters' theses of University of Windsor students from 1954 forward. These documents are made available for personal study and research purposes only, in accordance with the Canadian Copyright Act and the Creative Commons license—CC BY-NC-ND (Attribution, Non-Commercial, No Derivative Works). Under this license, works must always be attributed to the copyright holder (original author), cannot be used for any commercial purposes, and may not be altered. Any other use would require the permission of the copyright holder. Students may inquire about withdrawing their dissertation and/or thesis from this database. For additional inquiries, please contact the repository administrator via email (scholarship@uwindsor.ca) or by telephone at 519-253-3000ext. 3208.

INFORMATION TO USERS

This manuscript has been reproduced from the microfilm master. UMI films the text directly from the original or copy submitted. Thus, some thesis and dissertation copies are in typewriter face, while others may be from any type of computer printer.

The quality of this reproduction is dependent upon the quality of the copy submitted. Broken or indistinct print, colored or poor quality illustrations and photographs, print bleedthrough, substandard margins, and improper alignment can adversely affect reproduction.

In the unlikely event that the author did not send UMI a complete manuscript and there are missing pages, these will be noted. Also, if unauthorized copyright material had to be removed, a note will indicate the deletion.

Oversize materials (e.g., maps, drawings, charts) are reproduced by sectioning the original, beginning at the upper left-hand corner and continuing from left to right in equal sections with small overlaps.

Photographs included in the original manuscript have been reproduced xerographically in this copy. Higher quality 6" x 9" black and white photographic prints are available for any photographs or illustrations appearing in this copy for an additional charge. Contact UMI directly to order.

Bell & Howell Information and Learning
300 North Zeeb Road, Ann Arbor, MI 48106-1346 USA
800-521-0600

UMI[®]

Aging Characteristics of Solid Polymeric Materials used for Electrical Insulation

by

Hui Zhang

A Thesis

Submitted to the College of Graduate Studies and Research through the
Faculty of Engineering - Electrical and Computer Engineering
in Partial Fulfillment of the Requirements for
the Degree of Master of Applied Science at the
University of Windsor

Windsor, Ontario, Canada

2000

© 2000 Hui Zhang



National Library
of Canada

Acquisitions and
Bibliographic Services

395 Wellington Street
Ottawa ON K1A 0N4
Canada

Bibliothèque nationale
du Canada

Acquisitions et
services bibliographiques

395, rue Wellington
Ottawa ON K1A 0N4
Canada

Your file Votre référence

Our file Notre référence

The author has granted a non-exclusive licence allowing the National Library of Canada to reproduce, loan, distribute or sell copies of this thesis in microform, paper or electronic formats.

The author retains ownership of the copyright in this thesis. Neither the thesis nor substantial extracts from it may be printed or otherwise reproduced without the author's permission.

L'auteur a accordé une licence non exclusive permettant à la Bibliothèque nationale du Canada de reproduire, prêter, distribuer ou vendre des copies de cette thèse sous la forme de microfiche/film, de reproduction sur papier ou sur format électronique.

L'auteur conserve la propriété du droit d'auteur qui protège cette thèse. Ni la thèse ni des extraits substantiels de celle-ci ne doivent être imprimés ou autrement reproduits sans son autorisation.

0-612-52685-2

Canada

Abstract

Polymeric materials have been increasingly used as electrical insulation since 1960's, partly as a result of more and more new materials are being invented. Compared with historically traditional insulation materials such as porcelain and glass, aging performance is a big concern for polymeric insulation materials. Three most commonly used solid polymeric materials: polyvinyl chloride, epoxy resin and high temperature vulcanized silicone rubber were selected as the test objects in the study leading to this thesis. The aging characteristics for the three materials were revealed by experiments following elaborated test procedures. Variety of experimental methods for evaluating the aging characteristics of polymeric materials used for electrical insulation, which may be used to study other polymeric materials, have been presented in the thesis.

To my family
for love, inspiration and support

Acknowledgements

I wish to thank Dr. R. Hackam, my thesis advisor, for his supervision, guidance, support and encouragement throughout the course of this research work.

I would like to thank my department reader, Professor P. H. Alexander and my external reader, Dr. R. Aroca, for their valuable advice toward the fulfillment of the thesis work.

I also want to thank Mr. J. Robinson, the electron optics technologist at the Mechanical and Materials Engineering, and Dr. Vivi Lazarescu, the instrument technologist at the Chemistry and Biochemistry department, for their kind assistance and instruction on analytical experiments such as SEM, FTIR, GC-MS.

Appreciation must also be given to Mr. Alan Johns and Mr. Joe Novosad, the departmental technologists, as well as the staff at the Technical Support Center, for their technical support on the experiments.

Table of Contents

Abstract	iii
Dedication	iv
Acknowledgements	v
Table of Contents	vi
List of Abbreviations	ix
List of Figures	x
List of Tables	xv
 Chapter 1 Introduction	 1
 Chapter 2 A Study on Polyvinyl Chloride	 3
2.1 Introduction	3
2.2 Experimental Conditions and Procedures	6
2.2.1 Fog Test Conditions	6
2.2.2 Measurements of the Surface Resistance	6
2.2.3 Measurement of the Contact Angle	8
2.2.4 Measurement of the Diffusion Coefficient	9
2.3 Results and Discussions	12
2.3.1 Surface resistance of and contact angle on PVC as a function of aging time in salt-fog without ac stress	12
2.3.2 Recovery of Surface Resistance and Contact Angle of PVC after Exposure to salt-fog	23
2.3.3 Dependence of Surface Resistance on Rod Length	25
2.3.4 Effect of DC Stress on Surface Resistance Measurements	27
2.3.5 Effect of Combined Salt-fog and AC Electric Stress	

on Surface Resistance	29
2.3.6 Surface Tensions of PVC in the Presence of Salt-fog	35
2.3.7 Determination of γ_S , γ_{SD} and γ_{SH} from the Static Contact Angle	39
2.3.8 Diffusion Coefficient of Saline Water into PVC	42
2.4 Conclusions	47
Chapter 3 A Study on Epoxy Resin	49
3.1 Introduction	49
3.2 Experimental Conditions and Procedures	50
3.2.1 Electrodes Preparation	50
3.2.2 Description of the Test Cycle	50
3.2.3 Summary of Test Conditions	51
3.2.4 Measurements of the Surface Roughness	51
3.2.5 Measurements of the Contact Angle	52
3.2.6 Measurements of the Leakage Current	52
3.2.7 Analysis with Fourier Transform Infrared (FT-IR) Spectroscopy	53
3.3 Results and Discussions	53
3.3.1 Surface Roughness of Virgin Specimens	54
3.3.2 Surface Roughness as a Function of Number of Test Cycles	55
3.3.3 Contact angle of Virgin Specimens	63
3.3.4 Contact Angle as a Function of Number of Test Cycle	64
3.3.5 Leakage Current as a Function of Test Time	72
3.3.6 FT-IR Analysis on the White Powder Deposited on the Surface of Specimens	79
3.4 Conclusions	80
Chapter 4 A Study on the HTV Silicone Rubber	83
4.1 Introduction	83
4.2 Experimental Conditions and Techniques	84
4.3 Results and Discussions	89

4.3.1	Weight Loss Due to Heating	89
4.3.2	Loss of Fluid Due to Heating	91
4.3.3	LMW Fluid Content in Samples from Different Manufacturers	93
4.3.4	Regeneration of Fluid	94
4.3.5	GC-MS Analysis	99
4.4	Conclusions	107
References		109
Publications Supporting the Thesis		116
Vita Auctoris		118

List of Abbreviations

ATH	Alumina Trihydrate
FT-IR	Fourier Transform Infrared Spectroscopy
GC	Gas Chromatography
HEE	Heating - Extraction - Evaporation
HTV	High Temperature Vulcanized
LMW	Low Molecular Weight
MS	Mass Spectrometer
PDMS	Polydimethylsiloxane
PVC	Polyvinyl Chloride
SIR	Silicone Rubber

List of Figures

Figure 2.1 Test cycle of the salt-fog showing the on (t_1) and the off (t_2-t_1) periods	7
Figure 2.2 Surface resistance of and contact angle on a PVC cylindrical rod during exposure to un-energized salt-fog	20
Figure 2.3 Surface resistance of PVC rod during exposure to salt-fog	21
Figure 2.4 Recovery of contact angle during the rest period between the successive exposure to salt-fog shown in Figure 2.3	22
Figure 2.5 Surface resistance and contact angle of the PVC specimen as a function of rest time in air after 96h of exposure to salt-fog	24
Figure 2.6 Dependence of surface resistance on time of exposure to salt-fog for different length of PVC rods	26
Figure 2.7 Influence of dc stress on surface resistance during exposure to salt-fog	28
Figure 2.8 Average leakage current with aging time in the presence of salt-fog and ac stress	32
Figure 2.9 Surface resistance as a function of aging time for cycles 1-4 during exposure to a combined salt-fog and ac stress of 200 V _{rms} /cm	33
Figure 2.10 Recovery of surface resistance after exposure to a combined salt-fog and ac stress of 200 V _{rms} /cm	34
Figure 2.11 Recovery of contact angle of PVC in air at 23±2°C after immersion for 96h in saline solution with salinity of 1 mS/cm at	

23±2°C (curve 1) and after exposure for 96h to salt-fog produced by a saline solution of 1 mS/cm (curve 2)	38
Figure 2.12 Calculated surface tension of PVC from contact angle measured with distilled water and methylene iodide as a function of exposure time to salt-fog	41
Figure 2.13 Dependence of weight increase of PVC on time of immersion in a saline solution (1 mS/cm) at different temperatures	45
Figure 2.14 Dependence of $\Delta M(t)/\Delta M_{\infty}$ on $t^{0.5}$ in PVC immersed in a saline solution (1 mS/cm) at 98 and 74°C (Equation 4)	46
Figure 3.1 Surface roughness (Sa and Srms) of the virgin (before aging) specimens for #1 to #6	54
Figure 3.2 Average (Sa) and RMS (Srms) surface roughness of specimen #1 as a function of the number of test cycles	57
Figure 3.3 Surface roughness of specimen #2 as a function of the number of test cycles ...	58
Figure 3.4 Surface roughness of specimen #3 as a function of the number of test cycles ...	58
Figure 3.5 Surface roughness of specimen #4 as a function of the number of test cycles ...	59
Figure 3.6 Surface roughness of specimen #5 as a function of the number of test cycles ...	59
Figure 3.7 Surface roughness of specimen #6 as a function of the number of test cycles ...	60
Figure 3.8 Averaged surface roughness of specimens #1 and #2 (CY184) as a function of test cycles	60
Figure 3.9 Averaged surface roughness of specimens #3 and #4 (LMB5622) as a function of the number of test cycles	61
Figure 3.10 Averaged surface roughness of specimens #5 and #6 (LMB5623) as a function of the number of test cycles	61

Figure 3.11 Surface roughness (Sa and Srms) at the top area for specimens #1 to #6 after one cycle of aging	62
Figure 3.12 Surface roughness (Sa and Srms) at the top area for specimens #1 to #6 after 6 cycles of aging	62
Figure 3.13 Contact angle measured at top area for virgin specimens #1 to #6 (before aging)	63
Figure 3.14 Contact angle of #1 specimen as a function of number of test cycle	66
Figure 3.15 Contact angle of #2 specimen as a function of number of test cycle	66
Figure 3.16 Contact angle of #3 specimen as a function of number of test cycle	67
Figure 3.17 Contact angle of #4 specimen as a function of number of test cycle	67
Figure 3.18 Contact angle of #5 specimen as a function of number of test cycle	68
Figure 3.19 Contact angle of #6 specimen as a function of number of test cycle	68
Figure 3.20 Averaged contact angle of CY184 (#1 and #2) as a function of number of test cycle	69
Figure 3.21 Averaged contact angle of LMB5622 (#3 and #4) as a function of number of test cycle	69
Figure 3.22 Averaged contact angle of LMB5623 (#5 and #6) as a function of number of test cycle	70
Figure 3.23 Contact angle measured at the top area for specimens #1 to #6 after 24 h of aging and 24 h of recovery in cycle 1	71
Figure 3.24 Contact angle measured at top area for specimens #1 to #6 during the 6 th cycle of aging	71
Figure 3.25 Averaged leakage current of the three specimens as a function	

of test time during cycle 1	74
Figure 3.26 Averaged leakage current of the three specimens as a function	
of test time during cycle 2	74
Figure 3.27 Averaged leakage current of the three specimens as a function	
of test time during cycle 3	75
Figure 3.28 Averaged leakage current of the three specimens as a function	
of test time during cycle 4	75
Figure 3.29 Averaged leakage current of the three specimens as a function	
of test time during cycle 5	76
Figure 3.30 Averaged leakage current of the three specimens as a function	
of test time during cycle 6	76
Figure 3.31 Averaged leakage current for the last four hours of aging	
during cycle 1 for CY184, LMB5622 and 5623	77
Figure 3.32 Averaged leakage current for the last four hours of aging	
during cycle 6 for CY184, LMB5622 and 5623	77
Figure 3.33 Current pulse rate having amplitude in the range 14-20 mA	
as a function of test time in salt-fog for cycle 1	78
Figure 3.34 Current pulse rate having amplitude in the range 14-20 mA	
as a function of test time in salt-fog for cycle 6	78
Figure 3.35 Current pulse rate having amplitude in the range 20-24 mA	
as a function of test time in salt-fog for cycle 6	79
Figure 3.36 FT-IR spectrum for the white powder on specimens #1 and #2	81
Figure 3.37 FT-IR spectrum for the white powder on specimens #3 and #4	82

Figure 3.38 FT-IR spectrum for the white powder on specimens #5 and #6	82
Figure 4.1 Variation of the weight of a specimen after immersion at 43 °C for 480 h with evaporation time	86
Figure 4.2 Percentage weight increase of the specimens vs. immersion time in hexane at 43±2 and 23±3 °C	87
Figure 4.3 Amount of the LMW fluid extracted as a function of immersion time	89
Figure 4.4 Weight loss of the HTV silicone rubber specimens as a function of heating time at different heating temperature	91
Figure 4.5 Amount of fluid after 2 h heating	93
Figure 4.6 LMW fluid content by weight for samples from different manufacturers	94
Figure 4.7 Amount of fluid regenerated with different heating temperature	97
Figure 4.8 Production of fluid as a function of the number of heating-extraction-evaporation (HEE)	98
Figure 4.9 Production of fluid with accumulative time of heating	98
Figure 4.10 GC spectrum for HTV silicone rubber at the virgin status	102
Figure 4.11 GC spectrum for HTV silicone rubber treated with 4 cycles of heating-extraction-evaporation (HEE)	103
Figure 4.12 GC spectrum for HTV silicone rubber treated with 5 cycles of HEE	104
Figure 4.13 Mass spectra of peaks of GC spectrum shown in Figure 4.12	105

List of Tables

Table 2.1: Diffusion coefficients D of saline water (1 mS/cm)	
into PVC at 98 and 74°C	44
Table 3.1: Identification of the CIBA specimens	49
Table 3.2: Dimensions of the CIBA specimen	50
Table 4.1: Area for some peaks in Figure 4.10	106
Table 4.2: Calculation of the molecular weight for PDMS with small n and n^+	106
Table 4.3: Bond energies of various carbon and silicone bonds	107

Chapter 1

Introduction

As more and more new materials are being invented and cost becomes decreasing with technology advancing, polymeric materials have been increasingly used as electrical insulation since the 1960's.

Compared with historically traditional insulation materials such as porcelain and glass, polymeric materials have many advantages. For power equipment using polymeric materials, weight is reduced significantly. For manufacturers, reduced product weight means less raw material, more easy delivery and subsequently less manufacturing cost. The light weight equipment also helps utilities save funds on maintenance. A good example for this aspect is polymeric line insulators. The old pin-and-cap type suspension insulators were made of porcelain and steel and weighted about 20 kg each. A string of this kind of insulators normally consists of 28 pins each phase for a 500 kV ac transmission line. Without compromising on mechanical strength, composite insulators made of high temperature vulcanized (HTV) silicone rubber and glass fiber impregnated with epoxy resin have proved very successful as an alternate to the old porcelain insulator strings. Weight for the old insulator string is more than 500 kg each phase for 500 kV lines, which usually required a special utility vehicle to assist in replacing, while

composite insulators with the same length can be lifted and put on shoulder by one lineman.

Polymeric materials are organic. When enough saturated C-O bond is on the surface, the material is always found to be hydrophobic, i.e. having well water-repellent ability. This characteristic of polymeric material makes it very interested by insulation design engineer. Because surface of porcelain is hydrophilic, water spreads easily on the surface of insulators and causes lots of dry band arcs. Under fog and drizzle weather condition, porcelain insulators are apt to electrically breakdown if the dry band arcs shorted most of insulation length. With hydrophobic surface property, composite insulators are found to be able to withstand dry band arc pretty well.

Concerns for polymeric materials used for electrical insulation are mechanical and electrical aging characteristics. Electrical aging was dealt with in the thesis. Three most commonly used materials: polyvinyl chloride (PVC), epoxy resin and HTV silicone rubber, were selected as test objects. Chapters 2 to 4 cover the research results for each of the three materials respectively.

It is the thesis's purpose to introduce and investigate effective experimental procedures to reveal the aging characteristics of solid polymeric materials. Due to the lack of internationally recognized test standards, details for the relevant experiments have been presented as much as possible. It has to be pointed out that all the experimental methods are fitted to this laboratory's resources. Improved or modified methods can be useful to investigate other polymeric materials used for electrical insulation.

Chapter 2

A Study on Polyvinyl Chloride

2.1 Introduction

The hydrophobicity of the surface in the presence of pollution and moisture is one of the most important properties of polymeric insulating materials. A surface which has inherent ability to maintain a high level of hydrophobicity in the presence of moisture would have a low leakage current, much reduced dry band arcing and therefore a better overall electrical performance and hence a longer lifetime [1-3]. The measurement of the contact angle of a water droplet on the polymer surface provides an indication of the state of the hydrophobicity of the surface [4-6]. Although the measurement of the contact angle in a laboratory setting can readily be made with elaborately designed equipment, it is not a practical proposition on insulators suspended from high voltage towers. As polymeric insulators are being increasingly used, it is imperative to find a suitable test method that can be utilized to evaluate in situ the performance of composite insulators at various stages of their lifetime.

It has been suggested that the measurement of the electrical surface resistance might give indication on the state of the surface and thus on the electrical performance of the

insulation. The determination of the electrical resistance of the surface is relatively simple to conduct and is a nondestructive testing method [7, 8]. For polymer insulation, if the surface can keep a high resistance, detrimental surface activities such as dry band arcing will not be able to occur. Compared with porcelain and glass, it is well known that polymers are more readily damaged by degradation initiated from dry band arcings. Generally, in wet conditions, the lower is the surface resistance, the larger would be the leakage current and the shorter becomes the lifetime of the polymer insulation.

A degraded surface may have incurred much tracking and erosion caused by dry band arcings in the presence of wet and polluted conditions and other aging factors, such as ultra violet (UV) radiation from sun light, abrupt temperature change, etc. However, if the surface remains hydrophobic, the electrical performance of the insulation can be considered acceptable because the leakage current does not readily develop and further degradation is slowed down. On the other hand, if the hydrophobicity is lost or substantially reduced, the development of the leakage current accelerates and the degradation of the insulation surface grows. Therefore a polymeric insulation which loses its surface hydrophobicity needs to be identified by regular testing. The criterion is that in a wet and polluting environment the hydrophilic surface will have a much smaller surface resistance than that of a hydrophobic surface. This differentiation between the two states of the surface provides a possible method to evaluate the performance by measuring the resistance of the surface of the insulation. Albeit the insulation resistance has long been accepted as a reliable indication of the presence of conducting

contamination or degradation, many influencing factors on the measurement of the surface resistance of polymer insulation are yet to be elucidated.

Polyvinyl chloride (PVC) is very widely used in low voltage wire and cable insulation and extrusion applications. It is applied as a jacket material for coaxial cables, specialized power cables, as electrical insulation for military and aircraft wires [7, 9] and in nuclear power stations. The PVC constitutes a simple repetitious chain of $-(CH_2-CHCl)-$. This polymer is a commercial formulation and it can only be stated that it contains 50% polyvinyl chloride as the base polymer, 25-35% plasticizer with additives occupying the remainder.

The study presented in this paper is aimed at the identification of some of the parameters affecting the loss and the recovery of the surface resistance and its correlation with the hydrophobicity as represented by the contact angle of a droplet of water on the surface of a polymer. PVC is used in the present work and is widely employed in low voltage wires in motor vehicles, which in northern climates are exposed to moisture and salt that is prayed on roads in the winter. PVC is also exposed to moisture and hostile environment in the wiring of nuclear generating stations. It is planned to extend this work to other materials used in outdoor high voltage insulators including silicone rubber, epoxy and others. Since it was found that PVC could absorb moisture into the bulk and lower the insulation performance, the diffusion coefficient of the saline water into PVC was also determined at different temperatures.

2.2 Experimental Conditions and Procedures

2.2.1 Fog Test Conditions

PVC rods of different lengths were exposed to either salt-fog or to a combination of salt-fog and electrical stress in a fog chamber where they were hung vertically. Details of the fog chamber ($2.54 \times 2.54 \times 2.54 \text{ m}^3$), test supply (208V/14.4kV, 37.5kVA, 60Hz), four IEC nozzles to create the fog [10, 11] and data acquisition system [12] have been recently reported [13] and only essential information necessary for the present work will be briefly given here. In the present work, the conductivity of saline water was $1 \pm 0.03 \text{ mS/cm}$, the pressure of the compressed air used to create the fog was $0.65 \pm 0.02 \text{ MPa}$ ($94.3 \pm 3 \text{ psi}$), the water flow rate into the fog nozzles was $1.6 \pm 0.2 \text{ l/min}$ and the ambient temperature in the fog chamber was $23 \pm 2^\circ\text{C}$ during the test period. The saline solution was obtained by adding NaCl to tap water which has a conductivity of $275 \pm 25 \text{ }\mu\text{S/cm}$.

2.2.2 Measurements of the Surface Resistance

PVC specimens were aged as a function of time in three ways: 1. by exposure to salt-fog spray only, 2. by exposure to a combination of salt-fog and electrical stress and 3. by immersion in a saline solution. The tests were conducted using repeated cycles. Each test cycle (Figure 2.1) comprised of an aging time t_1 when the salt-fog was turned on.

This was followed by a period of $(t_2 - t_1)$ when the fog was turned off. $(t_2 - t_1)$ is termed the rest time during which both the recovery of hydrophobicity and the recovery of the surface resistance took place.

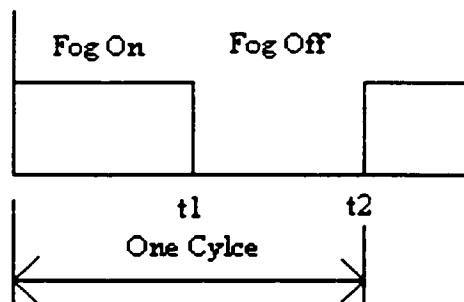


Figure 2.1 Test cycle of the salt-fog showing the on (t_1) and the off ($t_2 - t_1$) periods.

Graphite discs were screwed to both ends of the PVC rods using stainless steel screws. Graphite was employed to minimize corrosion, possible melting and subsequent evaporation during the intense arcing which might condense on the surface of the insulating rods. Other metals such as aluminum, stainless steel, brass and copper were previously tried in this laboratory and were found to be unsatisfactory [14] as they corrode and leave corrosions by-products on the surface of the specimens. The diameters of the PVC rods were kept constant at 19.5 mm for exposure to salt-fog only and 13.2 mm for the study of exposure to combined salt-fog and ac electric stress. Graphite discs of 31.8 mm in diameter and 3.1 mm thick were used with the 19.5 mm diameter PVC rods, and 25.7mm in diameter and 4.0mm thick

were used with the 13.2 mm diameter PVC rods. The length of the PVC rods was varied in the range of 25-300mm.

A dc stress in the range of 20-60 V/cm was applied to the rods to measure the surface resistance. The polarity of the dc stress was positive at the top end of the vertical rod. A sampling resistor (56.5 k Ω) was connected in series with the specimens. The current flowing in the rod was measured with the aid of a digital voltmeter (input resistance > 10 M Ω) which was connected in parallel with the sampling resistor.

2.2.3 Measurement of the Contact Angle

The contact angle between the tangent of a droplet of water and the horizontal plane of the surface of the insulating rod gives a measure of its hydrophobic property [15-17]. The static contact angle (θ) was determined on a stable horizontal plane using a goniometer with a resolution of $\pm 0.5^\circ$ [18]. A sessile drop of either deionized, or distilled water (conductivity $\leq 5.5 \mu\text{S/cm}$) and having a volume of about 5 μl was applied to the surface. The contact angle was previously reported to be independent of the volume of the droplet up to 9 μl [19] and 17 μl [20] as well as independent of its salinity in the range $2.5\text{-}10^5 \mu\text{S/cm}$ [20].

The rods were either immersed in a saline solution or exposed to salt-fog. After removing the rods from the salt-fog and from the saline solution, they were cleaned in

distilled water to remove the salt deposits which may have accumulated on the surface using an ultrasonic vibrator (115W) for about 2 min [21]. The specimens were then dried using forced air at $32\pm 2^\circ\text{C}$ for about 30 s. Unless stated otherwise, all values of θ reported here were measured after washing with distilled water. Since the surface of the polymer is both rough on a microscopic scale and heterogeneous, multiple measurements of θ at different locations on the surface are necessary to obtain reliable values. For the rod specimens, 16 readings of the contact angle were taken for each condition and the average value is reported. For each set of 16 readings, the maximum relative error was checked and found to be less than $\pm 3\%$. The maximum relative error, $e_{r\max}$, is defined as

$$e_{r\max} = \text{Max}\left(\frac{X_i - \bar{X}}{\bar{X}}\right) \times 100\% \quad (2.1)$$

where X_i is the value of the contact angle for the i th measurement, $i = 1, 2, \dots, 16$.

$\bar{X} = \frac{\sum X_i}{n}$ is the average value of the contact angle where $n=16$. If four data among the 16 readings had relative error $>\pm 3\%$, the measurements of the contact angle were repeated.

2.2.4 Measurement of the Diffusion Coefficient

The diffusion coefficient of a saline solution into PVC was determined over the temperature range from 74 to 98 °C. Circular flat discs of PVC having a thickness of 0.85 ± 0.01 mm were cut from the rods with a diameter of 26.2 mm. The discs were

immersed in a saline solution prepared by adding table salt (sodium chloride) to
Aging Characteristics of Solid Polymeric Materials used for Electrical Insulation Page 9

distilled water giving 1 mS/cm which was the same conductivity used to create the salt-fog. The added NaCl was supplied by the Canadian Salt Company, and was reported to contain traces of 0.01% potassium iodide, 0.03% dextrose, 0.4% calcium silicate and natural impurities of 0.15% calcium sulfate. Five temperatures of the saline solution of 0 ± 1 , 23 ± 2 , 44 ± 2 , 74 ± 3 and $98 \pm 2^\circ\text{C}$ were used to measure the diffusion coefficients. The absorption of the liquid into the bulk of the specimen saturates after an extended period of time.

The relationship describing the rate of absorption of liquid into a membrane was developed by Crank [22]. For the case where the diffusion is driven by a concentration gradient and there is no chemical reaction between the liquid and the membrane which results in weight changes, then the rate of absorption of the liquid into the membrane is initially linear with $t^{0.5}$, where t is the time of absorption. This process is described by [22]

$$\Delta M(t) / \Delta M_{\infty} = 2\sqrt{\frac{Dt}{\ell^2}} \left\{ \sqrt{\frac{1}{\pi}} + 2 \sum_{n=1}^{\infty} [(-1)^n \text{ierfc}\left(\frac{n\ell}{2\sqrt{Dt}}\right)] \right\} \quad (2.2)$$

where $\Delta M(t)$ is the increase in the weight ($M(t)-M(0)$) of the membrane (in kg) due to the absorption of liquid at time t , $M(t)$ is the weight at time t , $M(0)$ is the initial weight at $t=0$. ΔM_{∞} is the saturated increase in the weight (in kg) at infinity time ($t=\infty$) or at very long time, $\Delta M_{\infty} = (M_{\infty}-M(0))$ where M_{∞} is the saturated weight at infinity time ($t=\infty$) or after very long time. D is the diffusion coefficient in m^2/s , ℓ is the thickness of the membrane (in m). ierfc is a mathematical function which is defined as :

$$\text{ierfc}(x) = \sqrt{\pi} \exp(-x^2) - x \cdot \text{erfc}(x) \quad (2.3)$$

where erfc is the complementary error function. When $x \rightarrow 0$, $\text{ierfc}(x) \rightarrow \pi^{-1/2}$. When $x \rightarrow \infty$, $\text{ierfc}(x) \rightarrow 0$.

A circular disc of 26.2 mm in diameter and 0.85 mm in thickness is used which has a ratio of diameter to thickness as high as 30.8 and a corresponding ratio of the surface areas of the ends to the side of 15.4. This ensures that the diffusion from both ends of the membrane would be dominating over the diffusion from the sides. Equation (2.2) is for one-dimensional diffusion. Since the diffusion occurs from both ends of the disc for two-dimensional diffusion, ℓ is replaced by L , which is the thickness of the PVC disc which is $L=2\ell$. For the early stages of absorption, the second term in equation (2.2) may be neglected as D is very small, leading to an error function approaching zero. Therefore an equation from which the diffusion coefficient D may be determined is obtained as

$$\frac{\Delta M(t)}{\Delta M_{\infty}} = 4\left(\frac{D}{\pi L^2}\right)^{0.5} \cdot t^{0.5} \quad (2.4)$$

D may be determined from the linear dependence of the plot of $\frac{\Delta M(t)}{\Delta M_{\infty}}$ against $t^{0.5}$.

Alternatively, if a linear dependence can not be obtained over a sufficient range, D

can be determined from Equation (2.4) when $\frac{\Delta M(t)}{\Delta M_{\infty}} = 0.5$.

2.3 Results and Discussions

2.3.1 Surface resistance of and contact angle on PVC as a function of aging time in salt-fog without ac stress

In this part of the experiment, the polymer rods were not subjected to a high electrical stress that may result in dry band arcings in order that the observed changes in the surface properties can be attributed to water absorption only. The surface resistance of the PVC was measured during continuous exposure to salt-fog for 96h. A rod having 200 mm in length and 19.5 mm diameter was hung vertically in the fog chamber. The contact angle was measured on another rod. After each test cycle, one of the rods was taken out of the fog chamber, rinsed in distilled water to remove the deposits of salts which had been accumulated on the surface, dried using forced air, and the contact angle was measured. The rod was then returned to the fog chamber immediately thereafter.

Figure 2.2 shows the surface resistance and the contact angle as a function of time of exposure to salt-fog. It will be observed from Figure 2.2 that during exposure to salt-fog the surface resistance of PVC continued to decrease due to gradual wetting until it reached a saturated value. Typically from 0.1 to 1h after exposure to salt-fog the surface resistance decreased rapidly from 22.5 to 2.1M Ω while from 1 to 96h, the surface resistance decreased slowly from 2.1 to 1.65 M Ω only. After $t_1=24h$ in the salt-fog, the surface resistance reached a saturated value of 1.65 M Ω which remained constant up to

96 h. This is attributed to the complete wetting of the specimen. It will be shown that the surface tension of the PVC specimen at and after complete wetting at $t_1 \geq 24\text{h}$ has become larger than that of water.

It has been suggested [23] that the whole period of salt-fog aging can be divided into three parts: the early aging process (EAP), the middle aging process (MAP) and the late aging process (LAP). Generally there are two factors that cause the surface resistance of a polymer such as PVC to decrease with increasing aging time until saturation is reached. One is the loss of hydrophobicity. The other is the effect of wetting which results in the formation of a layer of water on the surface of the polymer.

At the EAP up to about 0.3h, the hydrophobicity of the surface, as evidenced by a relatively high θ , was still high (at $t_1=0.3\text{h}$, $\theta=80^\circ$, Figure 2.2). The wetting of the specimen was caused mainly by the impingement of the fog droplets and the condensation of moisture on the surface due to a slight temperature difference between the specimen and the salt-fog. Before the onset of the test, the specimen was hung vertically in the fog chamber for one day to eliminate possible temperature differences. The saline water was stored in a 0.25 m^3 high density polyethylene (HDPE) tank and had the same temperature as the ambient in the fog chamber. However, it was found that the temperature of the compressed air supplied from a central source was about $4 \pm 1^\circ\text{C}$ higher than that of the fog chamber. The fog droplets from the high pressure nozzles reach the central area of the fog chamber, where the rods are located, and wet the specimens during EAP. The speed of the fog droplets at the surface of the rods was found to be 2.5 m/s .

Because the hydrophobicity of the surface was still high, water could not form long filamentary paths on the surface during the EAP. Therefore, the surface resistance in EAP was large ($>7\text{M}\Omega$). However, transient small values of surface resistance were also measured. This was evidenced by the presence of large but unstable currents during the EAP. This arose when droplets of water became large enough to roll down toward the bottom electrode. When a continuous film of water connected the upper and the lower electrodes, a large current developed resulting in a lower surface resistance. This was a transient process since the long filamentary water disappeared quickly. The transitory low values of the surface resistance are not reported in this paper.

With increasing time of exposure to salt-fog, the surface tension of the PVC specimen increased and therefore the hydrophobicity decreased. It became possible for the filamentary water to cover the surface of the PVC across both electrodes. Whenever the filamentary water became temporarily disjointed and ceased to connect both electrodes, the surface resistance became transiently large which is defined as the MAP. In the LAP, the surface tension of the specimen was larger than that of water, resulting in a permanent and a continuous film of water on the surface because the surface had become hydrophilic (at $t_1 > 24\text{h}$, $\theta = 0^\circ$, Figure 2.2). The value of the surface resistance became saturated as the surface resistance was determined only by the saline water film which permanently covered the surface. During the LAP, the current in the specimen was stable.

The three stages of the aging process could be distinguished from each other by observing the stability of the current flowing in the specimen. In the EAP the current was small, but transiently high, giving a high but transient low surface resistance. In the MAP the current tends to be large, but occasionally transient towards lower values, giving a small but occasionally transient high surface resistance. In the LAP, the aging time is long, the current is stable and constant giving a saturated low value of the surface resistance. Applying this categorization, it was found that for the exposure of PVC to salt-fog shown in Figure 2.2, the EAP was up to 1h, the MAP from 1 to 24h and the LAP from 24 to 96h.

It is observed from Figure 2.2 that the largest reduction in the surface resistance occurred during the EAP while the surface resistance became relatively small in the MAP and LAP. This is because filamentary water had permanently connected both electrodes in the MAP and a continuous water film covered the whole surface of the PVC specimen in the LAP.

The formation of a continuous water film on the surface of the PVC specimen in the LAP means that the measured resistance is that of the volume resistance of the saline water film. The volume resistivity of PVC at 23°C is very large at $2 \times 10^{14} \Omega \cdot \text{m}$ [24] and therefore the measured resistance depicted in Figure 2.2 (1.65-22.5 M Ω) is largely due to the surface resistance of the specimen which includes the saline solution. If we make the reasonable assumption that the thickness of the water film is much less than the diameter of the rod, then the measured resistance in the LAP can be expressed as

$$R_s \approx \frac{x_1}{\sigma \pi \phi x_2} \quad (2.5)$$

where R_s (in Ω) denotes the surface resistance measured during the LAP, x_1 (in m) and ϕ (in m) are the length and the diameter of the rod, respectively; σ (in S/m) is the conductivity of the saline water used to produce the salt-fog and x_2 (in m) is the thickness of the water film. Substituting in Equation (2.5) $R_s=1.65 \text{ M}\Omega$ (Figure 2.2 for $t \geq 24 \text{ h}$), $x_1=0.2 \text{ m}$, $\sigma=0.1 \text{ S/m}$ and $\phi=0.0195 \text{ m}$ yields a value for $x_2=19.8 \text{ }\mu\text{m}$. This calculated value of the thickness of the water film covering the surface of PVC is in reasonable agreement with that of $30 \text{ }\mu\text{m}$ assumed recently in epoxy rods [23].

Figure 2.2 also shows the contact angle which was measured on PVC during exposure to salt-fog. The measured contact angle on the PVC rods, before the salt deposits were removed by washing in distilled water, describes the initial (up to 2h) gradual loss of the hydrophobicity of the surface during exposure to salt-fog. After 2h, θ decreased rapidly and steadily with time. The surface became completely hydrophilic ($\theta=0^\circ$) after 24h of exposure and remained in this state for up to 96h (Figure 2.2). This behavior is consistent with the observed reduction in the surface resistance which is also depicted in Figure 2.2.

Figure 2.2 also demonstrated that when the salt deposits were removed from the surface the contact angle became higher than when they were left on the surface. This is because sodium chloride is hydrophilic. θ decreased from 81.5° before the onset of the test to 62° after 96h of aging in salt-fog (Figure 2.2) and washing away the salt-deposit with the aid of distilled water in an ultrasonic cleaner.

In order to study the effects of repeated cycles of wetting and drying periods on the surface resistance of PVC, a specimen was exposed to salt-fog for four cycles. The salt-fog was left on for varying times from $t_1=2$ to 400h while the rest time in ambient air at $23\pm 2^\circ\text{C}$ outside the salt-fog chamber (t_2-t_1) was fixed at 1h. During the rest time the contact angle was measured. After this period the specimen was returned to the fog chamber. Since the specimen dried during the rest period ($t_2-t_1=1\text{h}$) the surface resistance at the beginning of cycles 2 to 4 was large (Figure 2.3). Figure 2.3 shows that during exposure to salt-fog the surface resistance continued to decrease due to gradual wetting until it reached a saturated value. Figure 2.3 also shows that the surface resistance at the beginning of each cycle has a different value. The reason is that the contact angle did not recover completely during the short rest period of 1h. After long exposure periods (50 to 400h, Figure 2.3) to salt-fog the values of the surface resistance were of the same order of magnitude and this is attributed to the completed wetting of the surface. The decrease of the surface resistance depicted in Figure 2.3 is consistent with that shown in Figure 2.2 and is attributed to the loss of hydrophobicity due to wetting.

Utilizing equation (2.5), the thickness of the water film when the resistance showed saturated and constant values at the end of cycles 1 to 4 are found to be 19.8, 25.1, 36.2 and 39.8 μm , respectively. These values are consistent with the value of 30 μm assumed for epoxy which was dipped in 0.5 mS/cm solution in a rotating wheel [23]. The thickness of the water film covering the surface of the PVC specimens after a long exposure (LAP) to salt-fog is influenced by both the quantity of water accumulated on the

surface and the specific surface tension of the material. The quantity of water accumulated on the surface is determined by the water flow rate supplied to produce the salt-fog. In the present study, the water flow rate was constant at 1.6 l/min. Therefore, the reason for the increase thickness of the water film with increasing test cycles is that the surface tension becomes larger with increasing test cycles. It will be shown in this paper that the surface tension of the specimen increases with increasing time of exposure to salt-fog.

In order to find a relationship between the surface resistance and the hydrophobic property of the surface, the specimens were temporarily removed from the fog chamber for 1h to measure the contact angle. θ was measured every 10 min in air at $23\pm3^{\circ}\text{C}$ and is shown in Figure 2.4 during a short period of recovery between exposure to salt-fog for 4 cycles.

It will be observed from Figure 2.4 that 1 min after removal from the salt-fog the θ values were low and close to each other at $73.3\pm0.2^{\circ}$ except for those measured after cycle 1 where the corresponding value was 74.8° . The contact angle of the virgin specimen was $81.5\pm0.3^{\circ}$ which is lower than the value of 87° reported previously [16, 25]. The difference could be due to different composition. The low values of θ at 1 min after removal from the salt-fog (Figure 2.4) correspond to the low values of the surface resistance found at the end of exposure to salt-fog shown in Figure 2.3. After a rest time of 1h, θ was different for different times of exposure to the salt-fog (Figure 2.3) because the hydrophobicity had not yet recovered to the same level due to their different history

of exposure to the salt-fog. The different values of θ shown in Figure 2.4 at the end of the rest period also explain the different surface resistances measured at the onset of each cycles of exposure to salt-fog shown in Figure 2.3. At 1h of rest subsequent to exposure to fog for 652h, θ had partially recovered to 78.8° (Figure 2.4, curve 4) while after exposure to only 2h it completely recovered within 1h in air (Figure 2.4, curve 1). The contact angle subsequent to the fourth cycle, when it was exposed to a total time of 652h, did not completely recover to 81.5° until after a rest time of 4.5 months in air.

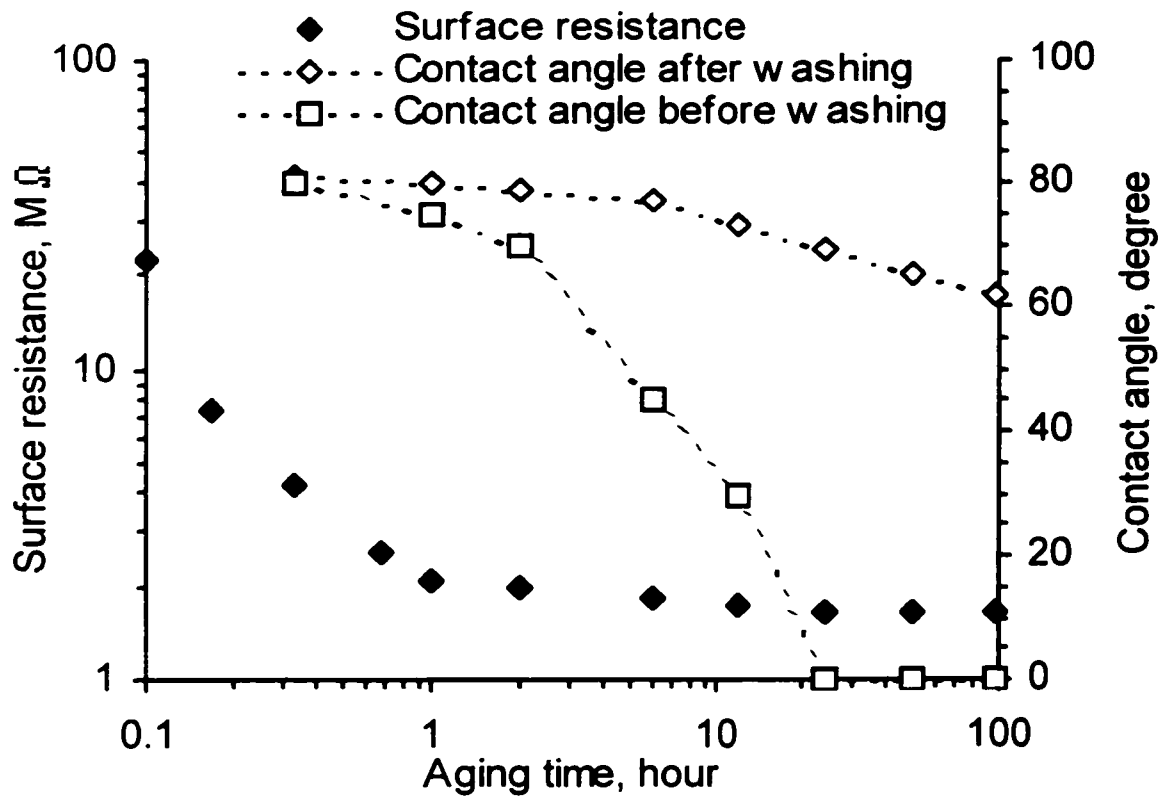


Figure 2.2 Surface resistance of and contact angle on a PVC cylindrical rod during exposure to un-energized salt-fog. Conductivity of the saline solution to produce the salt-fog, 1 mS/cm; water flow rate, 1.6 l/min; air pressure to produce the fog, 0.65 MPa; length of the rod, 200mm; diameter of rod, 19.5 mm; $t_1=96$ h; $t_2-t_1=0$; dc stress used to measure resistance, 20 V/cm; graphite electrodes: diameter, 31.8 mm; thickness, 3.1mm.

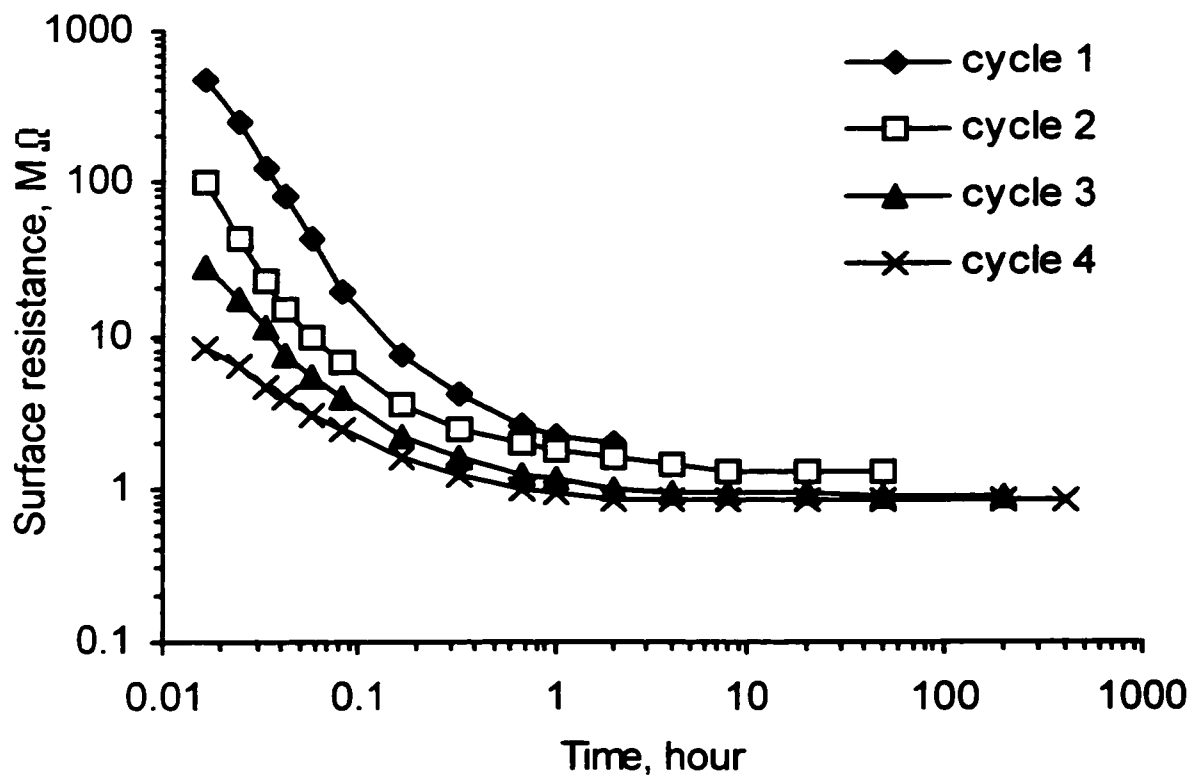


Figure 2.3 Surface resistance of PVC rod during exposure to salt-fog. For cycles 1 to 4, $t_1=2, 50, 200, 400\text{h}$, respectively. Rest time ($t_2 - t_1$) for cycles 1, 2, 3 was 1h. Other conditions are as in Figure 2.

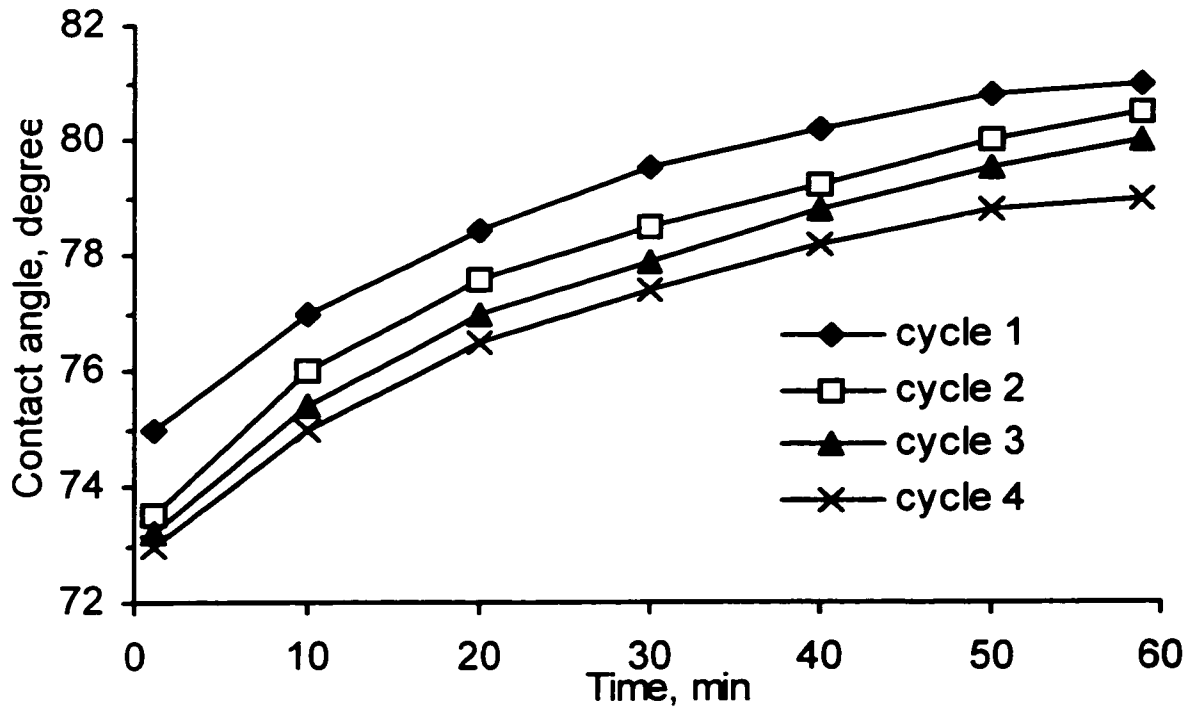


Figure 2.4 Recovery of contact angle during the rest period between the successive exposure to salt-fog shown in Figure 2.3. Rest period between successive cycles, 1h; other conditions are as in Figure 2.3.

2.3.2 Recovery of Surface Resistance and Contact Angle of PVC after Exposure to Salt-fog

Figure 2.5 shows the recovery of the surface resistance and the contact angle in air after an exposure to salt-fog for 96 h. Upon switching off the salt-fog one of the specimens was taken out of the fog chamber to measure the contact angle. It will be observed from Figure 2.5 that the recovery of the contact angle correlates well with the recovery of the surface resistance. After 8h of drying in air the surface resistance recovered from 20 M Ω to 210 G Ω while at the same period of rest time contact angle increased from 62° to 74°. Figure 2.5 shows that the surface resistance saturated after a rest time of 18h while the contact angle continued to increase with increasing rest time. The saturated high value of the surface resistance of $2.1 \times 10^{11} \Omega$ was close to the upper limit of our set-up for the measurements of the resistance.

The starting contact angle in Figure 2.5 is 62° which is lower than that shown in Figure 2.4 ($74 \pm 1^\circ$). This is in part due to the degree of severity of the initial salt deposits on the surface and also how effective was the washing used to remove them. Figure 2.5 shows a good correlation between the increasing contact angle and the surface resistance during recovery in air.

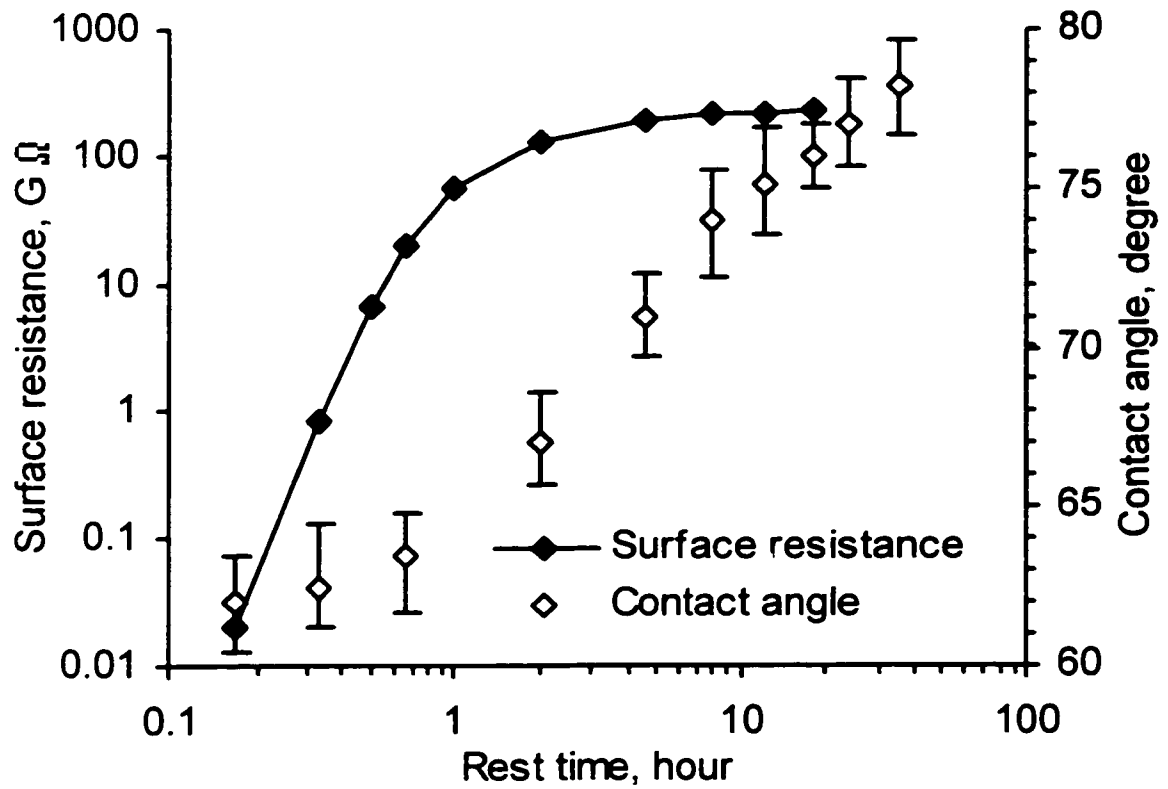


Figure 2.5 Surface resistance and contact angle of the PVC specimen as a function of rest time in air after 96h of exposure to salt-fog. Other conditions are as in Figure 2.

2.3.3 Dependence of Surface Resistance on Rod Length

PVC rods having different lengths in the range from 25 to 300 mm were used to investigate the dependence of the surface resistance on the length of the specimen. Figure 2.6 shows that the surface resistance decreases with increasing wetting duration for all lengths. Typically for the 300mm rod the surface resistance decreases from 4.8 G Ω after 1 min of exposure to salt-fog to 3 M Ω after 2h. The longer was the length of the rod, the more rapidly its surface resistance decreased with increasing time of exposure to salt-fog. Figure 2.6 indicates that the surface resistance before saturation is reached at long time of exposure, is not linearly dependent on the length of the rod as Equation (2.5) suggests. This is due to the non-uniform distribution of the voltage used to measure the resistance along the length of the rod and its dependence on the length [26]. The longer is the rod the less uniform is the voltage distribution along the rod. The saturated resistance values were 0.96, 1.45, 2.13 and 2.8 M Ω , respectively for the rod lengths 25, 100, 200 and 300 mm (Figure 2.6). The thickness of the water layer may also slightly change with varying length due to the effect of the gravity on the cascading water. However, since the rods were exposed to the same fog conditions it is expected that the water thickness would be silimilarly close for all four rods and the force contribute a smaller effect to the changing saturated resistance with varying rod lengths.

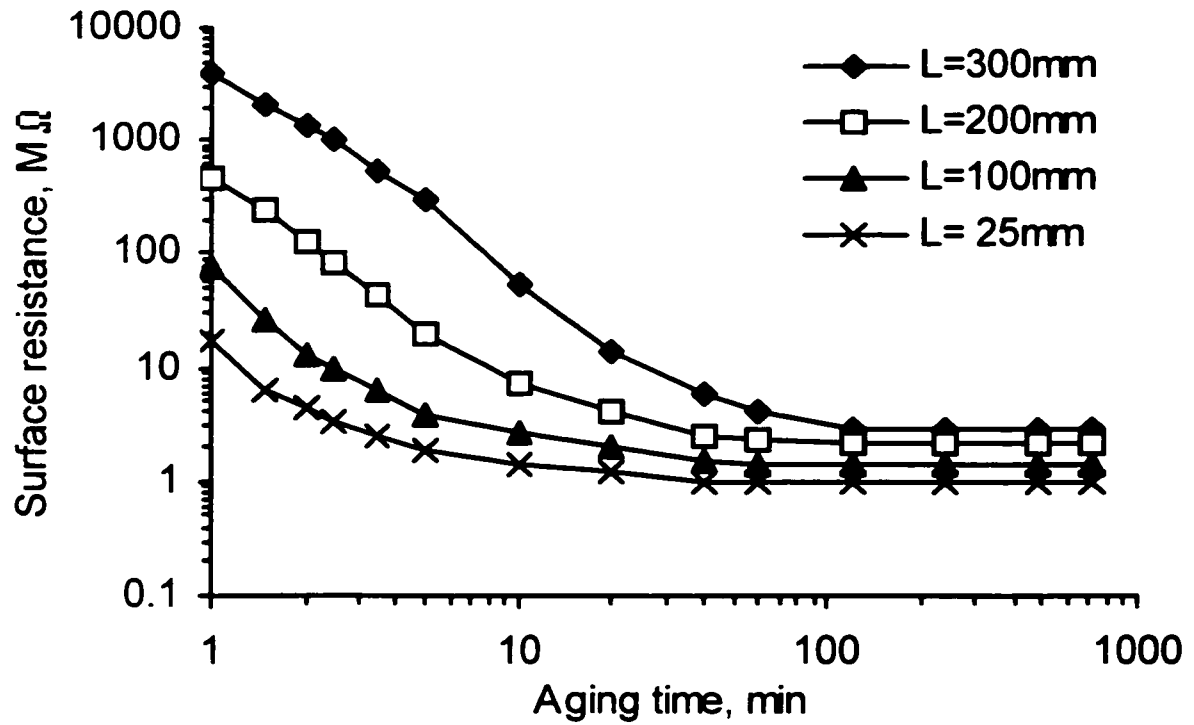


Figure 2.6 Dependence of surface resistance on time of exposure to salt-fog for different length of PVC rods. Other conditions are as in Figure 2.

2.3.4 Effect of DC Stress on Surface Resistance Measurements

The dc stress used to measure the surface resistance was varied in the range from 20 to 60 V/cm while keeping the length of the specimen constant at 200 mm. Figure 2.7 shows the surface resistance during salt-fog exposure of 96 h. It is shown in Figure 2.7 that for 20 and 40 V/cm the surface resistance at a given time of exposure had about the same values while for 60 V/cm higher values of resistance were obtained. This was because the larger current in the latter case caused a temporary and partial drying of the surface leading to a larger surface resistance.

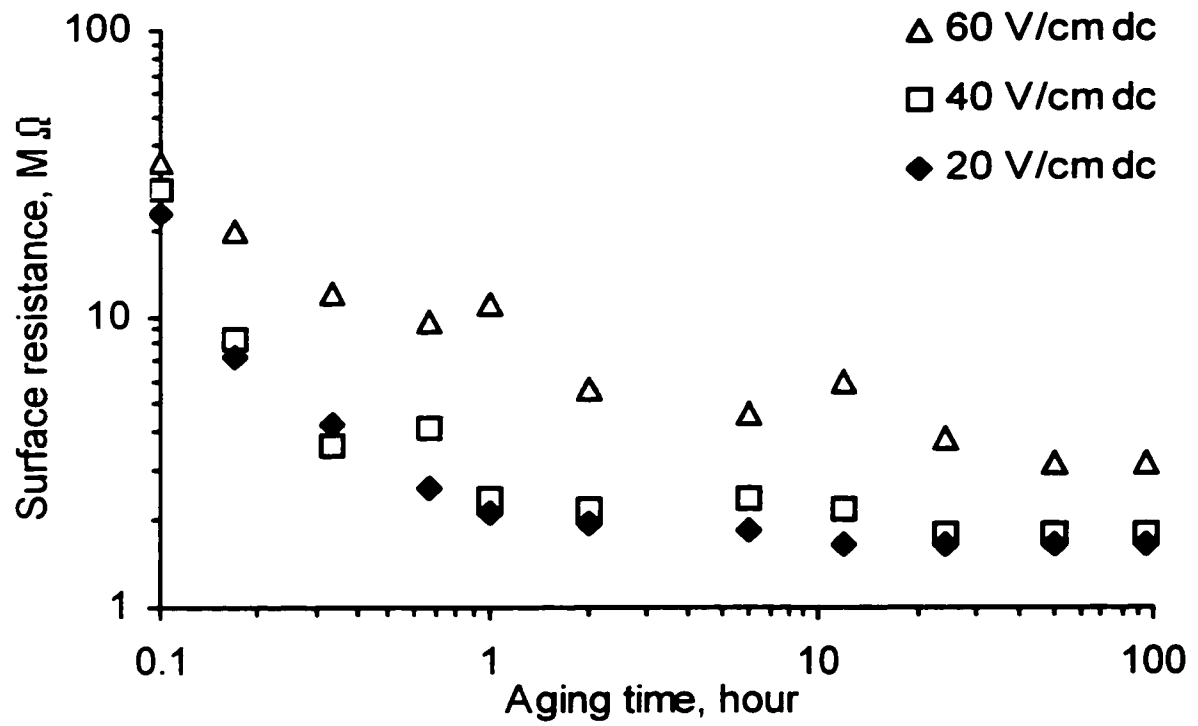


Figure 2.7 Influence of dc stress on surface resistance during exposure to salt-fog. Conditions are as in Figure 2.

2.3.5 Effect of Combined Salt-fog and AC Electric Stress on Surface Resistance

A combined salt-fog and ac electric stress of 200 V_{rms}/cm (60 Hz) was applied to PVC rods having a diameter of 13.2 mm and a length of 152 mm. Four cycles were applied with $t_1=12$ h in each cycle, followed by a rest period of 36 h. The average leakage current is shown in Figure 2.8. The average leakage current is defined as the value obtained by summing up the absolute values of all currents sampled during the positive (13 samples) and the negative (13 samples) portions of the 60 Hz, over a specified length of time, and dividing by the total number of the sampled currents [27]. Figure 2.8 shows that the leakage current increases with time of test until saturation is reached. This is due to the gradual loss of hydrophobicity of the surface. At the beginning of each cycle the current is larger due to the incomplete recovery of the hydrophobicity during the rest period of 36 h between successive cycles. This is consistent with similar observations reported with silicone rubber coating [21]. Erosion tracks on the surface were visible after cycle 1. These were caused by dry band arcings during exposure to energized salt-fog. Although after each test cycle the specimen was cleaned with vinegar (5% acetic acid), washed with distilled water and dried in air, the tracks were readily wetted soon after exposure to salt-fog which resulted in a rapid increase of the average leakage current for cycles 2-4 (as shown in Figure 2.8).

During the aging with the energized salt-fog, the surface resistance of the specimen was measured. After switching off the ac stress only, a dc stress of 20 V/cm was applied to

the PVC rod. The measurement was carried out within 2 min and the ac stress was re-applied as soon as the measurement of resistance was completed. Figure 2.9 shows that the surface resistance decreased with increasing aging time and cycles. There is also a big decrease after cycle 1. This is due to erosion tracks which were found after the first 12 h of exposure to the energized salt-fog. The tracks were permanent on the surface and caused a decreased surface resistance for cycles 2-4. For the increasing number of test cycles, the tracks extended from the upper electrode to the lower one and caused decreasing surface resistances (Figure 2.9, cycle 2-4). This resulted in much lower resistance values (Figure 2.9) compared to the case when the rods were subjected to unenergized salt-fog (Figure 2.3). An insulation failure on the PVC rod happened on cycle 5 when the current protective switch, whose action current was set at 50 A, disconnected automatically the supply for the ac test transformer.

During the rest time, the surface resistance was also measured using a dc stress of 20 V/cm while both the salt-fog and the ac stress were turned off. Figure 2.10 shows that the surface resistance decreased with increasing number of testing cycles during the rest period. The largest decrease was also found after cycle 1. This agrees with the large increase of the average leakage current after cycle 1 which is depicted in Figure 2.8. The tracks caused by the dry band arcing were concentrated in the area close to the upper electrode. Near the bottom electrode there was no dry band arcing and therefore no visible tracks. Immediately after turning off the salt-fog, the specimen was still wet. At the beginning of the rest time in air, the resistance of the wetted surface in all cycles in

Figure 2.10 was very low at about 2 M Ω . After 36 h of recovery in air the resistance of the dried surface tended to reach the same high value of 5.5×10^5 M Ω (Figure 2.10).

It is also shown in Figure 2.10 that the onset of the recovery of the surface resistance is delayed during the rest time outside the salt-fog with increasing number of cycles and therefore with increasing time of exposure to fog. This is because it takes longer time for the hydrophobicity to recover with increasing time of exposure to combined salt-fog and ac electric stress. Typically after the first cycle ($t_1=12$ h) the resistance started to recover after 2 min of rest time (Figure 2.10, cycle 1). While after the fourth cycle ($\Sigma t_1=48$ h) the onset of recovery of the surface resistance was delayed by 10min (Figure 2.10, cycle 4).

Generally, increasing the time of exposure to combined salt-fog and ac stress resulted in a lower surface resistance at a fixed time after removing the combined salt-fog and electric stress. After 36 h of rest time the surface resistance is at about the same level 5.5×10^{11} Ω (Figure 2.10) because by then the surface had completely dried.

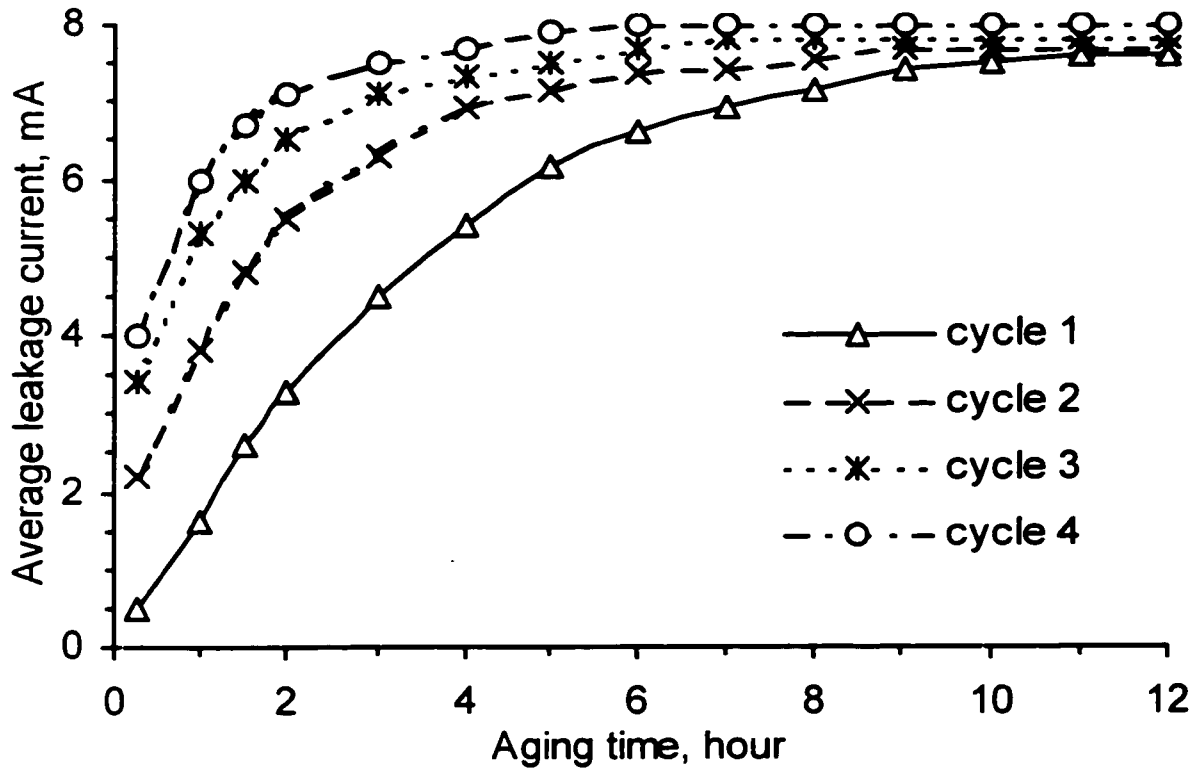


Figure 2.8 Average leakage current with aging time in the presence of salt-fog and ac stress. $t_1=12\text{h}$, $(t_2 - t_1)=36\text{h}$. ac stress was $200 \text{ V}_{\text{rms}}/\text{cm}$. Length of the rod, 152mm ; diameter of the rod, 13.2mm . Fog conditions are as in Figure 2.

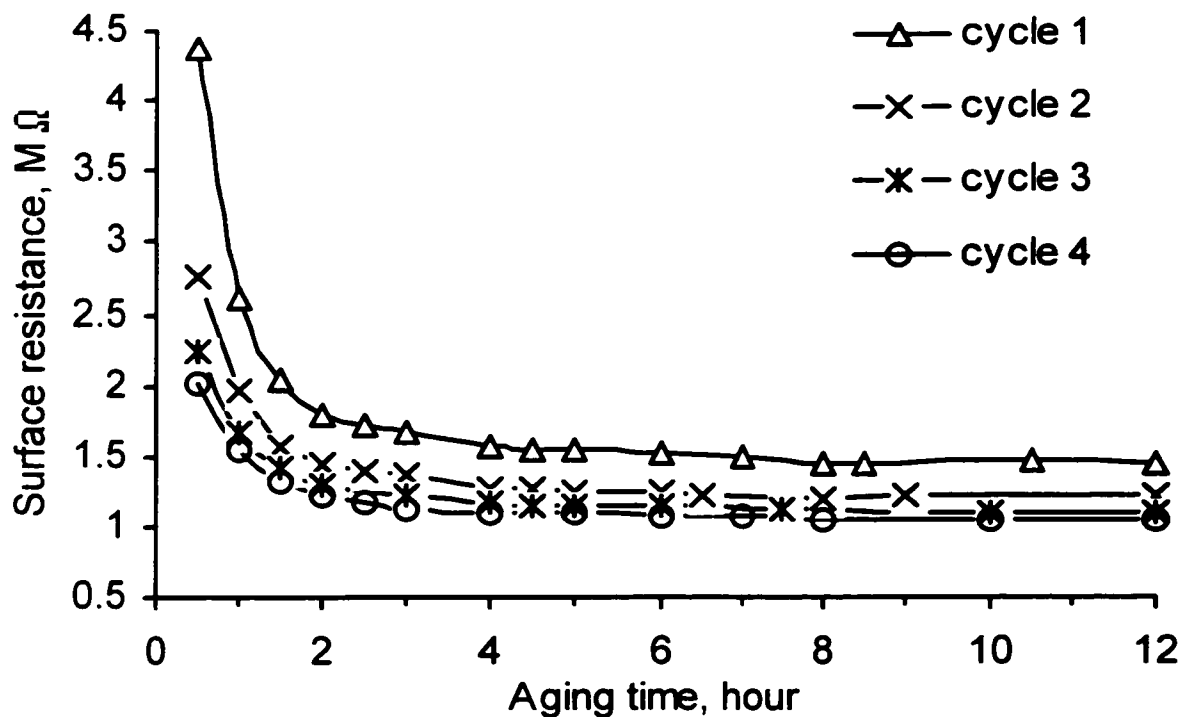


Figure 2.9 Surface resistance as a function of aging time for cycles 1-4 during exposure to a combined salt-fog and ac stress of 200 V_{rms}/cm. dc stress to measure resistance, 20 V/cm. Other conditions are as in Figure 2.8.

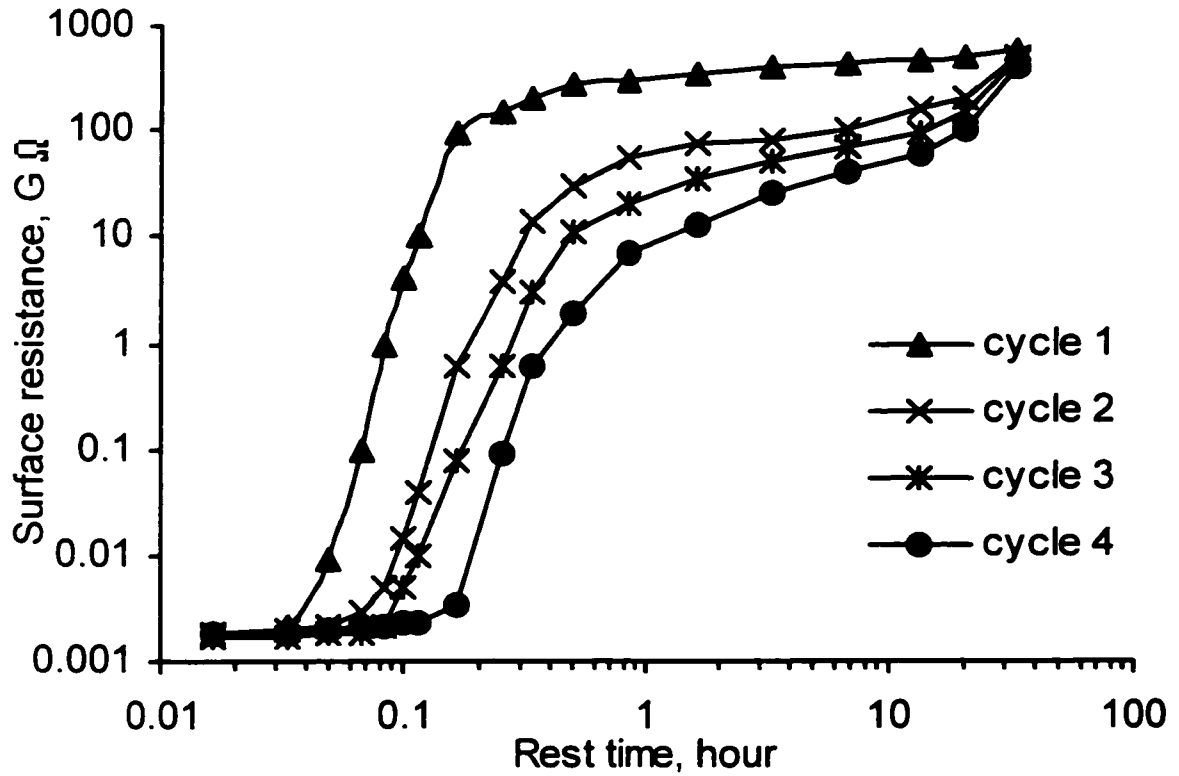


Figure 2.10 Recovery of surface resistance after exposure to a combined salt-fog and ac stress of 200 V_{rms}/cm. dc stress to measure surface resistance, 20V/cm; sampling resistor in series with PVC specimen, 200kΩ. Other conditions are as in Figure 2.8.

2.3.6 Surface Tensions of PVC in the Presence of Salt-fog

The loss of hydrophobicity of PVC after exposure to salt-fog for a long time is attributed to the interaction between water and the surface which resulted in a higher surface tension (γ_s). Microscopically, the increase of γ_s is due to the chemical functional groups present on the surface during aging [28]. The chemical functional groups possibly come from additives.

The surface tension, also called the surface free energy per unit area, is in unit of J/m^2 . Basically, it can be divided into a dispersion (non-polar) component due to the London dispersive force and a polar component due to the polar force. Therefore the surface tension for a solid can be expressed as [5, 15, 16]

$$\gamma_s = \gamma_{SD} + \gamma_{SH} \quad (2.6)$$

and for a liquid,

$$\gamma_L = \gamma_{LD} + \gamma_{LH} \quad (2.7)$$

where the suffixes D and H denote dispersion and polar component, respectively; L and S for liquid and solid, respectively. The London dispersion force arises from instantaneous dipole interaction produced by the motion of electrons within molecules. The polar force arises from dipole-dipole interaction or dipole-induced dipole interaction by polarization [16].

For PVC, γ_{SD} and γ_{SH} are responsible for the hydrophobicity and hydrophilicity, respectively. The contact angle (θ) is related to the surface tension via Young's equation [16, 17],

$$\gamma_s = \gamma_{SL} + \gamma_L \cos \theta \quad (2.8)$$

where γ_{SL} is the surface tension of the solid-liquid interfacial surfaces. For the system of saline water and PVC, the polarizabilities of the interacting elements are not too different. Therefore the Harmonic-Mean approximation is applicable and the relationship among γ_{SL} , γ_s and γ_L can be expressed as [16]

$$\gamma_{SL} = \gamma_s + \gamma_L - \frac{4\gamma_{SD}\gamma_{LD}}{\gamma_{SD} + \gamma_{LD}} - \frac{4\gamma_{SH}\gamma_{LH}}{\gamma_{SH} + \gamma_{LH}} \quad (2.9)$$

From equations (2.8) and (2.9),

$$(1 + \cos \theta)\gamma_L = \frac{4\gamma_{SD}\gamma_{LD}}{\gamma_{SD} + \gamma_{LD}} + \frac{4\gamma_{SH}\gamma_{LH}}{\gamma_{SH} + \gamma_{LH}} \quad (2.10)$$

or, by combining (2.7) and (2.10),

$$(3 - \cos \theta)\gamma_L = \frac{4\gamma_{LD}^2}{\gamma_{SD} + \gamma_{LD}} + \frac{4\gamma_{LH}^2}{\gamma_{SH} + \gamma_{LH}} \quad (2.11)$$

Equation (2.11) indicates that for given polymeric material and wetting environment the larger are γ_{SD} and γ_{SH} , the smaller would be the static contact angle θ . Therefore, when the surface tension (γ_s) of the solid surface is increased, a smaller contact angle will be observed. This agrees with the experimental results [29, 30].

For a virgin polymer insulating material, $\gamma_{SD} \gg \gamma_{SH}$. γ_s is therefore determined mainly by γ_{SD} on the surface of a non-aged polymeric surface. During aging, γ_s is changing with

time of interfacial interaction between PVC and the saline water. Specifically, γ_{SH} increased with time of exposure to salt-fog [5, 16]. Therefore the surface tension of PVC is increased because of the absorption of saline water and the adhesion of the saline water to the surface. This causes a decrease of the contact angle.

To investigate the recovery of the contact angle of PVC after wetting, two specimens were immersed in a saline solution (1 mS/cm) for 96h at $23 \pm 2^\circ\text{C}$. After this time of immersion the contact angle decreased to a value of about 60° . Figure 2.11 shows the recovery the contact angle after exposure for 96h to salt-fog (curve 1) and after immersion for 96h in a saline solution (curve 2). It will be observed that after 96h of immersion in saline solution with a salinity of 1 mS/cm it took 300h for the contact angle to recover to 81° (Figure 2.11, curve 1). This is very close to the original contact angle of the PVC of 81.5° . The recovery of the contact angle on the specimens which had been exposed to salt-fog for 96h took 150 h to recover to 81.3° (Figure 2.11, curve 1).

In general the recovery of hydrophobicity on a polymeric surface after aging is attributed to the thermodynamic driving force to minimize the surface free energy. It is believed that the chemical functional groups responsible for the loss of hydrophobicity tend to migrate away from a surface which was exposed to dry air to the interior of the polymeric material. The migration is facilitated by the local motion of polymer chains and is dependent on the molecular mobility of the polymer chains [28]. The recovery of the contact angle on the drying PVC (Figure 2.11) is

primarily due to the loss of moisture on the surface but it may also be related to the diffusion process of the hydrophobic groups from the bulk to the surface.

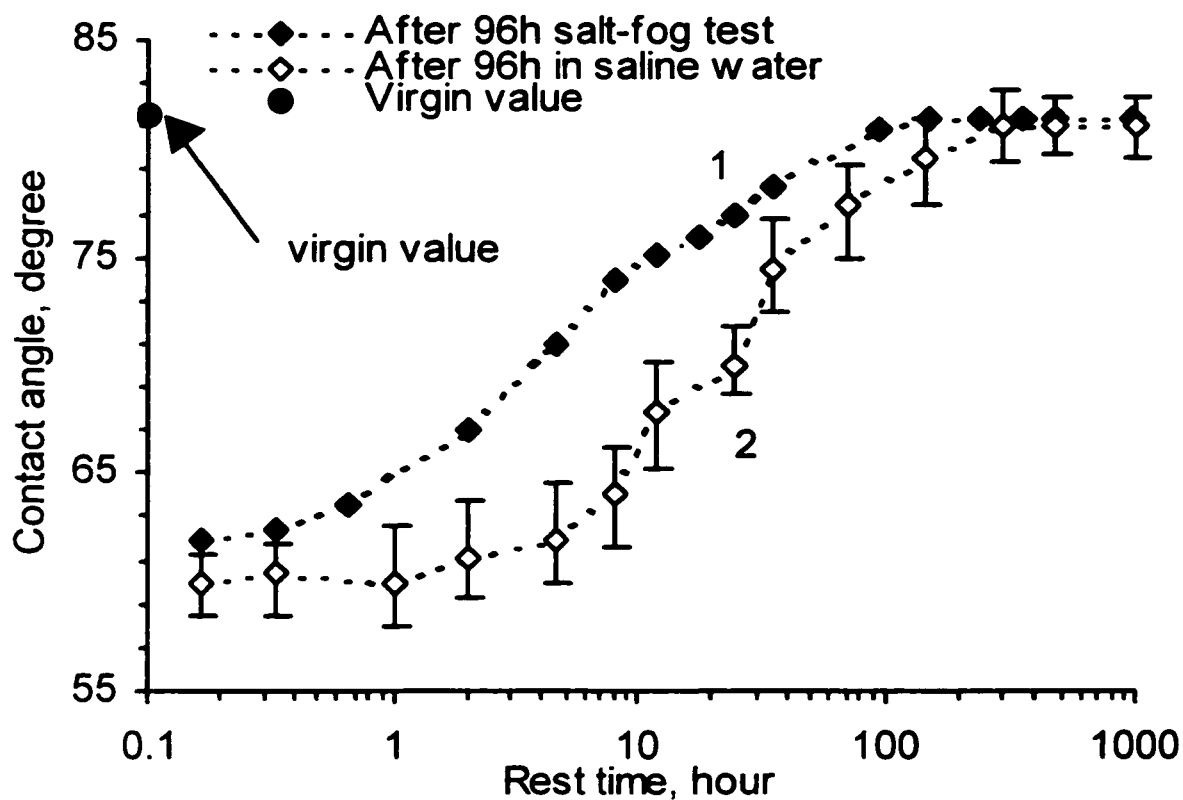


Figure 2.11 Recovery of contact angle of PVC in air at $23 \pm 2^\circ\text{C}$ after immersion for 96h in saline solution with salinity of 1 mS/cm at $23 \pm 2^\circ\text{C}$ (curve 1) and after exposure for 96h to salt-fog produced by a saline solution of 1 mS/cm (curve 2).

2.3.7 Determination of γ_s , γ_{SD} and γ_{SH} from the Static Contact Angle

For polymeric materials used as electrical insulation, keeping a low surface free energy (γ_s) is always preferable. In practice, it is difficult to measure γ_s directly. By means of equation (2.10), γ_s for PVC may be calculated by measuring the static contact angle with two different testing liquids. This method is called the Harmonic-Mean method [16]. Using distilled water and methylene iodide (CH_2I_2), two contact angles θ_w and θ_m , respectively were measured and γ_{SD} and γ_{SH} were determined by solving a set of two simultaneous equations in form of equation (2.10). For distilled water, the literature values of γ_{L1} , γ_{L1D} and γ_{L1H} are 72.8×10^{-3} , 22.1×10^{-3} and $50.7 \times 10^{-3} \text{ J/m}^2$, respectively [16]. For methylene iodide (MI), γ_{L2} , γ_{L2D} and γ_{L2H} are 50.8×10^{-3} , 44.1×10^{-3} and $6.7 \times 10^{-3} \text{ J/m}^2$, respectively [16]. The contact angle with water, θ_w was measured as 81.5° while the contact angle with MI, θ_m was measured as 35° on a virgin PVC specimen. The calculated values on a virgin PVC at 23°C are: $\gamma_s = 43.1 \times 10^{-3} \text{ J/m}^2$, $\gamma_{SD} = 34.4 \times 10^{-3} \text{ J/m}^2$ and $\gamma_{SH} = 8.7 \times 10^{-3} \text{ J/m}^2$. Our calculated values agree well with literature values of $\gamma_s = 41.9 \times 10^{-3} \text{ J/m}^2$, $\gamma_{SD} = 35.8 \times 10^{-3}$ and $\gamma_{SH} = 6.1 \times 10^{-3} \text{ J/m}^2$ at 20°C [16]. All values are reported here at $23 \pm 2^\circ\text{C}$.

During the aging test with salt-fog (shown in Figure 2.2), both θ_w and θ_m were measured on the PVC specimen. Figure 2.12 shows the calculated values of γ_{SH} , γ_{SD} and γ_s using equation (2.10). It will be observed from Figure 2.12 that γ_{SH} (curve C) steadily increased

with increasing time until saturation is reached while γ_{SD} (curve B) changed only slightly during the aging process. This was because γ_{SH} reflects the polarity of the surface while γ_{SD} reflects non-polar component of the surface tension and is independent of the polar forces. As the surface was wetted gradually the polarity of the surface increased due to the enhanced effect of the hydrogen bonding forces. Figure 2.12 shows that after the aging time reached 2h, θ_m decreased to 0° (curve E). This is because γ_s of the PVC surface increased to $52.8 \times 10^{-3} \text{ J/m}^2$ which was larger than γ_L of MI ($50.8 \times 10^{-3} \text{ J/m}^2$) after exposure to the salt-fog for 2h. When γ_L of PVC became larger than γ_L of water at $t_1=24\text{h}$, θ_w also decreased to 0° (Figure 2.12, curve D). This means that a continuous water film has been formed on the surface of the PVC specimen. The saturated values shown in Figure 2.12 of γ_{SD} (curve B), γ_{SH} (curve C) and γ_s (curve A) for $t_1 > 24\text{h}$ are attributed to the error of the Harmonic-Mean method. In the model described by equations (2.9)-(2.11), γ_{SH} and γ_{SD} are to be determined by θ_m and θ_w . When both θ_m and θ_w decreased to zero, they reached the physical minimum and could not decrease further. Therefore the calculated γ_{SH} and γ_{SD} became constant.

It will be observed from Figure 2.12 that the surface tension of the PVC surface γ_s was $50.1 \times 10^{-3} \text{ J/m}^2$ at $t_1=1\text{h}$ (curve A) and $76.8 \times 10^{-3} \text{ J/m}^2$ at $t_1=24\text{h}$ (curve A). This means that γ_s increased from 43.1×10^{-3} to only $50.1 \times 10^{-3} \text{ J/m}^2$ (Figure 2.12, curve A) in the EAP and therefore the hydrophobicity of the surface of the PVC specimen was still relatively good. The calculated small increase of the surface tension during the EAP was consistent with the large surface resistance shown in Figure 2.2. Between aging times of 1 and 24h, the surface tension of PVC increased quickly and by the time $t_1=24\text{h}$, the surface tension

$\gamma_s = 76.8 \times 10^{-3} \text{ J/m}^2$ (Figure 2.12, curve A) became larger than that of water ($72.8 \times 10^{-3} \text{ J/m}^2$ [16]). Therefore, after exposure to the salt-fog for 24h, the surface of the PVC specimens lost their hydrophobicity completely and a continuous film of water was formed on the surface. This agrees with the saturated value of the surface resistance for $t_1 > 24\text{h}$ shown in Figure 2.2.

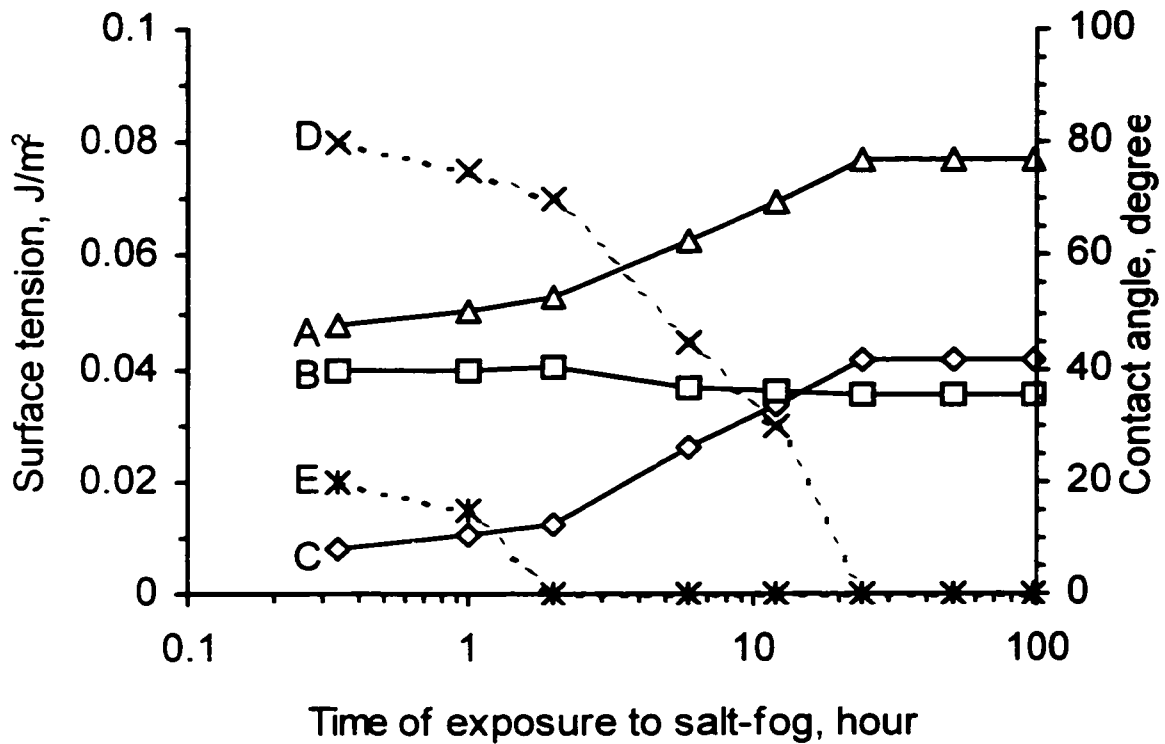


Figure 2.12 Calculated surface tension of PVC from contact angle measured with distilled water and methylene iodide as a function of exposure time to salt-fog. Curves A, B and C are γ_s , γ_{SD} and γ_{SH} , respectively. Curves D and E are contact angles measured with distilled water (θ_w) and methylene iodide (θ_m), respectively. Conditions are as in Figure 2.

2.3.8 Diffusion Coefficient of Saline Water into PVC

The diffusion of water into the polymer bulk contributes to the formation of water trees and subsequent degradation of the insulation. The present study may be used to give information on the lifetime of the material from the amount of and the rate of water absorption as determined from the diffusion coefficient of water into the PVC.

After immersing a disc of PVC (26.2 mm in diameter and 0.85 mm in thickness) in a saline solution (1 mS/cm) for about 14,616 hours, saturation in the weight of the specimens was observed at temperatures of 98 and 74°C. Figure 2.13 shows the percentage weight increase as a function of immersion time. It is shown in Figure 2.13 that the change on the weight of PVC specimens increases with increasing temperature of the saline solution (1 mS/cm). At 98 and 74°C, periods of 1,919.5 and 7,248 hours (Figure 2.13) were required to reach saturation in the weight (Equation 2.4), respectively. The saturated increases in the weights were 44.4 and 16.7%, respectively at 98 and 74°C (Figure 2.13). After immersion for 14,616 hours, the weight of the specimen at 44°C increased by only 3.52% and no saturation was reached at the end of this period (Figure 2.13). At 98°C, after the immersion of 385 hours in 1 mS/cm saline solution, it was noted that the color of the PVC specimen changed from the original gray blue to light brown. This is attributed to the decomposition or the diffusion of the pigment additives from the specimens into the water at high temperatures. Since the concentration of the added pigments to the compound is very small and the

specimens remained physically intact, it was concluded that there were no other chemical reactions and therefore the procedure for determining the diffusion coefficients was still valid.

Figure 2.13 indicates that the lower is the temperature the longer the time it takes to reach a saturation in the weight increase and the saturated value is higher for specimens at higher temperatures. Equation (2.4) shows that $\Delta M(t)/\Delta M_{\infty}$ is proportional to $D^{0.5}$ for a fixed thickness L and at a given immersion time t . Therefore since Figure 2.13 shows that the percentage weight increase of the specimens as a function of immersion time decreases with decreasing temperature, the diffusion coefficient of water into PVC must also decrease with decreasing temperature.

Figure 2.14 illustrates the relationship between $\Delta M(t)/\Delta M_{\infty}$ and $t^{0.5}$ for specimens immersed at 98 and 74°C. Equation (2.4) can be simplified for $\Delta M(t)/\Delta M_{\infty} = 0.5$, which occurs at $t = t_{0.5}$. The diffusion coefficient, D , is obtained from

$$D = \frac{\pi}{64} \frac{L_{0.5}^2}{t_{0.5}} = 0.049 \frac{L_{0.5}^2}{t_{0.5}} \quad (2.12)$$

where $t_{0.5}$ is the time at which $\Delta M(t)/\Delta M_{\infty} = 0.5$ and $L_{0.5}$ is the thickness of the specimen at $t_{0.5}$. From equation (2.12), the diffusion coefficients for PVC specimens immersed in saline solution (1 mS/cm) at 98 and 74°C were determined. The values obtained are listed in Table 2.1. It will be observed from Table 2.1 that D increases with increasing temperature from 2.8×10^{-15} at 74°C to 1.6×10^{-14} m²/s at 98°C. These

values are lower than those reported in cross linked polyethylene for the diffusion of moisture of $8.8 \times 10^{-13} \text{ m}^2/\text{s}$ at 89°C and $3.7 \times 10^{-13} \text{ m}^2/\text{s}$ at 74°C [31]. In cycloaliphatic epoxy resins values of $(1.49 \pm 0.27) \times 10^{-13} \text{ m}^2/\text{s}$ and for bisphenol epoxy resin $1.5 \times 10^{-12} \text{ m}^2/\text{s}$ were reported at 75°C [32]. At 44°C the increase in the weight of the specimen had not reached a saturated value even after 14,616 h and therefore the diffusion coefficient of water into PVC at that temperature could not be determined.

Table 2.1: Diffusion coefficients D of saline water (1 mS/cm)
into PVC at 98 and 74°C

$t_{0.5}$ is the time at which $\Delta M(t)/\Delta M_\infty = 0.5$ where $\Delta M(t)$ and ΔM_∞ are the increases in the weights of the specimen at time t and at saturation. $L_{0.5}$ is the thickness of the specimen at $t = t_{0.5}$.

Temperature of the solution, $^\circ\text{C}$	$t_{0.5}$, hour	$L_{0.5}$, mm	D, m^2/s
98	25.0^2	0.85	1.6×10^{-14}
74	58.6^2	0.84	2.8×10^{-15}

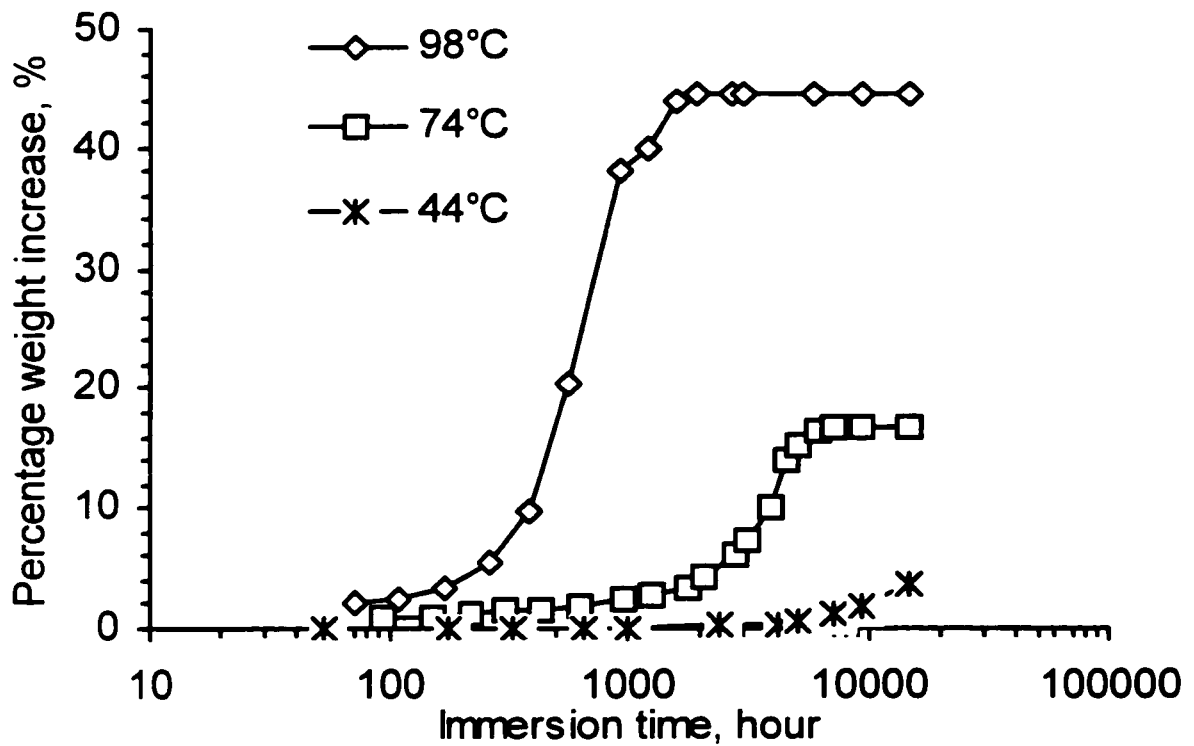


Figure 2.13 Dependence of weight increase of PVC on time of immersion in a saline solution (1 mS/cm) at different temperatures. Thickness of virgin PVC discs, 0.85 mm; diameter, 26.2 mm.

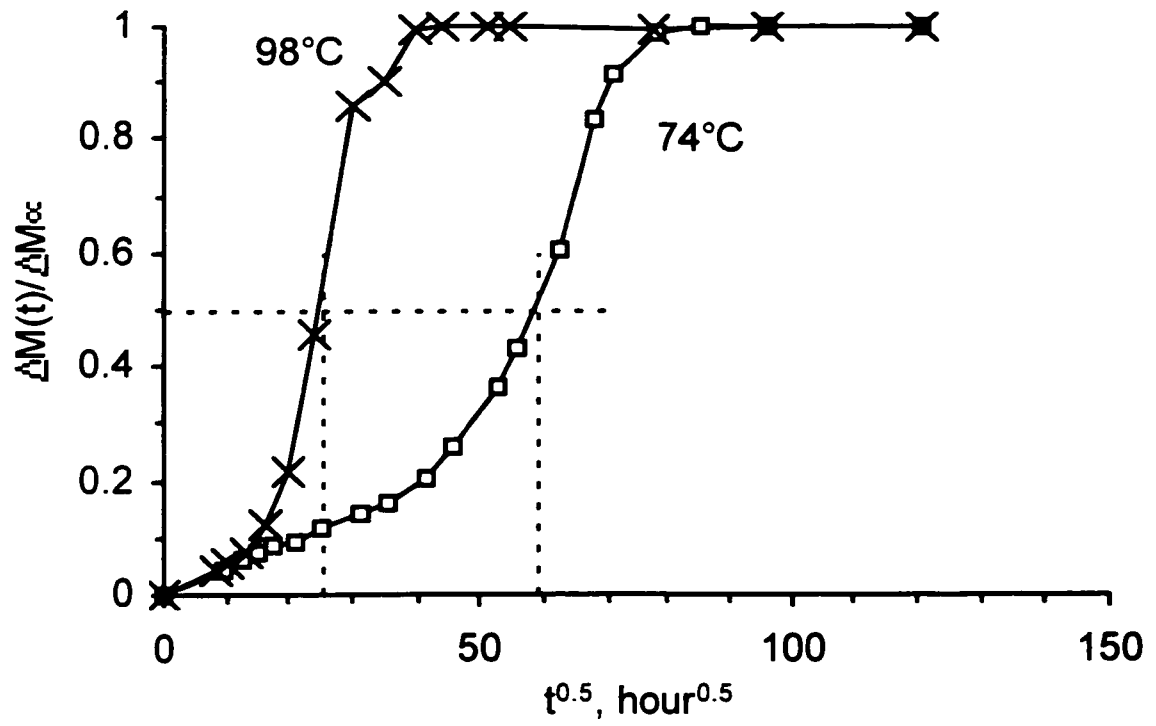


Figure 2.14 Dependence of $\Delta M(t)/\Delta M_{\infty}$ on $t^{0.5}$ in PVC immersed in a saline solution (1 mS/cm) at 98 and 74°C (Equation 4).

2.4 Conclusions

1. The surface resistance of PVC specimens decreased rapidly with increasing time of exposure to salt-fog without ac electrical stress until saturation is reached. This is attributed to the loss of hydrophobicity of the surface which is followed by a presence of water layer on the surface.
2. The saturated value of the resistance is that of the film of water on the surface of the PVC.
3. After removal from the salt-fog, the surface resistance of PVC increased with increasing recovery time in air. The contact angle also increased with time during recovery in air and it correlated well with the recovery of the surface resistance particularly during the early recovery time.
4. The surface resistance of PVC rods exposed to salt-fog depends on the length of the specimen. It increased with increasing length but not linearly.
5. A high magnitude of the dc stress (60 V/cm) used to measure the surface resistance has an influence on the measured values. This is due to a partial drying of the surface of the PVC. Low values of the dc stress (20-40 V/cm) have no influence on the measured values of the surface resistance.

6. A combination of salt-fog with ac stress accelerates the aging of the PVC surface.
7. The loss of hydrophobicity on the surface of the PVC during exposure to salt-fog is due to the increased surface tension. The contact angle of the PVC surface eventually recovered to its original value of 81.5° after drying in air subsequent exposure to wither salt-fog for 96h or after immersion in a saline water (1 mS/cm) for 96h. Different times were required for the complete recovery of the contact angle.
8. The Harmonic-Mean method was used to calculate the surface tension of PVC in virgin specimens and during exposure to salt-fog. At 23°C , the calculated values of a virgin PVC specimen are: $\gamma_s=43.1\times 10^{-3} \text{ J/m}^2$, $\gamma_{SD} = 34.4\times 10^{-3} \text{ J/m}^2$ and $\gamma_{SH} = 8.7\times 10^{-3} \text{ J/m}^2$. γ_s increased with increasing time of exposure to salt-fog to $50.1\times 10^{-3} \text{ J/m}^2$ after 1 h and to $76.8\times 10^{-3} \text{ J/m}^2$ after 24 h.
9. The percentage weight increase of PVC due to absorption of water depends on temperature. At higher temperatures, it took shorter time to reach saturation and the saturated value was higher than that at lower temperatures.
10. The diffusion coefficients of saline solution (1 mS/cm) into PVC are 1.6×10^{-14} at 98°C and $2.8\times 10^{-15} \text{ m}^2/\text{s}$ at 74°C .

Chapter 3

A Study on Epoxy Resin

3.1 Introduction

Contracted by a major epoxy resin manufacturer, a comparison experiment was conducted on three epoxy resin systems. The purpose of this comparison is to find which system has the best properties. Table 3.1 shows the identification of the specimens.

Table 3.1: Identification of the CIBA specimens

Factory Numbering	Lab Numbering
CY184 No. 1	#1
CY184 No. 2	#2
LMB5622 No. 1	#3
LMB5622 No. 2	#4
LMB5623 No. 1	#5
LMB5623 No. 2	#6

Table 3.2: Dimensions of the CIBA specimen

	#1	#2	#3	#4	#5	#6
Diameter, mm	30.44	30.40	29.90	30.30	29.89	30.05
Length, mm	118.69	118.53	118.87	119.29	117.16	118.02

The specimens were fabricated in the form of cylindrical rods. Data in Table 3.2 were measured with a digital caliper, type Mitutoyo CD-S6”P (Japan).

3.2 Experimental Conditions and Procedures

3.2.1 Electrodes Preparation

Two graphite electrodes were attached to both ends of the epoxy specimens with a thin layer (about 0.1 mm) of silicone rubber glue. The diameter of the circular electrodes was 38.14 mm and its thickness 3.22 mm.

3.2.2 Description of the Test Cycle

Specimens were aged in a fog chamber simultaneously with salt-fog and ac stress for 24 hours after which they were taken out and left in air at room temperature (23 ± 2 °C) for additional 24 h for the hydrophobicity to recover. One test cycle is defined

as 24 h of aging and the following 24 h of rest. Specimens were aged for six consecutive cycles.

3.2.3 Summary of Test Conditions

Test cycle: 24 h of aging in salt-fog followed by 24 h of rest in air

Number of test cycles: 6

During aging: both salt-fog and ac stress were applied

Conductivity of the water to generate the salt-fog: 0.5 ± 0.02 mS/cm

Pressure of the compressed air supplying the fog nozzles: 0.65 ± 0.02 MPa

Water flow rate: 1.6 ± 0.2 l/min

Nozzles: Four IEEE-IEC type were used. Two were placed on each of opposite walls.

Ac stress: 0.6 kVrms/cm, 60 Hz

Size of fog chamber: 2.54 m \times 2.54 m \times 2.54 m

Test supply: 208/14.4 kV, 37.5 kVA, 60 Hz

Composition of the salt-fog: table salt (NaCl) was added to the tap water. The latter had a conductivity of about 275 ± 25 μ S/cm.

3.2.4 Measurements of the Surface Roughness

Two quantities to separate the kinds of surface roughness, Sa and Srms, were measured after each test cycle. Sa is the arithmetic average of the absolute magnitude of the roughness profile. Srms is the root mean square value of the surface roughness. In each

specimen the measurements were conducted after the top, the center and the bottom areas of the vertically tested rod.

A Mitutoyo Surftest 212 (Japan) surface roughness tester was employed for the surface roughness measurement. The resolution of the instrument is 0.05 μm .

3.2.5 Measurements of the Contact Angle

The static contact angle (θ) was determined on a stable horizontal plane using a goniometer with a resolution of $\pm 0.5^\circ$. A sessile drop of distilled water (conductivity $\leq 5.5 \mu\text{S/cm}$) and having a volume of about 5 μl was applied to the surface. The contact angle was previously reported to be independent of the volume of the droplet up to 9 μl [1] and 17 μl as well as independent of its salinity in the range 2.5-105 $\mu\text{S/cm}$.

16 readings of the contact angle were taken for each condition and the average value is reported. For each set of 16 readings, the maximum relative error was checked and found to be less than $\pm 3\%$. If four data among the 16 readings had a relative error $> \pm 3\%$, the measurements of the contact angle were repeated.

3.2.6 Measurements of the Leakage Current

The leakage current given in this report is defined as the sum of the absolute values of all current impulses sampled during both the positive and the negative portions of the current wave, over a specified length of time (0.5 h), divided by the total number of the sampled

signals. The data acquisition system employed an eight-bit, 16-channel A/D converter having a sampling time of 16 μs . In order to have an increased sampling speed, only 6 channels were used.

Each sampling took about 104.1 μs . Thus 13 times of sampling can be obtained for each specimen within a half cycle of the ac (60 Hz) when using 6 specimens.

3.2.7 Analysis with Fourier Transform Infrared (FT-IR) Spectroscopy

A Nicolet 5DX Fourier Transform Infrared (FT-IR) spectrometer was applied to analyze the white powder deposited on the surface of the specimens after completion of the aging. Wave numbers in the range of 400-4000 cm^{-1} were used. A small amount of the powder scratched from the specimen was mixed with KBr and pressed to form a transparent circular disc for FTIR scanning.

3.3 Results and Discussions

Because of the unavailability of specific information on the composition of the specimens, these are referred to here in general term as epoxy resin. Discussions in this part are aimed to help understanding the results and to draw up appropriate conclusions.

3.3.1 Surface Roughness of Virgin Specimens

Figure 3.1 shows the surface roughness at the top area for virgin specimens #1 to #6 respectively. It is observed from Figure 3.10 that LMB5623 (#5 and #6) has the smallest S_a and S_{rms} while LMB5622 (#3 and #4) has the largest surface roughness at virgin status. The reason for the differences in the surface roughness of the virgin specimens of the three materials is related to the formulation and compositions which were not disclosed to the authors.

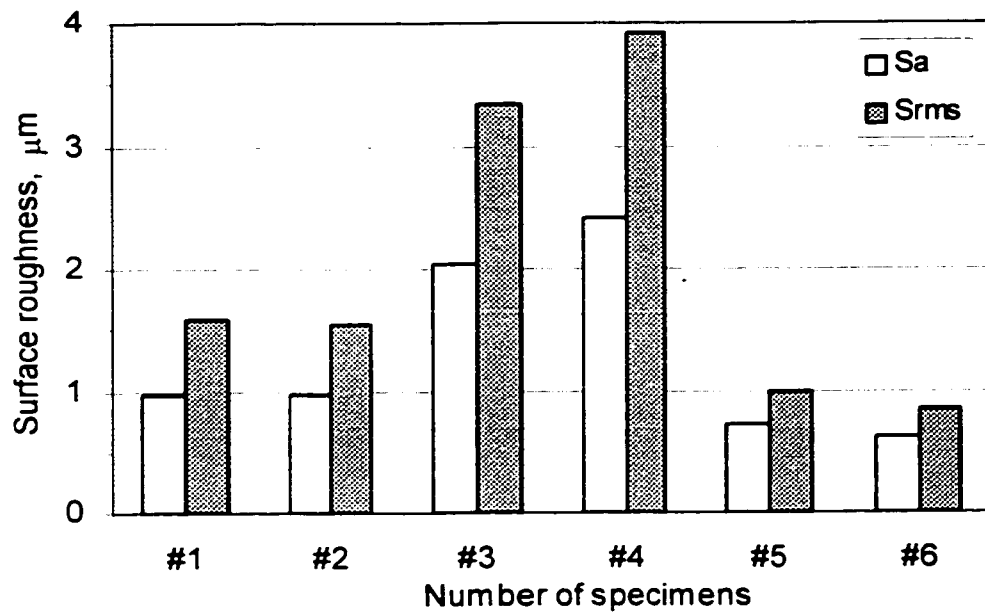


Figure 3.1 Surface roughness (S_a and S_{rms}) of the virgin (before aging) specimens for #1 to #6.

3.3.2 Surface Roughness as a Function of Number of Test Cycles

Figures 3.2 to 7 show the surface roughness of specimens #1 to #6 as a function of test cycles. Cycle 0 stands for the virgin status (i.e. before testing). In all figures, “top” means near the top high voltage electrode, and “bottom” near the bottom electrode (grounded via 56Ω) of the vertically tested rods. The measurements of the surface roughness were taken at the end of each cycle.

It is shown in Figures 3.2 to 7 that both S_a and S_{rms} generally increased with increasing test cycles except after cycle 2 in Figures 3.2, 6 and 7. The increase of S_a and S_{rms} with increasing test cycles is due to the effects of dry band discharges during aging in the energized salt-fog. The dry band arcing generates heat and gradually damages the surface. Even after the first cycle, an erosion of material in the area close to the top electrode was observed. The erosion was not uniformly distributed because the arcing on the surface is highly unstable. This led to an error in the surface roughness measurement because the value of S_a and S_{rms} which were measured at the eroded area were large while those measured at other locations had lower values of the surface roughness. The decrease in S_a and S_{rms} after cycle 2 (Figures 3.2, 6 and 7) is because these measurements were made in locations which were not eroded. It was observed during these tests that all the six epoxy specimens had the ability to maintain some areas on their surface which were free of erosion. These local uneroded areas were surrounded by eroded tracks. Within them, the surface roughness was very small and comparable to the values measured on virgin specimens.

Figures 3.8 to 10 show the average surface roughness of three materials as a function of the number of test cycles. A reference to Table 3.1 shows that Figures 3.8, 9 and 10 correspond to CY184, LMB5622 and LMB5623, respectively. A close examination of Figures 3.8 to 10 shows that LMB5623 (Figure 3.10) has the smallest surface roughness after 6 cycles of aging in the energized salt-fog. Figures 3.2 to 10 show that the surface roughness at the top area has the largest while at the bottom area has the smallest increase following the test.

Figure 3.11 shows the surface roughness at the top area for specimens #1 to #6 after one cycle of aging. A comparison with Figure 3.1 shows that specimens #5 and #6 incurred the largest increase of surface roughness. S_a for the specimen #5 increased from 0.72 to 3.89 μm (a ratio of 5.4). S_a for the specimen #6 increased from 0.62 to 4.14 μm (a ratio of 6.7). The corresponding ratios for #1 to #4 were 4.0, 2.6, 2.5, 2.8, respectively. This large increase on the surface roughness for specimens #5 and #6 indicates that the epoxy resin with the symbol of LMB5623 lost its surface smoothness at the early aging period.

Figure 3.12 shows the surface roughness (S_a and S_{rms}) at the top area for specimens #1 to #6 after 6 cycles of aging. Figure 3.12 shows that after a lengthy exposure to dry band arcing in salt-fog all specimens incurred an increase in the surface roughness. However, the S_a in specimens #5 and #6 appears to have increased somewhat less to $11.1 \pm 1.2 \mu\text{m}$ compared to $16.1 \pm 1.5 \mu\text{m}$ for specimens #1 to #4.

Conclusion by studying the change of surface roughness:

Figure 3.12 shows that the surface roughness of LMB5623 is marginally lower than that of LMB5622 and CY184 after testing for 6 cycles. The materials identified as LMB5622 and CY184 had similar values of surface roughness.

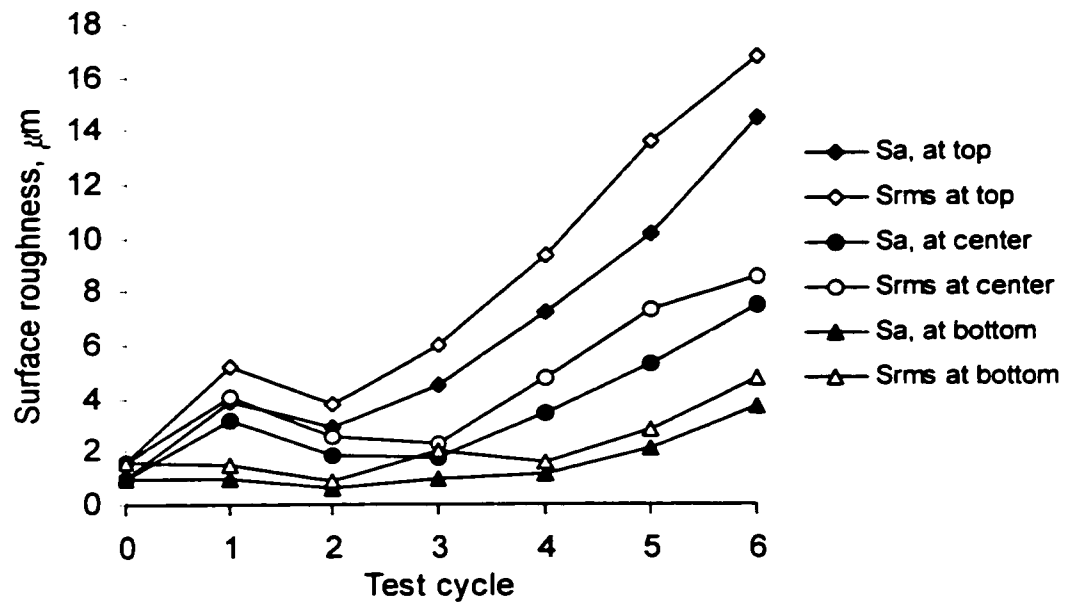


Figure 3.2 Average (S_a) and RMS (S_{rms}) surface roughness of specimen #1 as a function of the number of test cycles. Each cycle of the salt-fog is 24 h on followed with 24 h off. The measurements of surface roughness were taken at the end of the cycle.

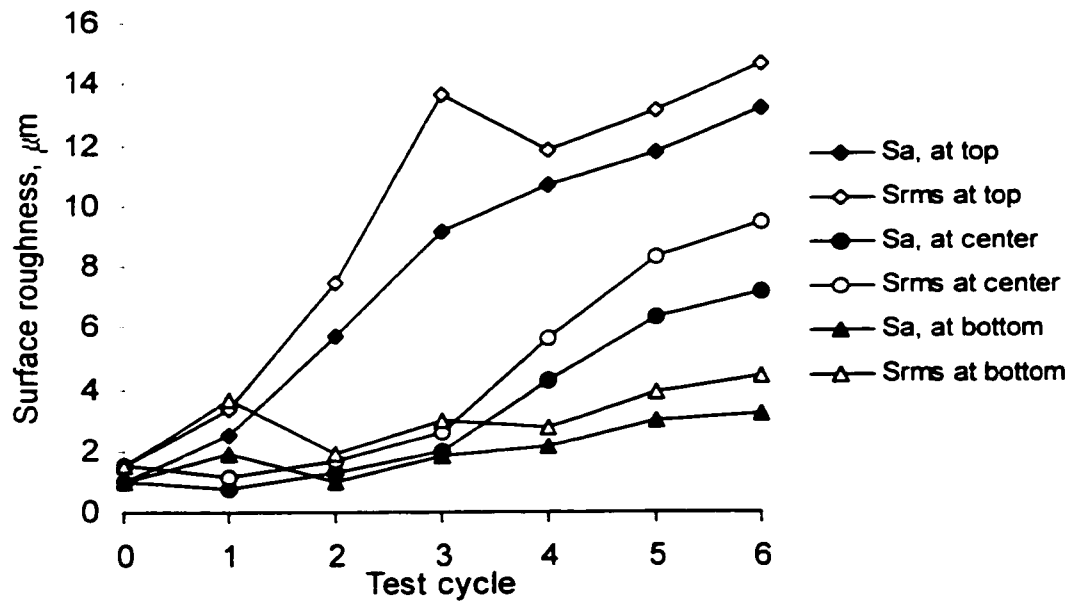


Figure 3.3 Surface roughness of specimen #2 as a function of the number of test cycles.

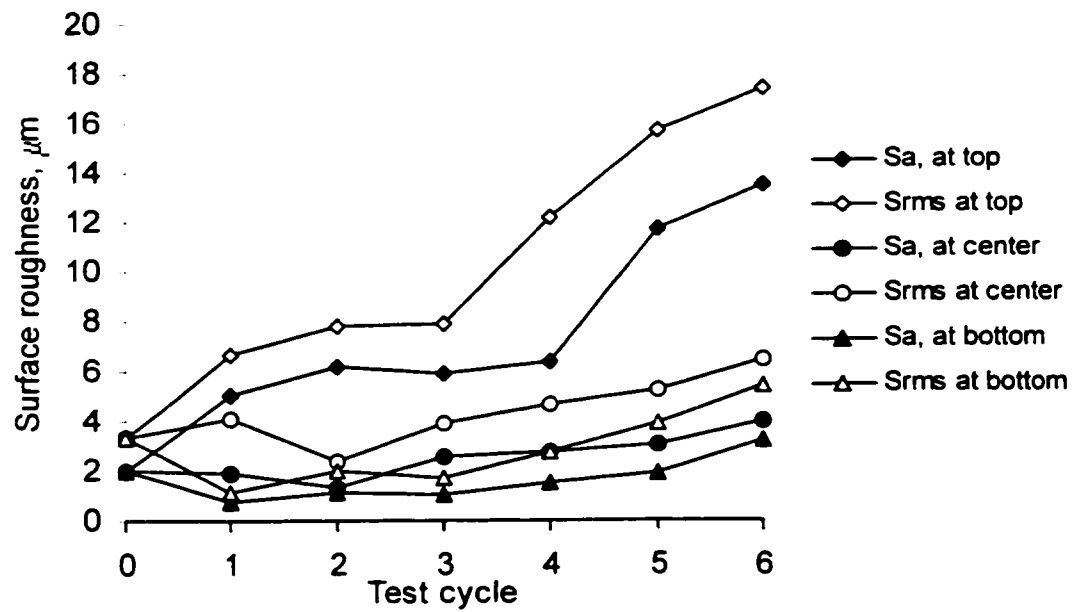


Figure 3.4 Surface roughness of specimen #3 as a function of the number of test cycles.

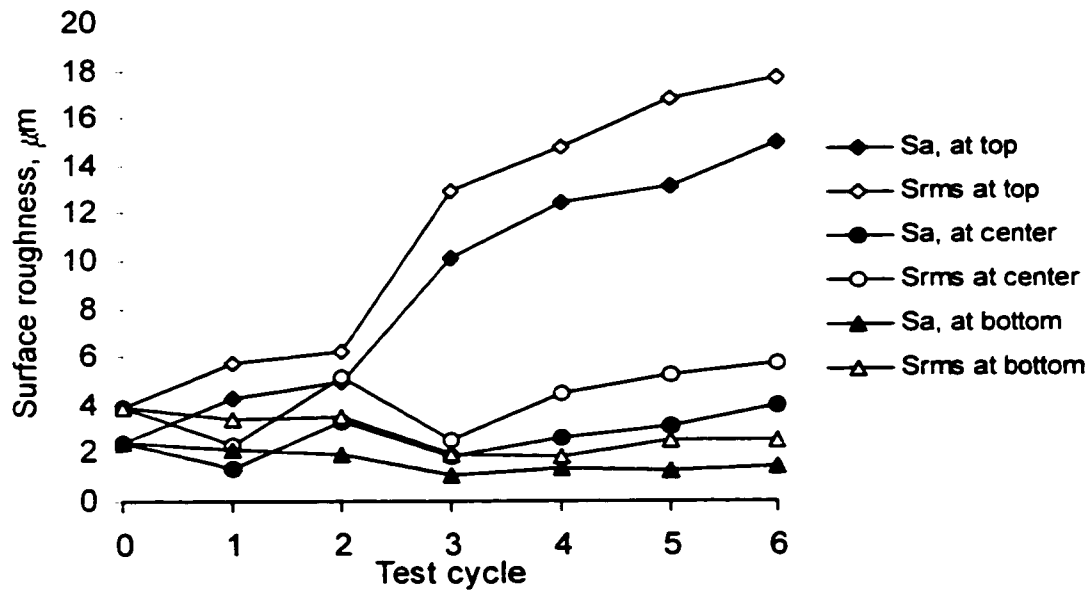


Figure 3.5 Surface roughness of specimen #4 as a function of the number of test cycles.

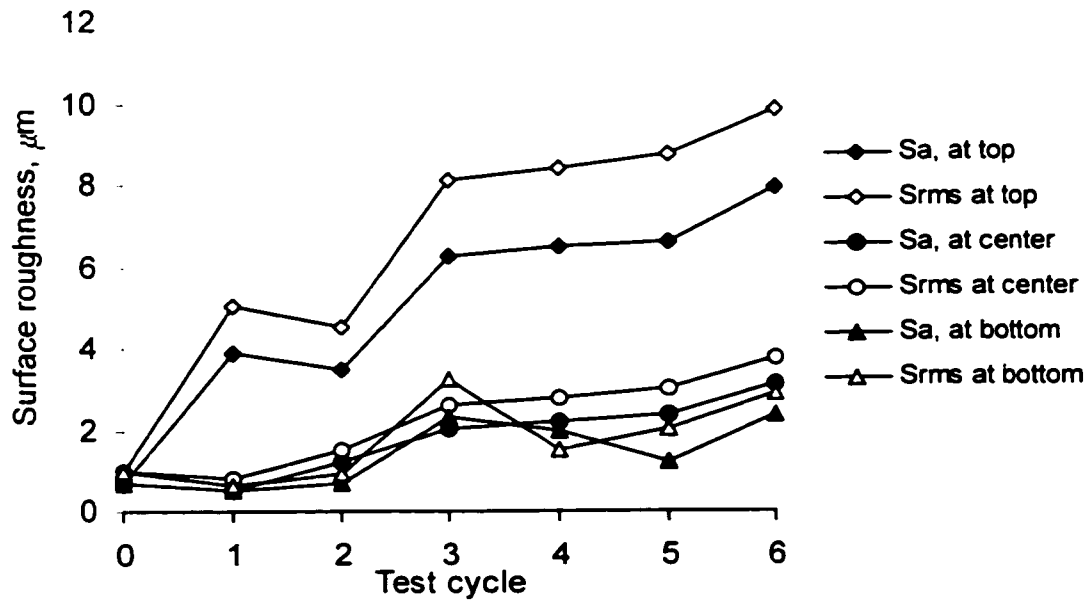


Figure 3.6 Surface roughness of specimen #5 as a function of the number of test cycles.

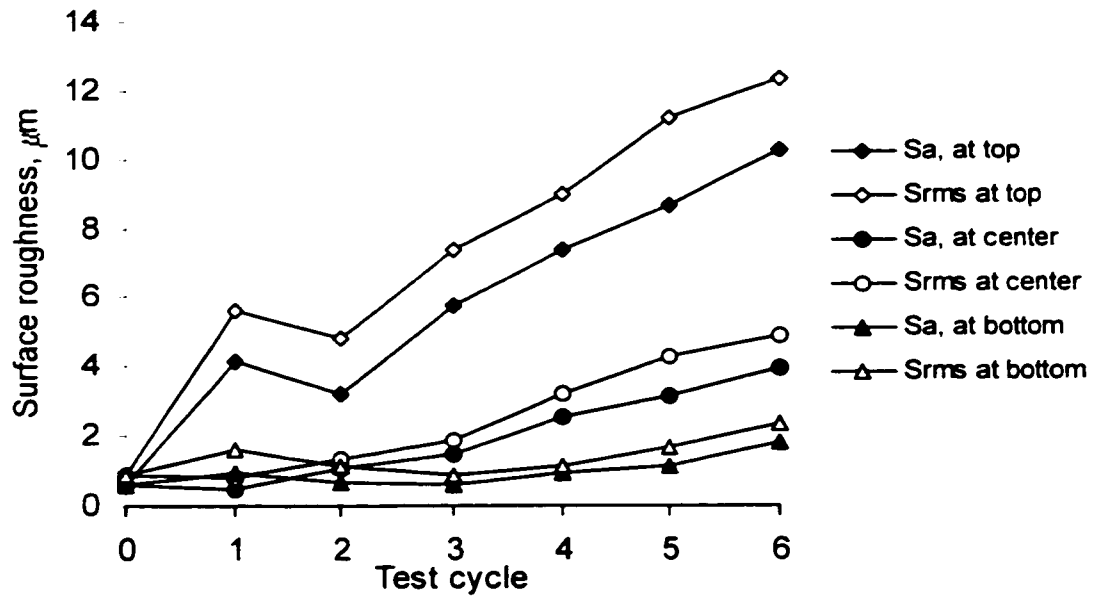


Figure 3.7 Surface roughness of specimen #6 as a function of the number of test cycles.

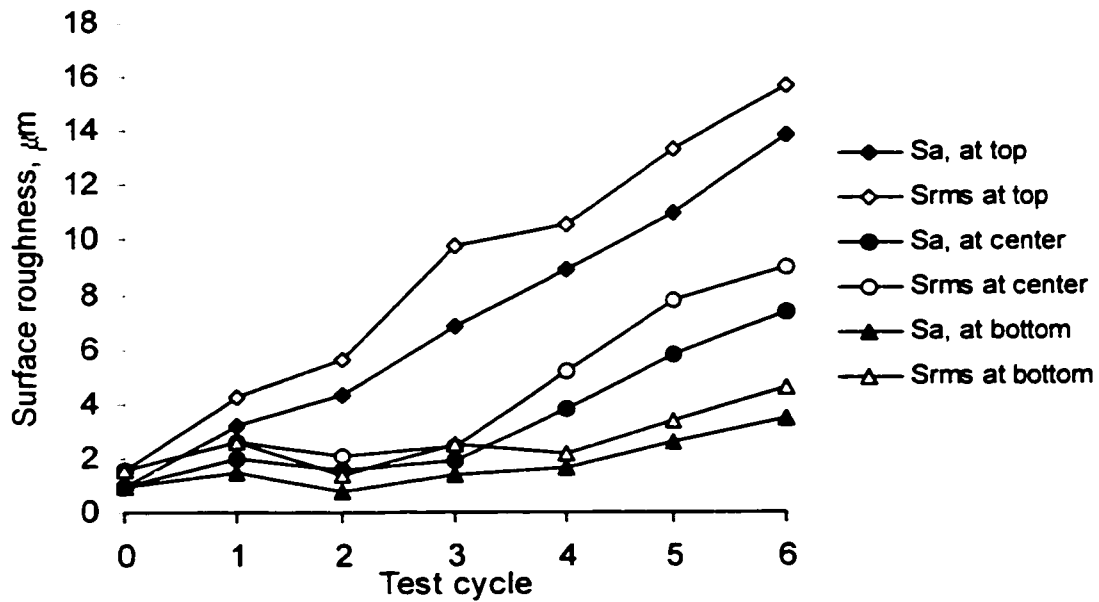


Figure 3.8 Averaged surface roughness of specimens #1 and #2 (CY184) as a function of test cycles.

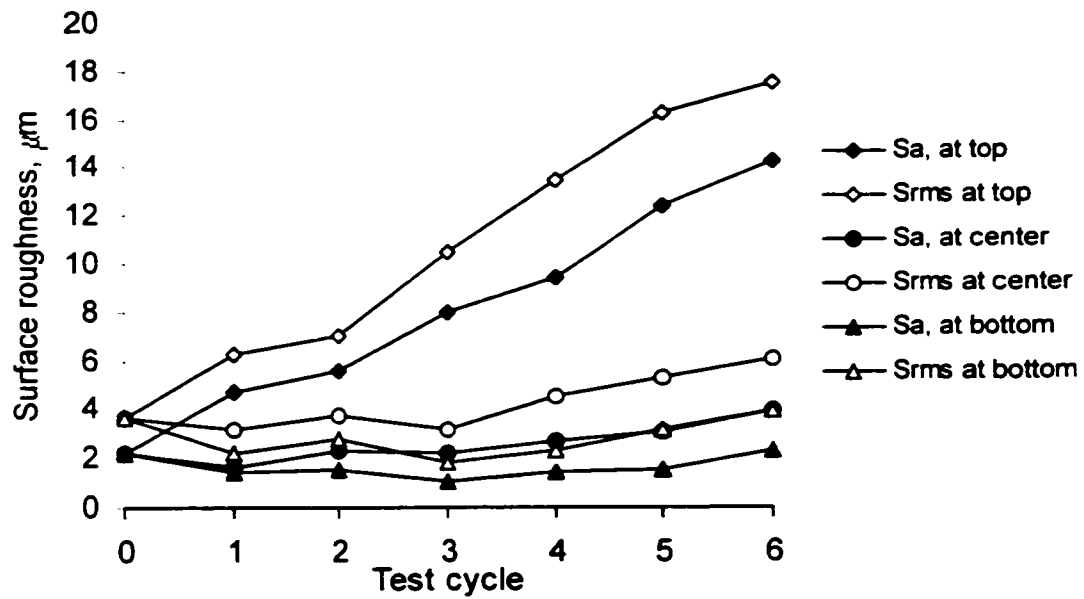


Figure 3.9 Averaged surface roughness of specimens #3 and #4 (LMB5622) as a function of the number of test cycles.

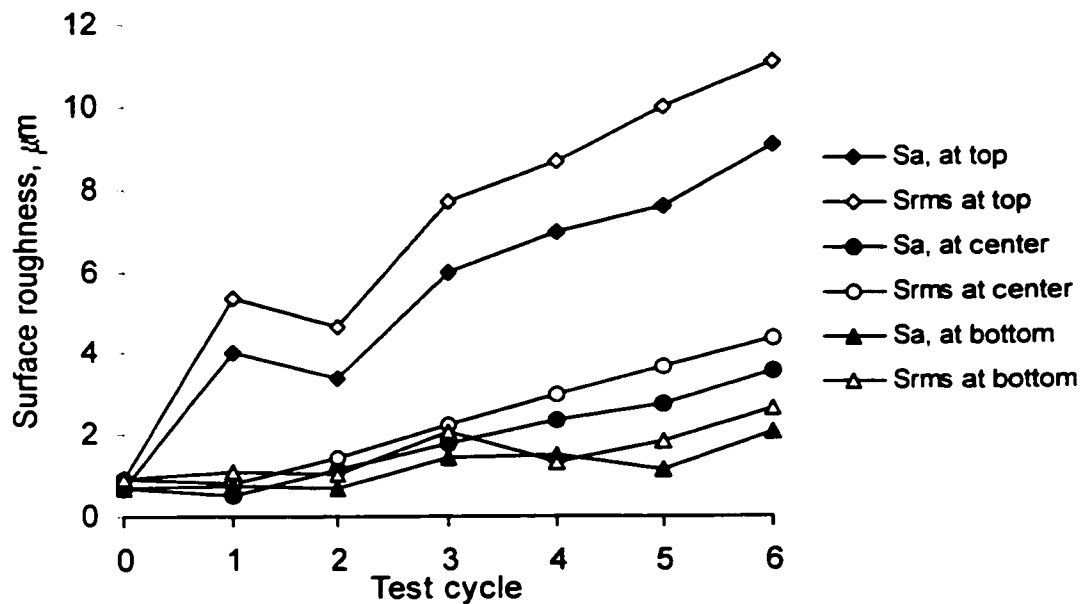


Figure 3.10 Averaged surface roughness of specimens #5 and #6 (LMB5623) as a function of the number of test cycles.

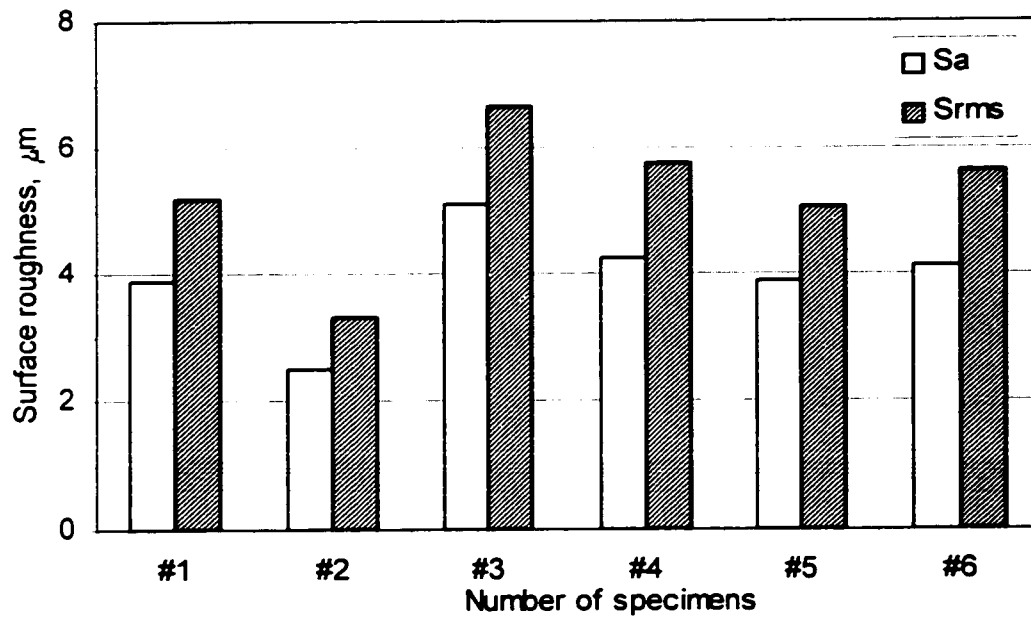


Figure 3.11 Surface roughness (S_a and S_{rms}) at the top area for specimens #1 to #6 after one cycle of aging.

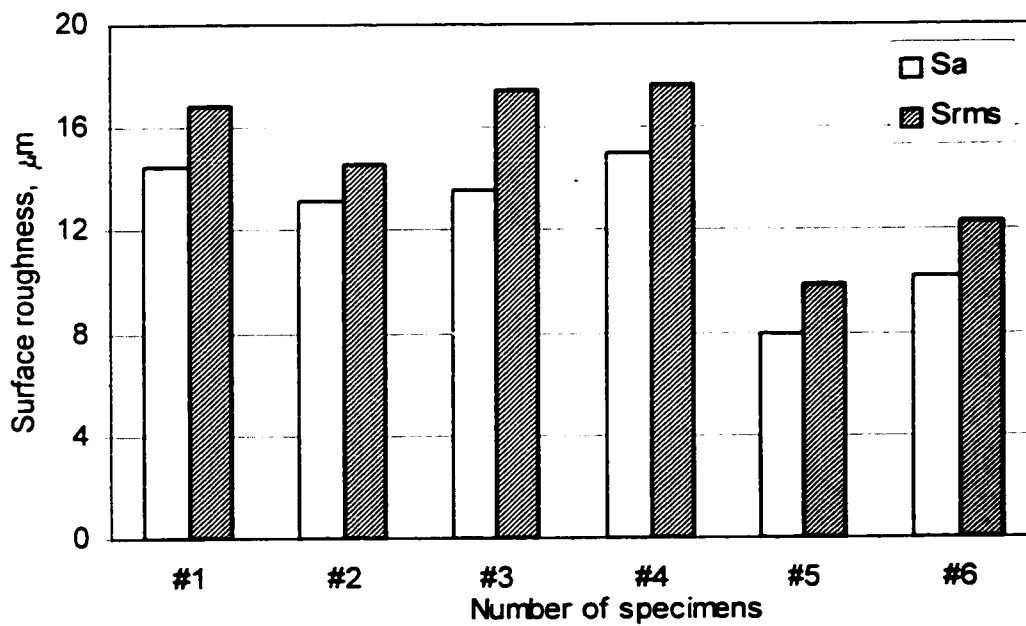


Figure 3.12 Surface roughness (S_a and S_{rms}) at the top area for specimens #1 to #6 after 6 cycles of aging.

3.3.3 Contact angle of Virgin Specimens

Figure 3.13 shows the contact angle measured at the top area for specimens #1 to #6 at the virgin status. It can be seen from Figure 3.13 that the contact angle for all specimens are similar at $97.8 \pm 3.8^\circ$. Therefore before the onset of the aging test all specimens were hydrophobic and did not permit the water to form a continuous film on the surface.

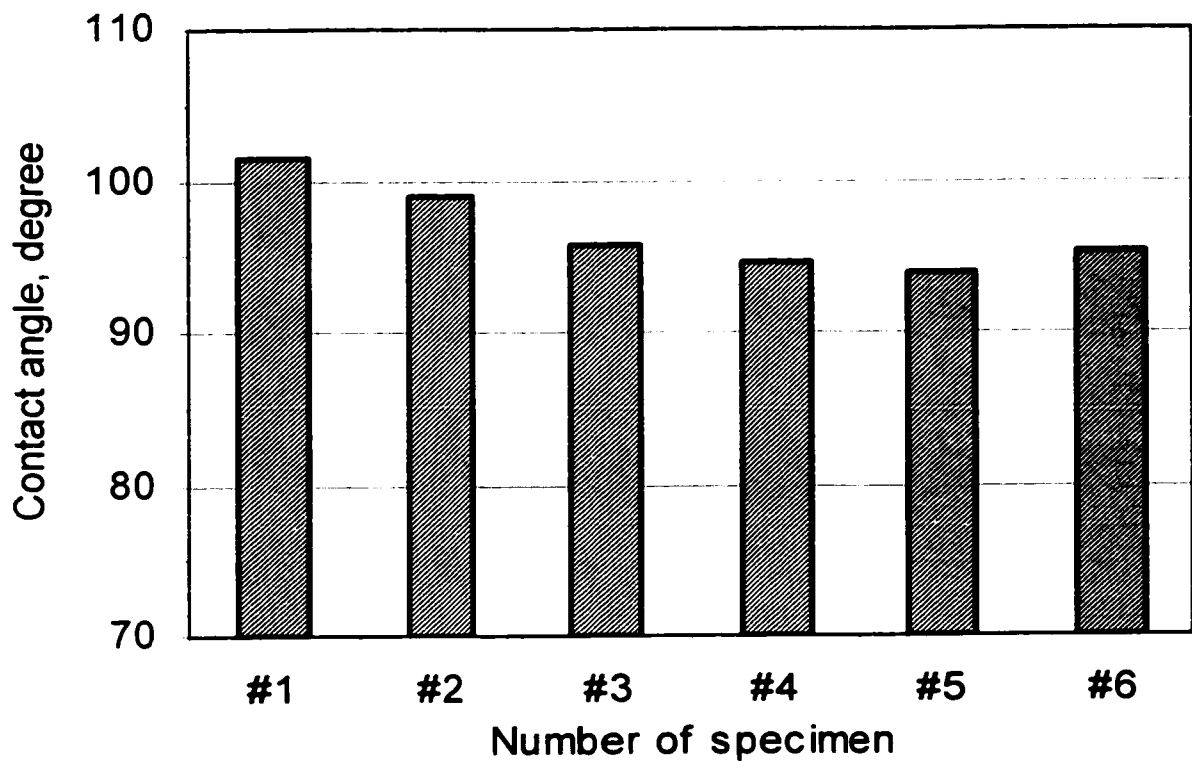


Figure 3.13 Contact angle measured at top area for virgin specimens #1 to #6 (before aging).

3.3.4 Contact Angle as a Function of Number of Test Cycle

Figures 3.14 to 19 show the contact angle as a function of test cycles for specimens #1 to #6, respectively. Each cycle consisted of 24 h of aging followed by a rest of 24 h in air at $23\pm 2^{\circ}\text{C}$. The contact angle was measured at the end of the aging and the rest periods. Figure 3.12 shows that contact angle decreased after the first cycle of aging and then partially recovered during the rest period of 24 h. The contact angle continued to decrease after each aging and to partially recover after each rest of 24 h. The partial recovery of the contact angle is attributed to the drying of the surface of the specimens. When the specimens were taken out of the fog chamber it was observed that some areas were clearly wet while others were still hydrophobic. The wet areas became covered with a layer of white powder after the surface dried. The contact angle for these areas, no matter whether they were in the wet or dried state, was almost zero. Therefore the reported contact angle in Figures 3.14 to 19 is not in these hydrophilic areas.

Figures 3.20 to 22 show the contact angle after end of aging period and as a function of test cycles for CY184, LMB5622 and LMB5623, respectively. Data reported in these three figures were averaged from Figures 3.14 to 19. It is shown that in Figures 3.20 to 22 that the contact angle at the end of the series of test and at the top of the rod for CY184 has decreased (to 12°) more than LMB5622 (29°) and 5623 (26.4°). For the later two specimens, the contact angle measured at the center and the bottom areas did not change much during the test period. This is because the dry band arcing activity was largely confined to area near the high voltage electrode. In Figure 3.20, the contact angle

on the bottom of CY184 specimens changed from 99.4° (on the virgin specimens) to 35.5° (at the end of cycle 6). In Figures 3.21 and 22, the contact angle measured on the bottom of LMB5622 changed from 94.3 to 90° and for LMB5623 from 96.6 to 75.5° . This is because the bottom area of the specimens had less surface discharge activities than areas close to the upper electrode. The larger decrease of the contact angle on the bottom area of CY184 indicates that the surface hydrophobicity there was lost more easily than for LMB5623 and LMB5622.

Figures 3.23 and 24 show the contact angle measured at the top area for specimens #1 to #6 during cycle 1 and cycle 6. A comparison with Figure 3.13 suggests that all the specimens lost hydrophobicity after aging. After six cycles of aging in the energized salt-fog, #1 and #2 (CY184) had the largest decrease in the contact angle. It is also found that #3 and #4 (LMB5622) had the smallest change on the contact angle from one cycle of aging to six cycles of aging.

Conclusion by studying the change of contact angle:

After 6 cycles of aging in salt-fog, the contact angles of LMB5622 ($9.4 \pm 1.8^\circ$) and LMB5623 ($13.9 \pm 0.3^\circ$) are higher than CY184 ($2.8 \pm 0.7^\circ$). After recovery of 24 h in the 6th cycle the corresponding contact angles were 28.9 ± 0.5 , and 26.1 ± 0.2 and $11.4 \pm 1.1^\circ$ (Figure 3.24).

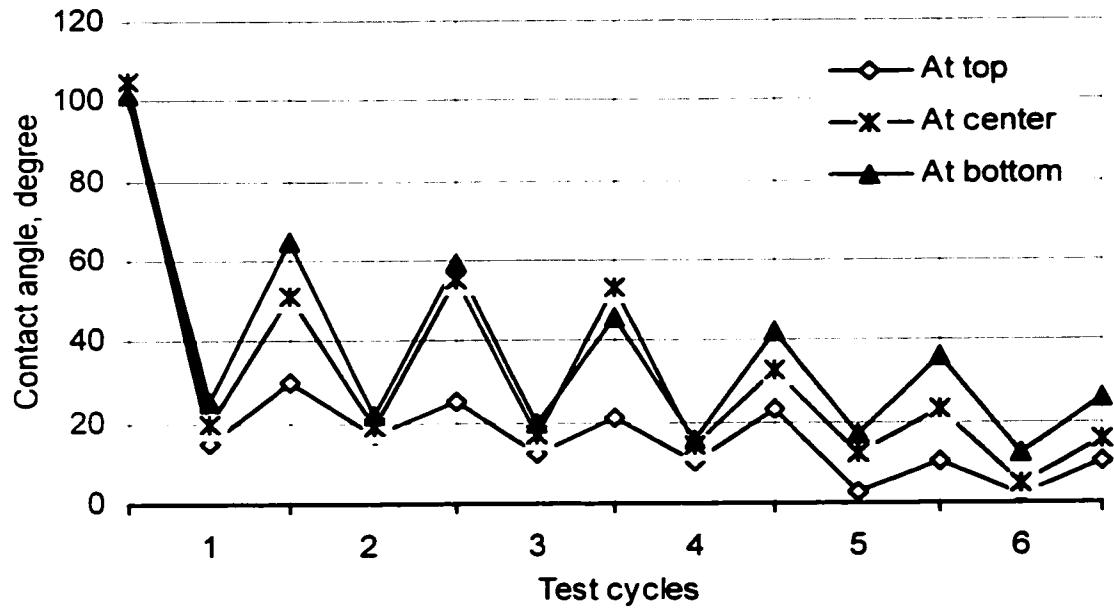


Figure 3.14 Contact angle of #1 specimen as a function of number of test cycle.

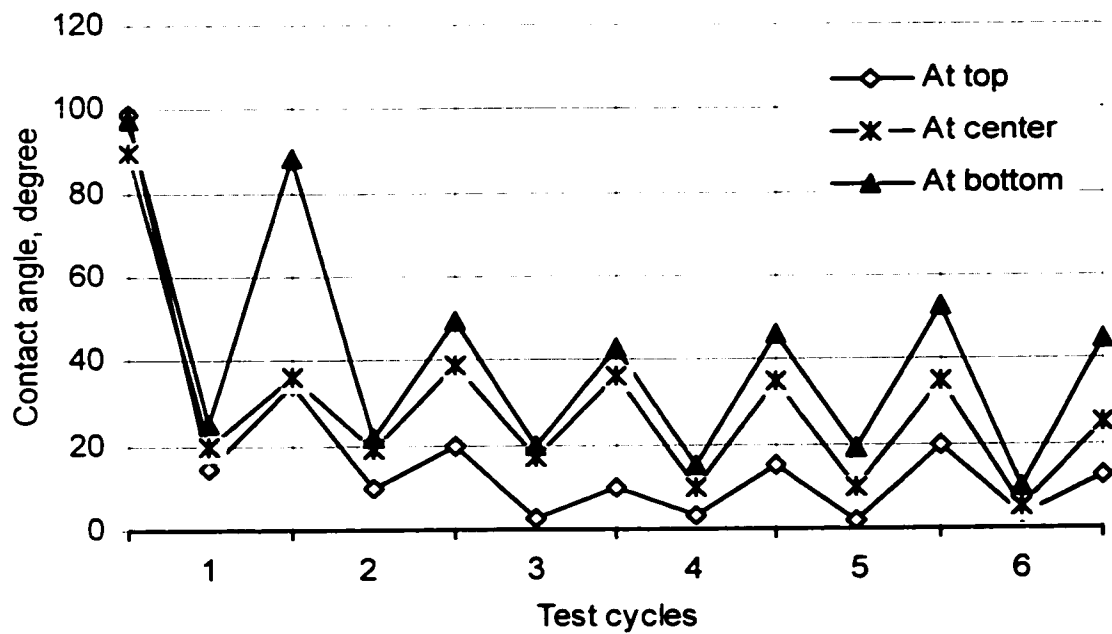


Figure 3.15 Contact angle of #2 specimen as a function of number of test cycle.

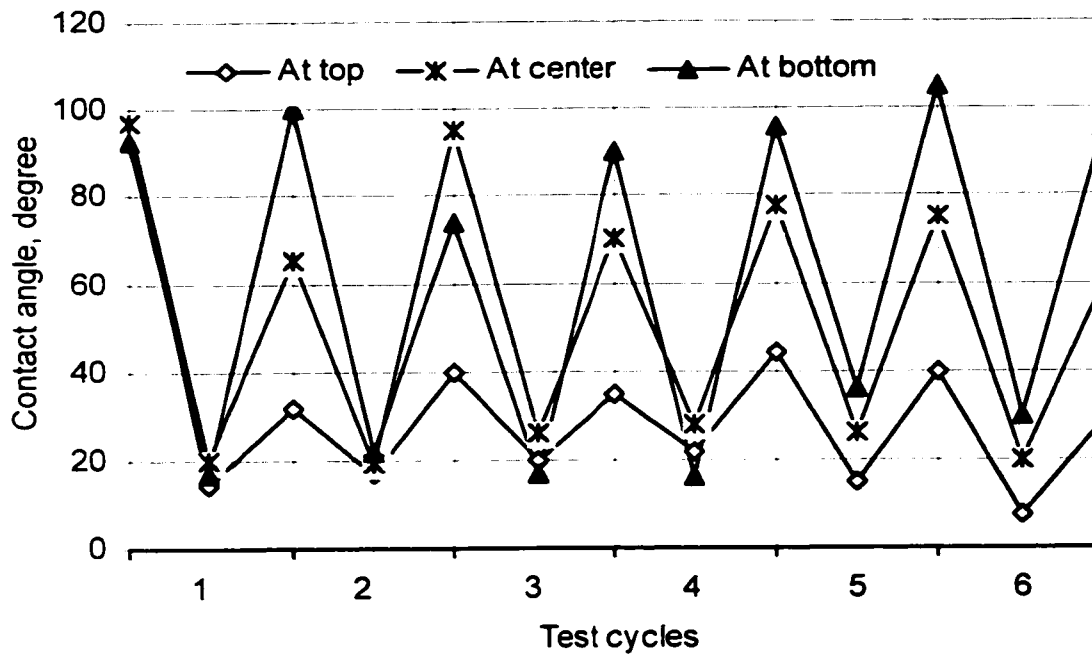


Figure 3.16 Contact angle of #3 specimen as a function of number of test cycle.

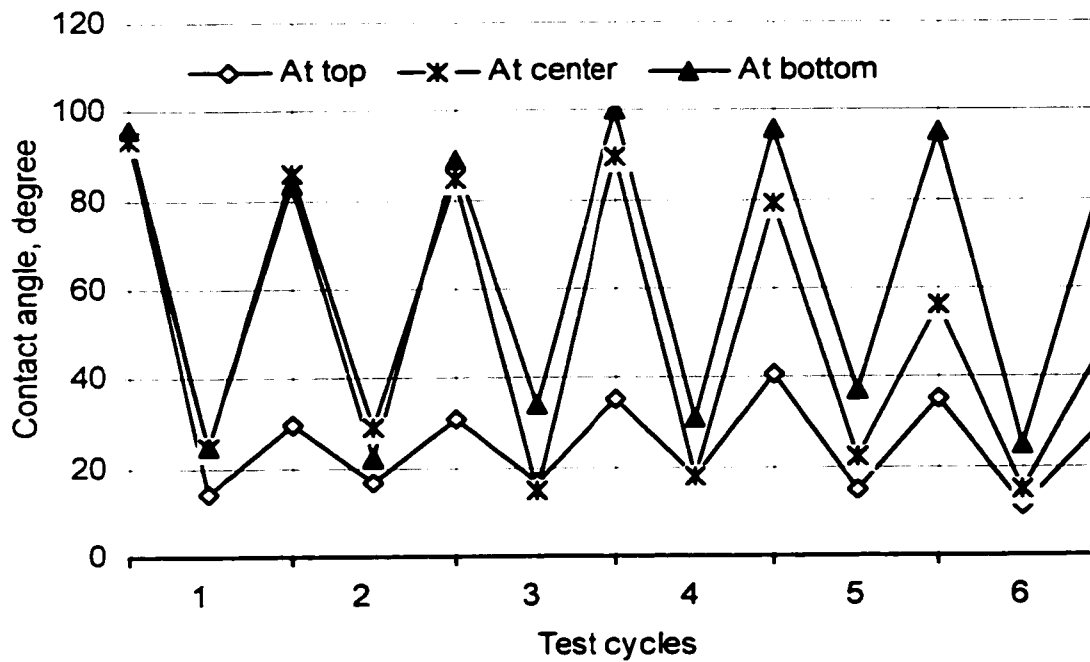


Figure 3.17 Contact angle of #4 specimen as a function of number of test cycle.

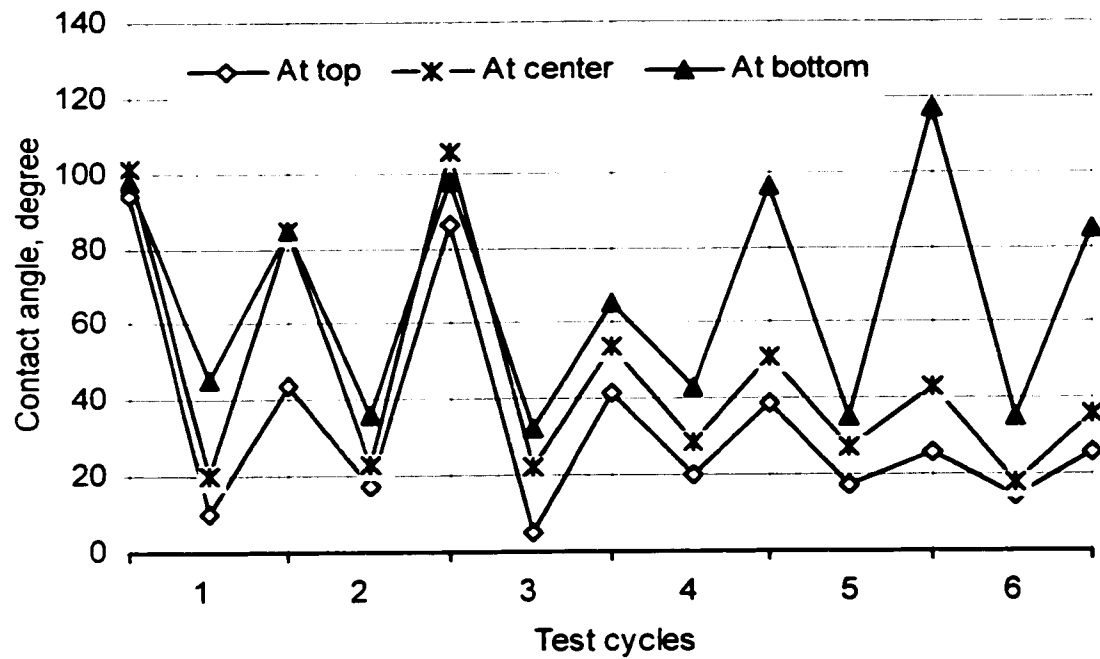


Figure 3.18 Contact angle of #5 specimen as a function of number of test cycle.

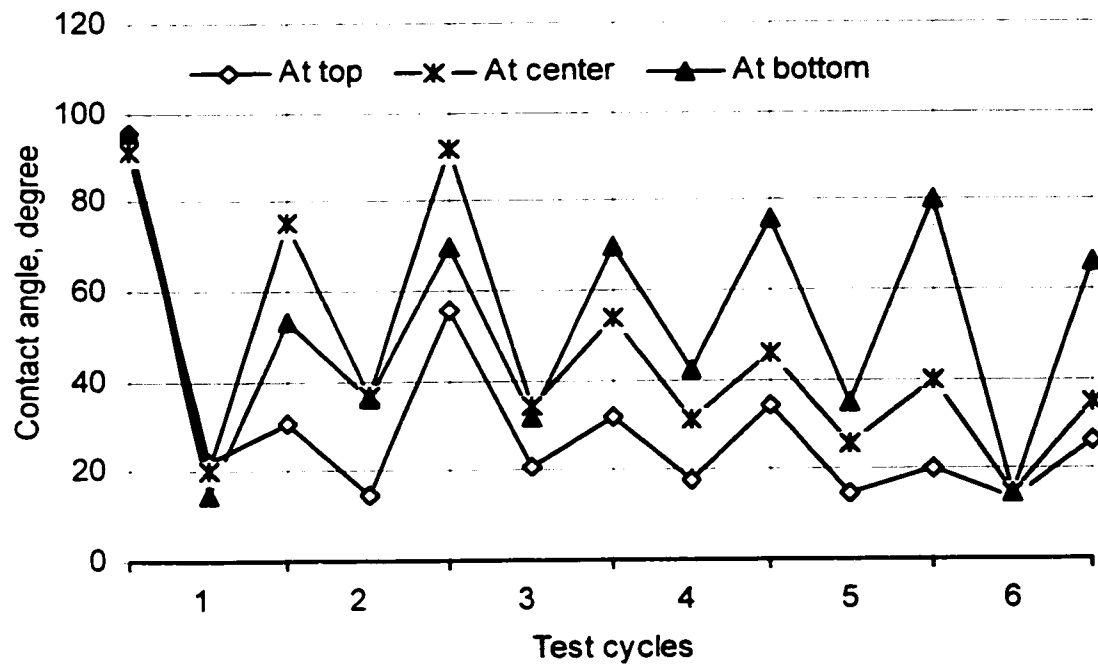


Figure 3.19 Contact angle of #6 specimen as a function of number of test cycle.

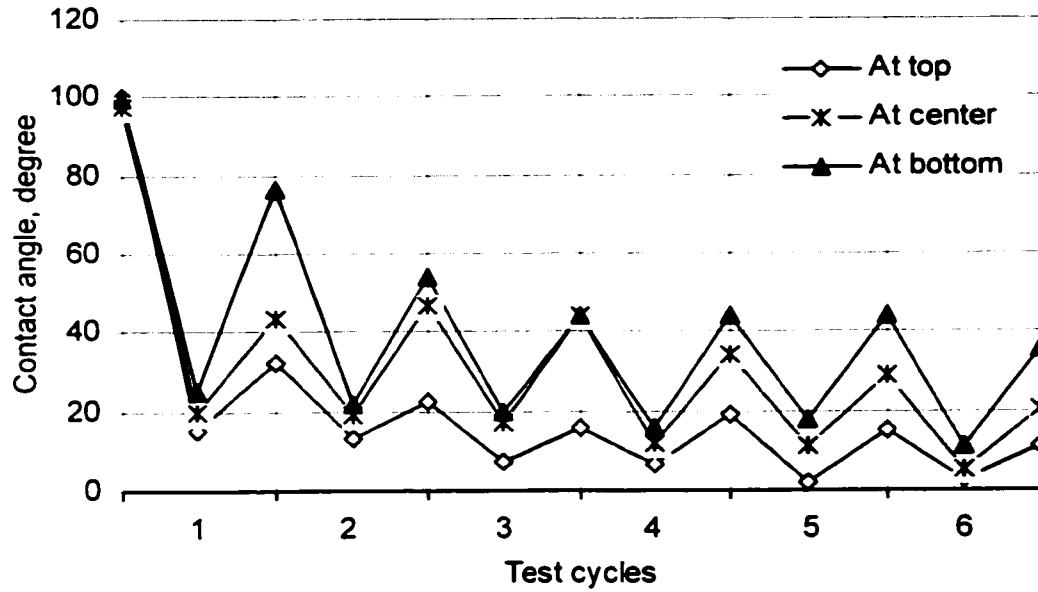


Figure 3.20 Averaged contact angle of CY184 (#1 and #2) as a function of number of test cycle. θ was measured at the end of the aging period.

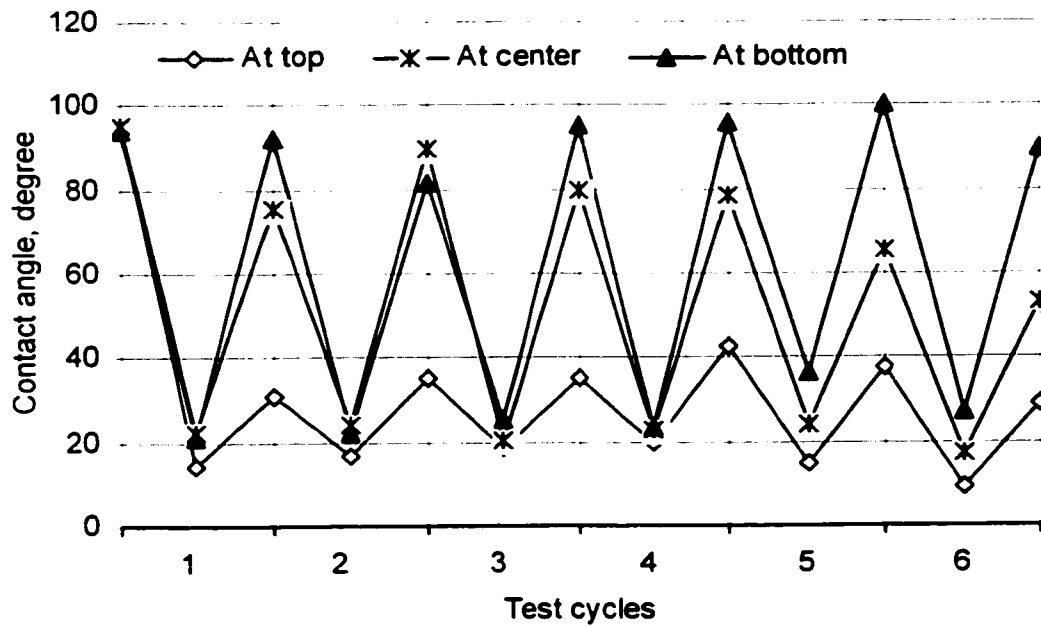


Figure 3.21 Averaged contact angle of LMB5622 (#3 and #4) as a function of number of test cycle. θ was measured at the end of the aging period.

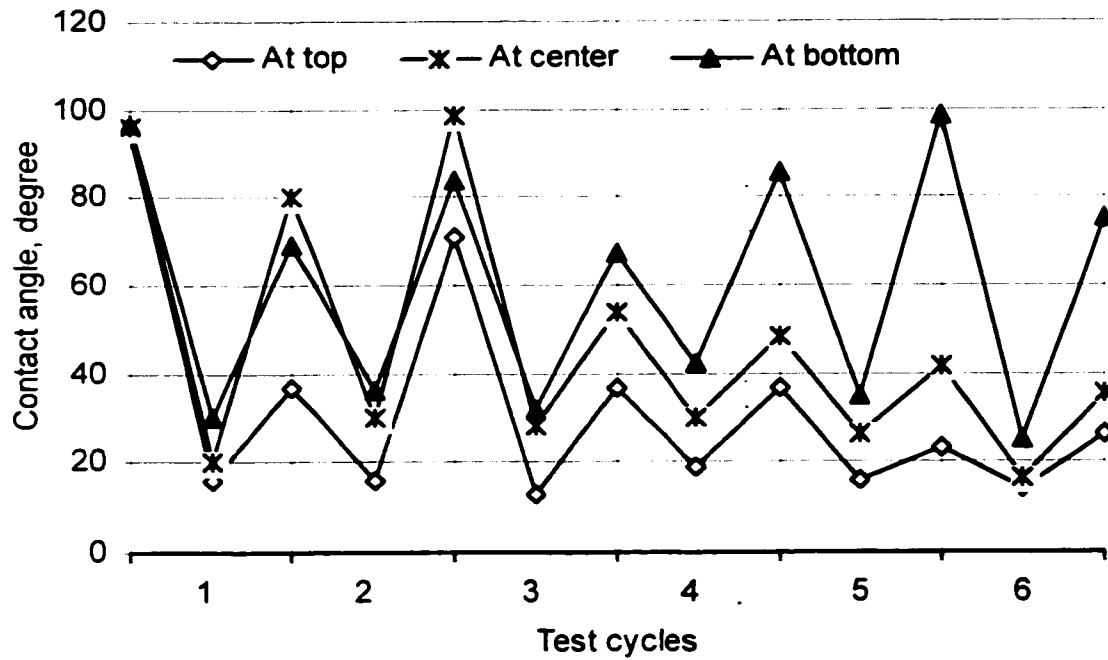


Figure 3.22 Averaged contact angle of LMB5623 (#5 and #6) as a function of number of test cycle. θ was measured at the end of the aging period.

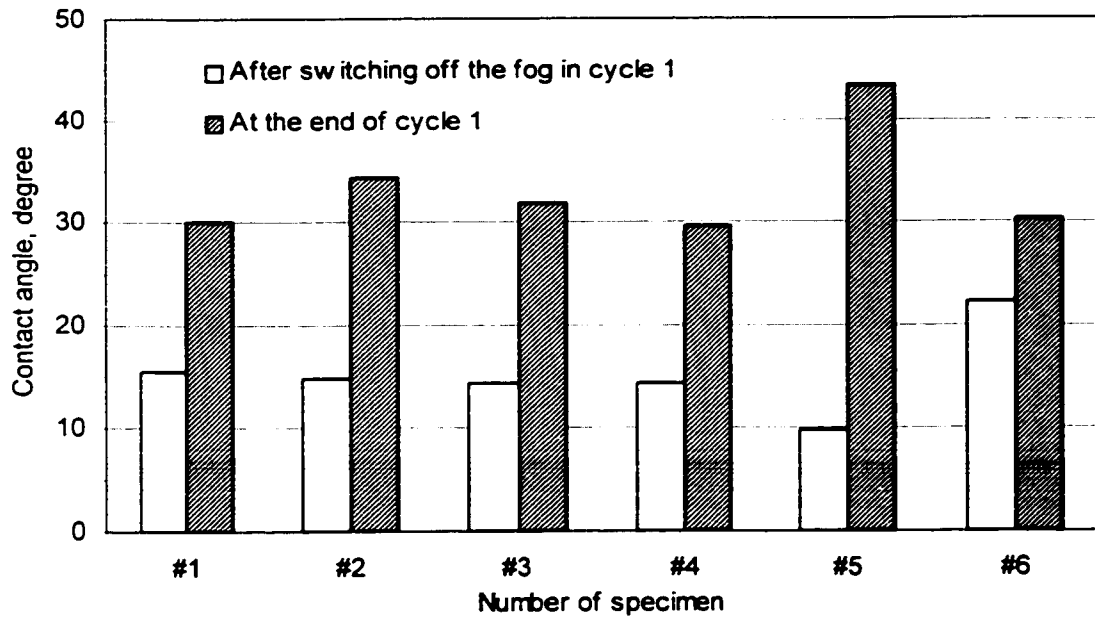


Figure 3.23 Contact angle measured at the top area for specimens #1 to #6 after 24 h of aging and 24 h of recovery in cycle 1.

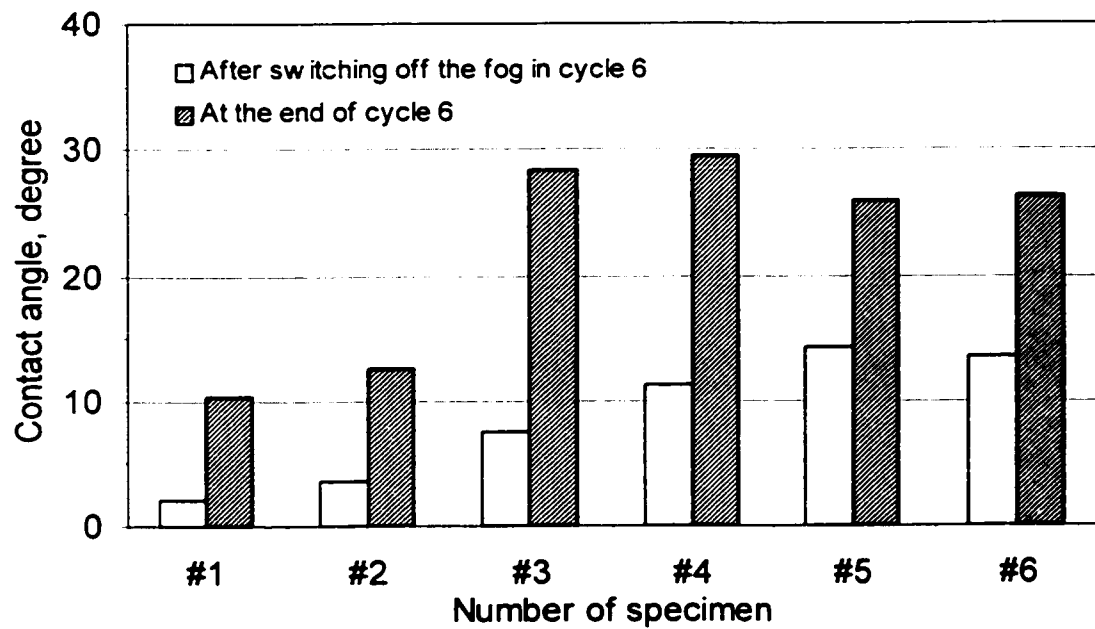


Figure 3.24 Contact angle measured at top area for specimens #1 to #6 during the 6th cycle of aging.

3.3.5 Leakage Current as a Function of Test Time

Figures 3.25 to 30 show that the leakage current for CY184, LMB5622 and LMB5623 during exposure to the energized salt-fog in cycle 1 to 6, respectively.

Figures 3.31 and 32 show the averaged leakage current for the last four hours of aging during cycle 1 and cycle 6 respectively for CY184, LMB5622 and 5623. In Figure 3.31, during the first cycle of aging the averaged leakage current is 8.3, 7.8, 8.3 mA for CY184, LMB5622 and 5623, respectively. During the 6th cycle (Figure 3.32), the corresponding values are 13.9, 13.1 and 13.4 mA. It is observed in both Figure 3.31 and 32 that the currents are essentially have the same magnitude of 8.1 ± 0.2 mA (Figure 3.31) and 13.5 ± 0.4 mA (Figure 3.32).

Figures 3.33 and 34 show the pulse rate of leakage current in the range of 14-20 mA as a function of test time in cycle 1 and 6, respectively. It will be observed that after extensive test in energized salt-fog (Figure 3.34) the pulse rate increased steadily with time of test during the 6th cycle for specimens 3 to 6 while the variations in specimens #1 and #2 were small. However, specimens #1 and #2 showed a much larger pulse rate right from the beginning of the test (Figure 3.34). This is because of their much lower contact angle which indicated a faster loss of hydrophobicity of this material (Figures 3.20 to 24).

Figure 3.35 shows the pulse rate of leakage current in the range of 20-24 mA as a function of test time in cycle 1 and 6, respectively. Figure 3.35 indicates that the amplitude of the current pulse was increasing with increasing cycle of testing (from cycle 1 to 6).

Conclusion by measuring the leakage current:

The currents in all specimens are of the same order of magnitude. During the last four hours of aging in cycle 6 the currents were within $\pm 3\%$ of each other 13.5 ± 0.4 mA (Figure 3.32).

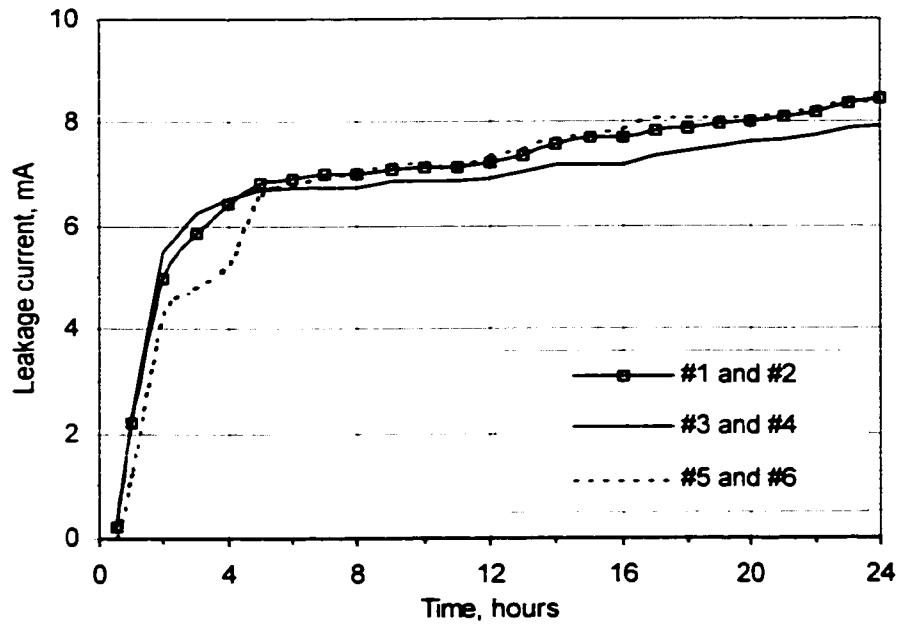


Figure 3.25 Averaged leakage current of the three specimens as a function of test time during cycle 1.

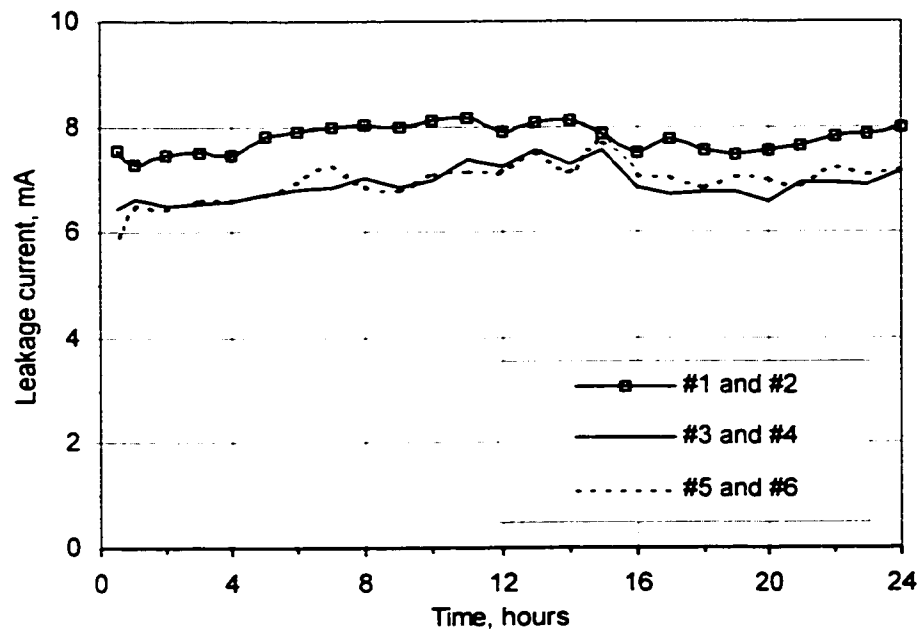


Figure 3.26 Averaged leakage current of the three specimens as a function of test time during cycle 2.

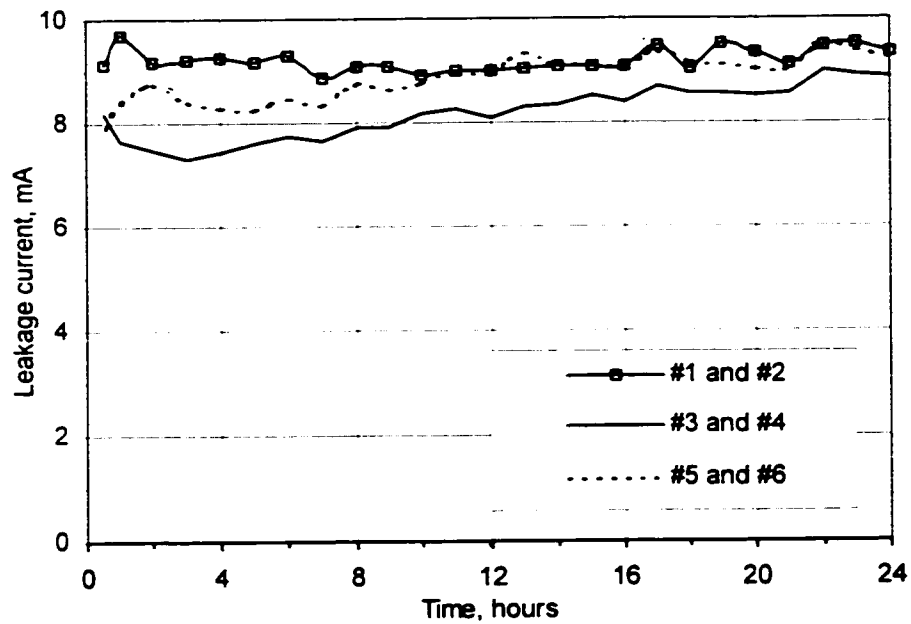


Figure 3.27 Averaged leakage current of the three specimens as a function of test time during cycle 3.

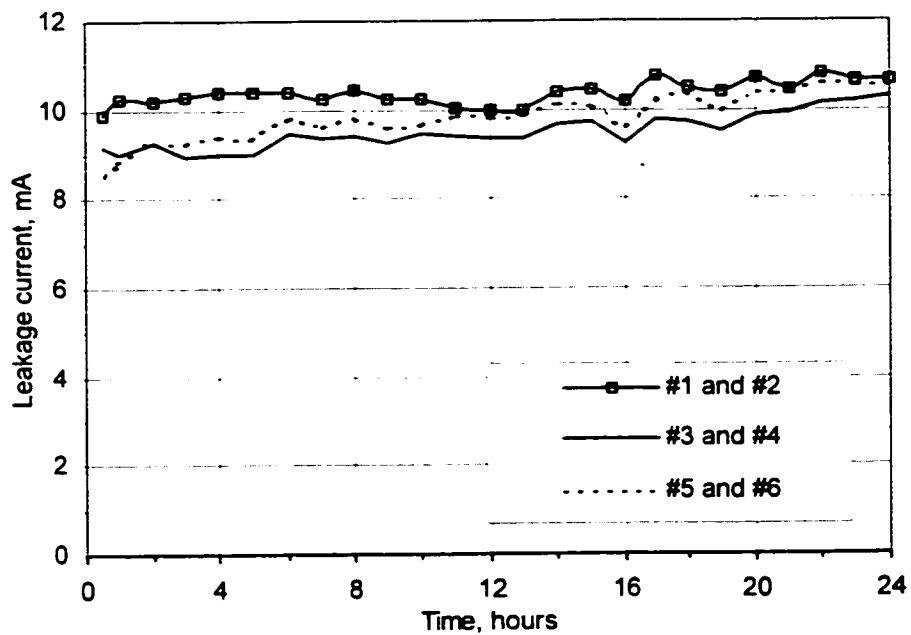


Figure 3.28 Averaged leakage current of the three specimens as a function of test time during cycle 4.

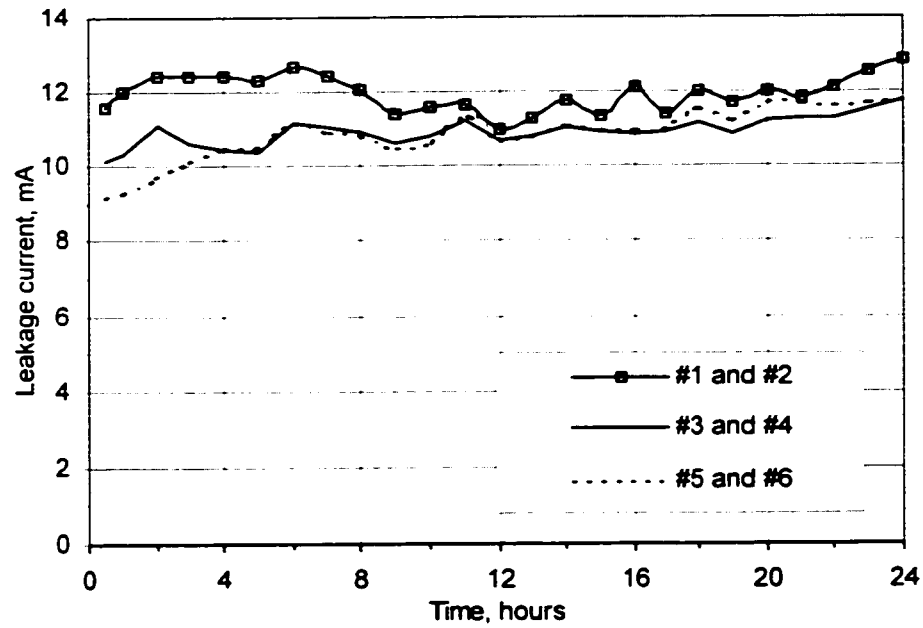


Figure 3.29 Averaged leakage current of the three specimens as a function of test time during cycle 5.

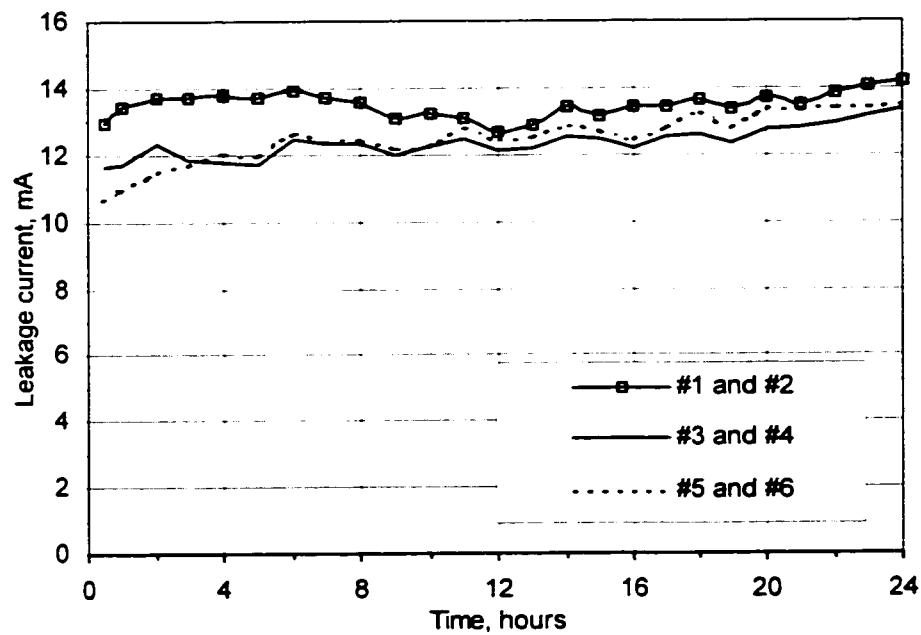


Figure 3.30 Averaged leakage current of the three specimens as a function of test time during cycle 6.

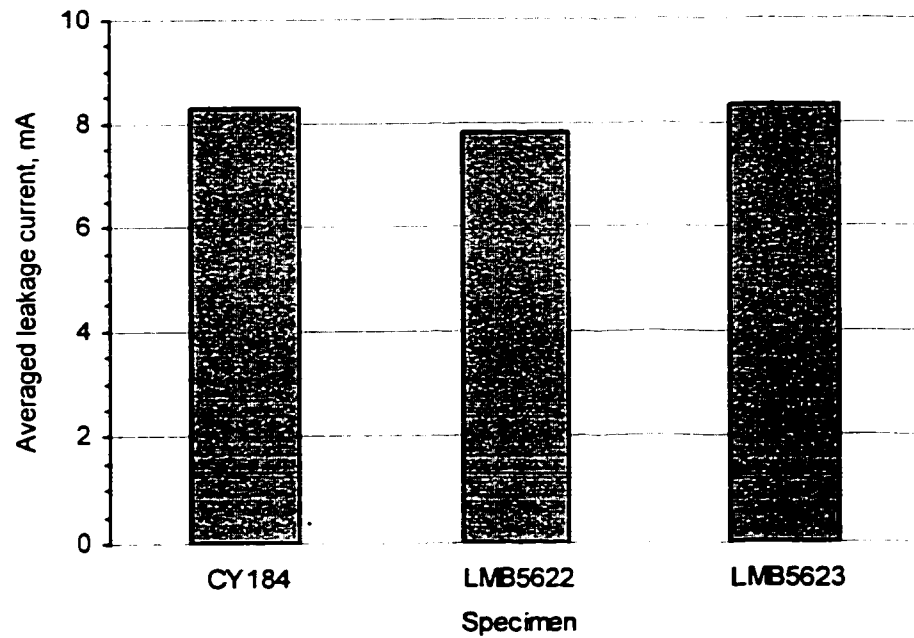


Figure 3.31 Averaged leakage current for the last four hours of aging during cycle 1 for CY184, LMB5622 and 5623.

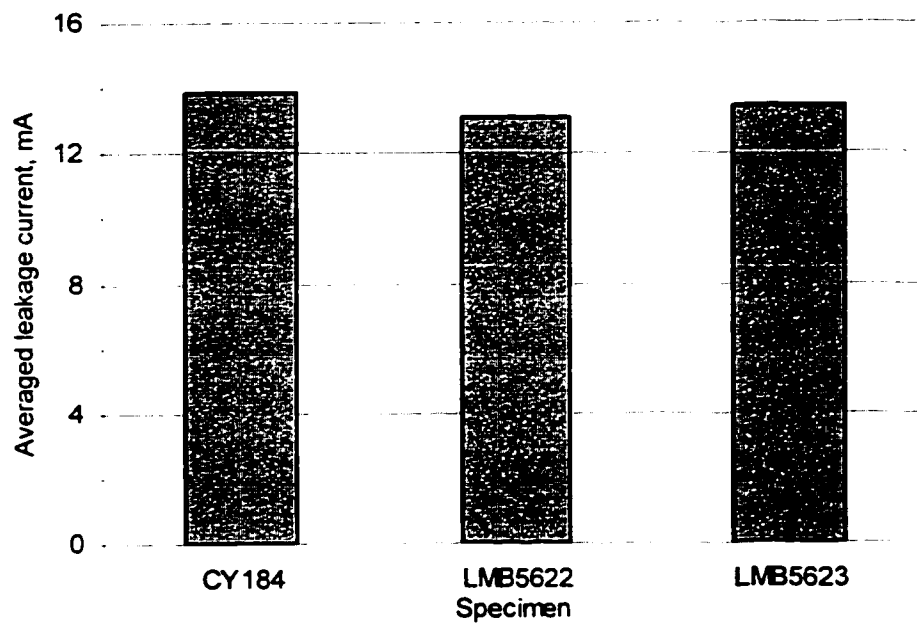


Figure 3.32 Averaged leakage current for the last four hours of aging during cycle 6 for CY184, LMB5622 and 5623.

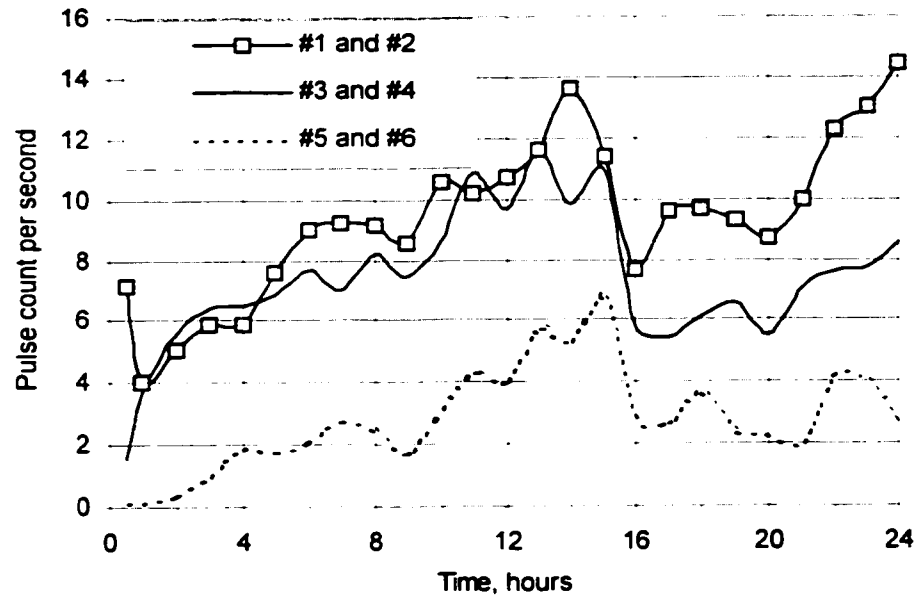


Figure 3.33 Current pulse rate having amplitude in the range 14-20 mA as a function of test time in salt-fog for cycle 1.

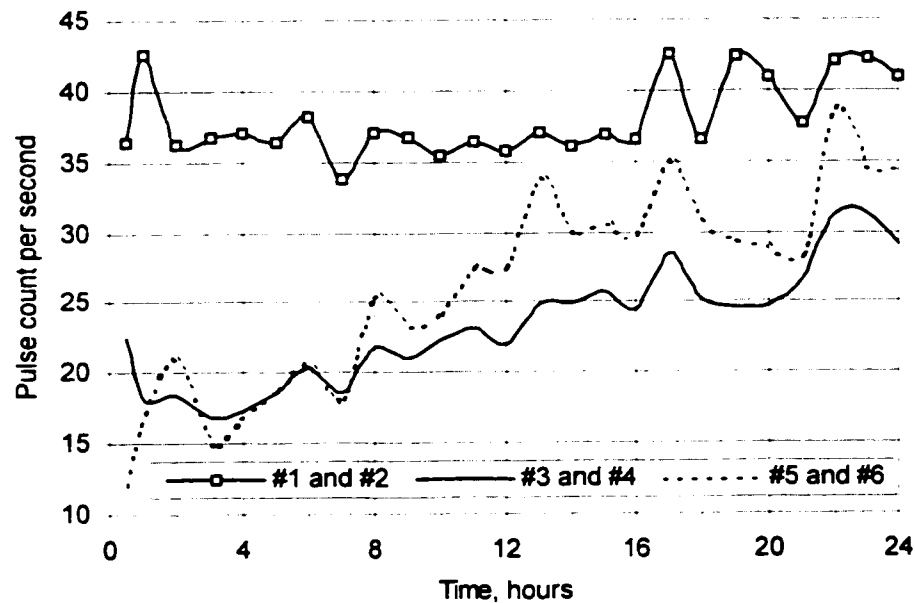


Figure 3.34 Current pulse rate having amplitude in the range 14-20 mA as a function of test time in salt-fog for cycle 6.

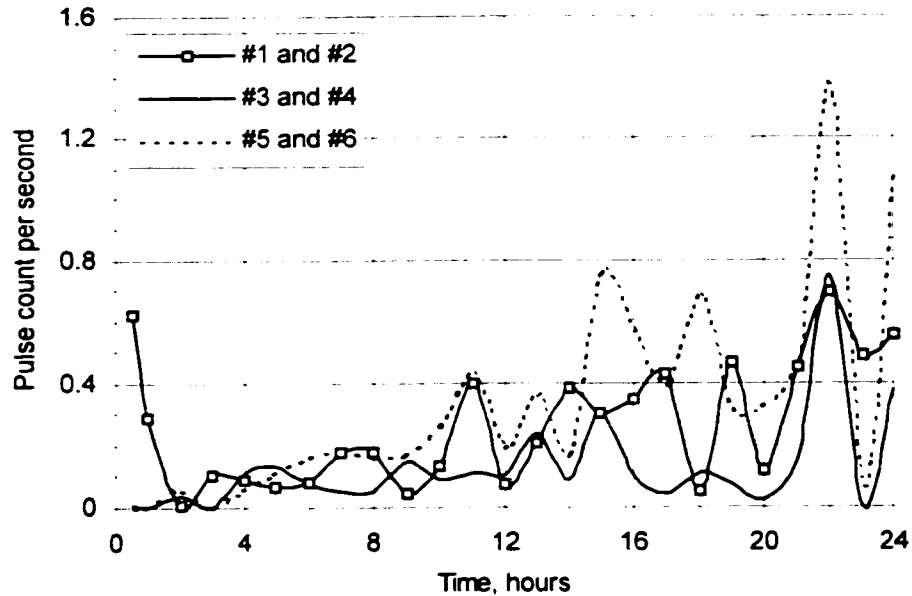


Figure 3.35 Current pulse rate having amplitude in the range 20-24 mA as a function of test time in salt-fog for cycle 6.

3.3.6 FT-IR Analysis on the White Powder Deposited on the Surface of Specimens

During the test, white powder was found deposited on the surface of all the epoxy rods. Figures 3.36 to 38 show the results of FT-IR spectroscopy for the powder which was collected after cycle 2, 4 and 6 for CY184, LMB5622 and 5623, respectively. The base line of those figures is slightly different from each other. The similar wavenumbers for peaks, for different specimens and the different cycles imply that the composition of the white powder is independent of the type of the specimen and also independent of the number of test cycles. The peaks revealed that the characteristic peaks for CO_3^{2-} and SO_4^{2-} are presented in these charts. Characteristic peaks for CO_3^{2-} are two medium peaks

from 460 to 410, 650 to 550 cm^{-1} and a broad peak at 1200-950 cm^{-1} . For SO_4^{2-} , a strong band at 1620-1450 cm^{-1} , and two medium peaks at 900-720, 810-735 cm^{-1} , respectively. Other peaks are caused by moisture and contamination during the FT-IR operation. As Ca^{2+} , CO_3^{2-} and SO_4^{2-} are the most common ions in the tap water, we conclude that the white powder deposited on the surface of the epoxy specimens originates from the salt in the tap water deposited during the test and becomes visible after complete drying of the surface. Since the surface close to the top electrode was exposed to the dry band arcings during aging in the energized salt-fog, saline water evaporated by the heat generated from the arcing and salts accumulated on the surface. This is the reason why white powder was found to extend from the area close to the upper electrode to the center area.

3.4 Conclusions

1. The surface roughness increased for all three types of epoxy specimens with increasing test cycles. LMB5623 showed the best performance while CY184 showed the fastest increase of surface roughness.
2. Measurement of contact angle on the aged epoxy specimens was dependent strongly on the location since the contact angle measured on the white powder was zero. By studying the change of contact angle, LMB5622 is better than LMB5623. The later is better than CY184.

3. Amplitude of the average leakage current and the pulse current rate increased with increasing test cycles in the energized salt-fog test. LMB5622 has smallest current pulse rate while CY184 has the largest.
4. The white powder deposited on the surface of all specimens was identified as salts from the tap water which was used to produce fog.

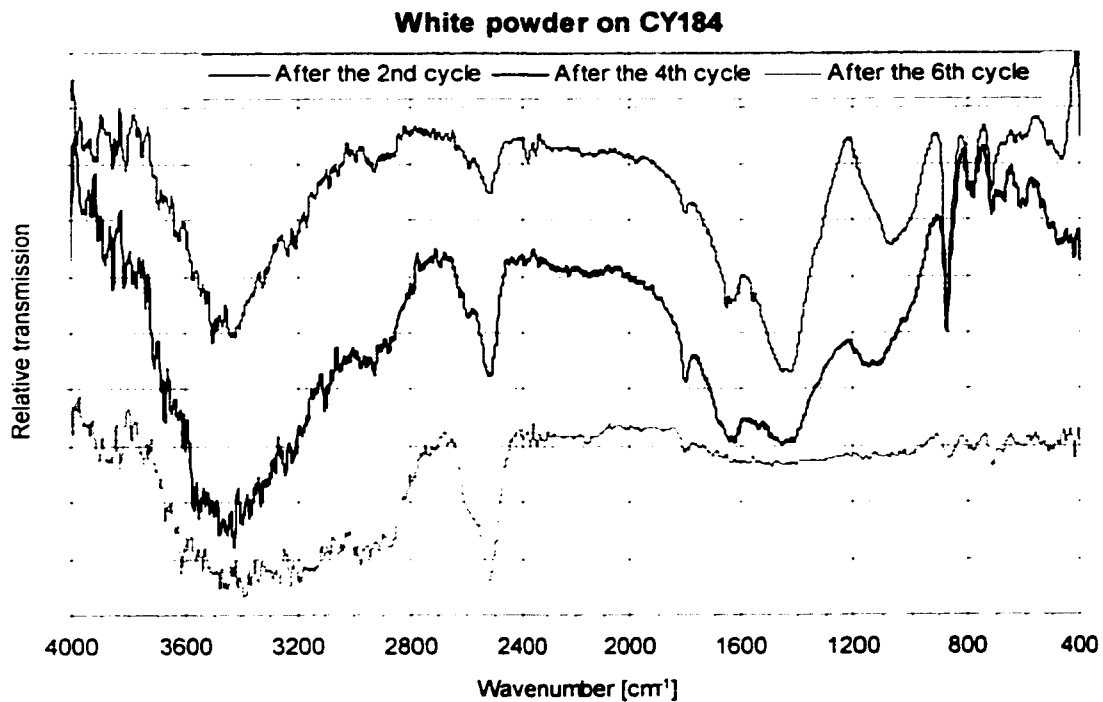


Figure 3.36 FT-IR spectrum for the white powder on specimens #1 and #2.

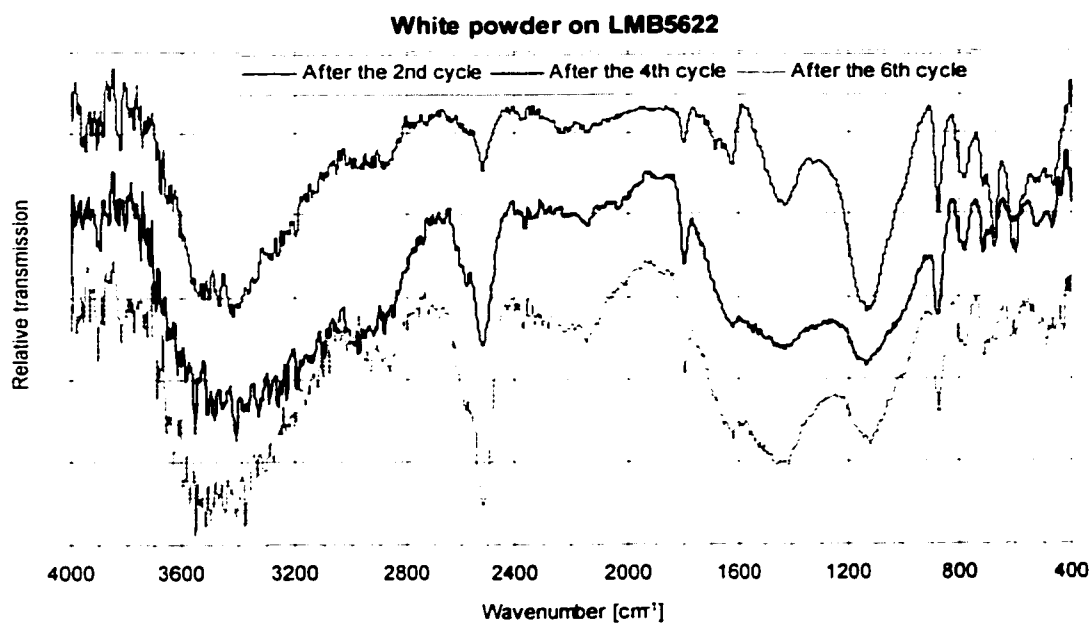


Figure 3.37 FT-IR spectrum for the white powder on specimens #3 and #4.

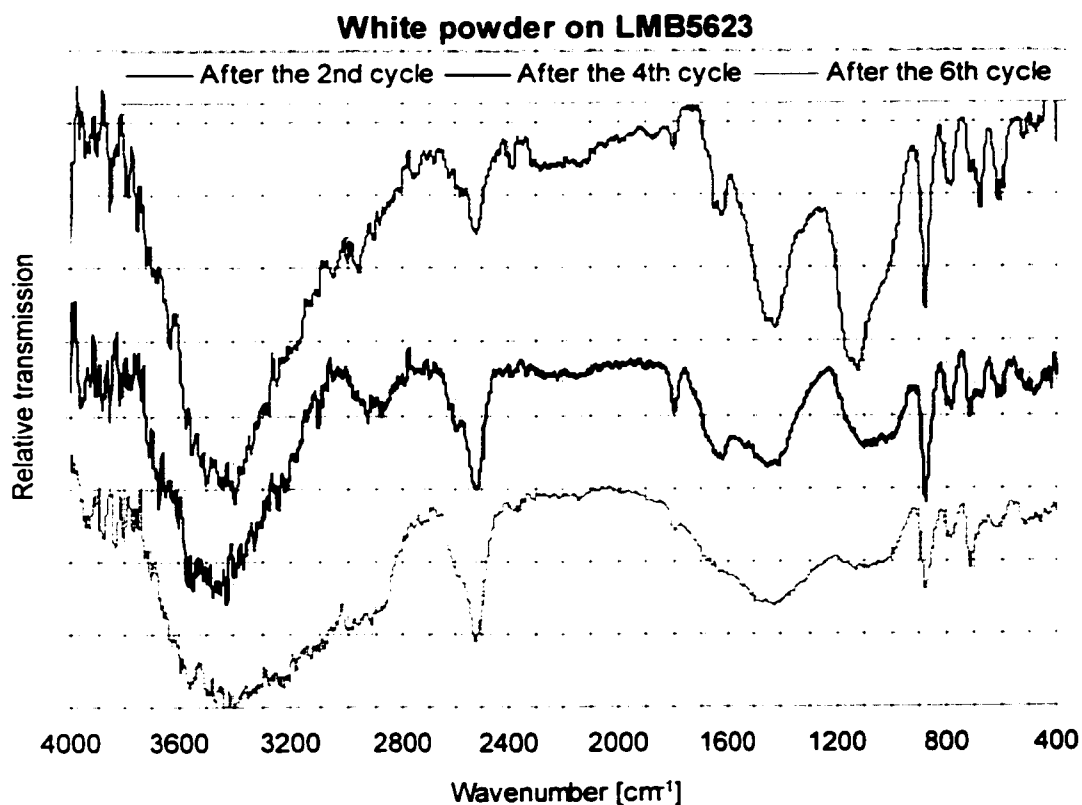


Figure 3.38 FT-IR spectrum for the white powder on specimens #5 and #6.

Chapter 4

A Study on the HTV Silicone Rubber

4.1 Introduction

One of the most attractive advantages of high temperature vulcanized (HTV) silicone rubber applied as the weather-shed material for manufacturing high voltage insulators is the ability for hydrophobicity to transfer to the surface of the polluted layer [33, 34]. Most high voltage polymeric insulators are not washed with high-pressured water/air during their lifetime because of a relatively vulnerable surface. For those used in polluted areas, the insulators suffer less surface discharging if the hydrophobicity can come out and capsule the particles of pollutants. Thus the transferability provides a longer life expectancy for composite insulators using HTV silicone rubber as weather-shed than any other polymeric material.

Today it has already been accepted that the transferring phenomenon in HTV silicone rubber is attributed to the diffusion of the mobile low molecular weight (LMW) fluid from the bulk of silicone rubber to the surface of insulator and polluted layer, if any [14,

19]. Considering the time-dependent degradation of silicone rubber in the actual running conditions, whether or not the transferability can be upheld during the service life is a highly interested question. Since the whole process is dominated by diffusion, the answer depends strongly on whether the bulk, i.e. the source of the diffusion can keep generating fluid.

In this thesis, forced heating was applied as an accelerated aging as well as an externally stimulating factor to study the loss and regeneration of fluid in the HTV silicone rubber. The optimized experimental procedures could make the HTV silicone rubber specimen completely devoid of the mobile LMW fluid inside the bulk and then regenerate within short time period. The experimental results indicate that the HTV silicone rubber does have an ability to regenerate the LMW fluid in appropriate temperature after each time of being depleted by extraction.

4.2 Experimental Conditions and Techniques

Cut from an HTV silicone rubber rod with the diameter of 23.5 mm, the specimens were circular slices with an average thickness of 2.0 mm. The density for the material was about $1.68 \times 10^3 \text{ kg/m}^3$ and the alumina trihydrate (ATH) filler was at the level of 140 pph by weight.

The LMW fluid was extracted by being immersed in the analytical hexane (C_6H_{14} with a boiling point of $68.5\text{ }^{\circ}\text{C}$) at $43\pm 2\text{ }^{\circ}\text{C}$. This extraction method has been shown effective in [35-37]. After the immersion, the specimens were taken out for a complete evaporation of hexane in the room temperature. The monitored weight difference before and after this complete extraction-evaporation process gives the amount of the mobile LMW fluid in the specimens. A high precision electronics balance with resolution of 10^{-4} g was employed for measuring the weight of the specimens at room temperature of $23\pm 3\text{ }^{\circ}\text{C}$ and humidity of $42\pm 4\%$. According to the experiment on a control specimen with a normal weight of 1.4693 g , the systematic error on weight measurement was found less than $\pm 0.04\%$. The systematic error was caused by the possible inconsistent humane operation between different times of measurement during the long period ($>3000\text{ h}$) and by the specimen's intake or evaporation of the moisture from the air in an environment with small humidity changing ($42\pm 4\%$).

Using an electric oven with a negative-feedback thermostat the specimens were subjected to different temperatures for different duration to study the effect of heating on the generation of fluid. In the present work, four temperature points, 50, 150, 250 and $380\text{ }^{\circ}\text{C}$, were selected.

To optimize evaporation time, one specimen was immersed in hexane for 480 h at $43\text{ }^{\circ}\text{C}$ and then taken out for evaporation at room temperature. Figure 4.1 shows the weight changing process during the evaporation. It is observed that after 10 h the weight became constant. This illustrates that all the hexane absorbed in the specimen was evaporated by

10 h. For more reliable and convenient considering, 24 h was set for complete evaporation.

It was recorded that after 480 h immersion the geometrical size of the specimen was increased by 33.1% while after 10h evaporation both the diameter and the thickness of the specimen recovered to the origin value. The size of the specimen was measured using a digital caliper with resolution of ± 0.01 mm.

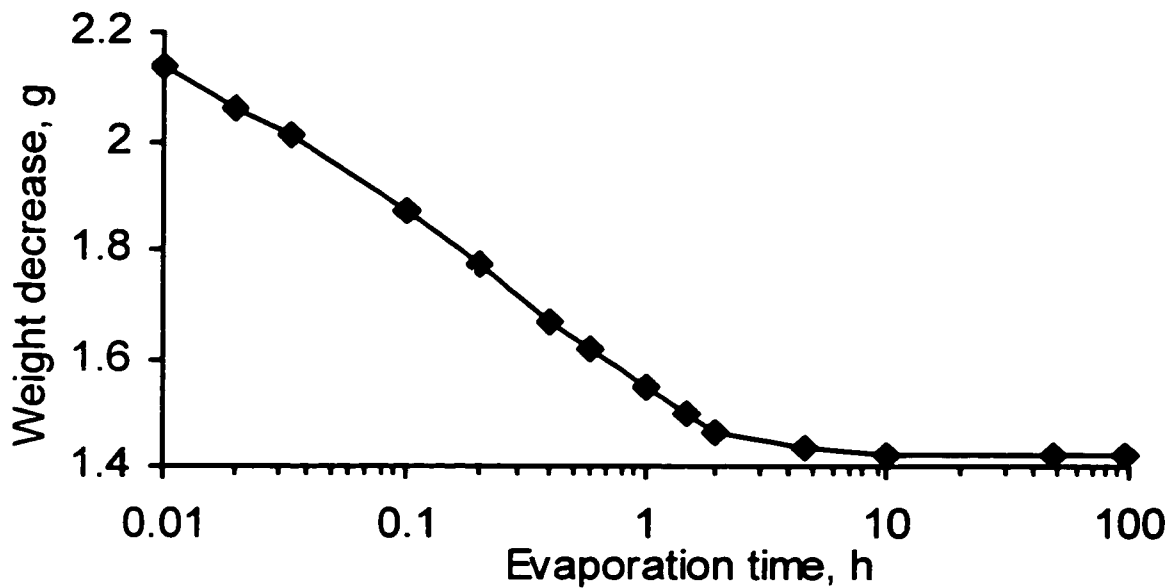


Figure 4.1 Variation of the weight of a specimen after immersion at 43 °C for 480 h with evaporation time. During evaporation in air, room temperature was 23 ± 3 °C and relative humidity of the air was $42 \pm 4\%$.

To optimize the immersion time, the specimens were firstly immersed in hexane for 480 h at 43 ± 2 and 23 ± 3 °C to clarify the effect of temperature. Figure 4.2 shows the percentage weight increase of the specimen as a function of immersion time. It is observed from Figure 4.2 that at higher immersion temperature the specimen absorbed more hexane. It took 10 h for specimens at 43 °C to reach the saturation value of 48.0% while at 23 °C it took 48 h to reach the saturation value of 44.3%. This indicates that the absorption speed to reach the saturated value is faster at higher temperature. Considering the fluid could not be extracted completely without a complete absorption of hexane, a faster speed to reach the saturation of absorption is preferred and an electric oven set at 43 °C was employed to store the specimens immersed in hexane.

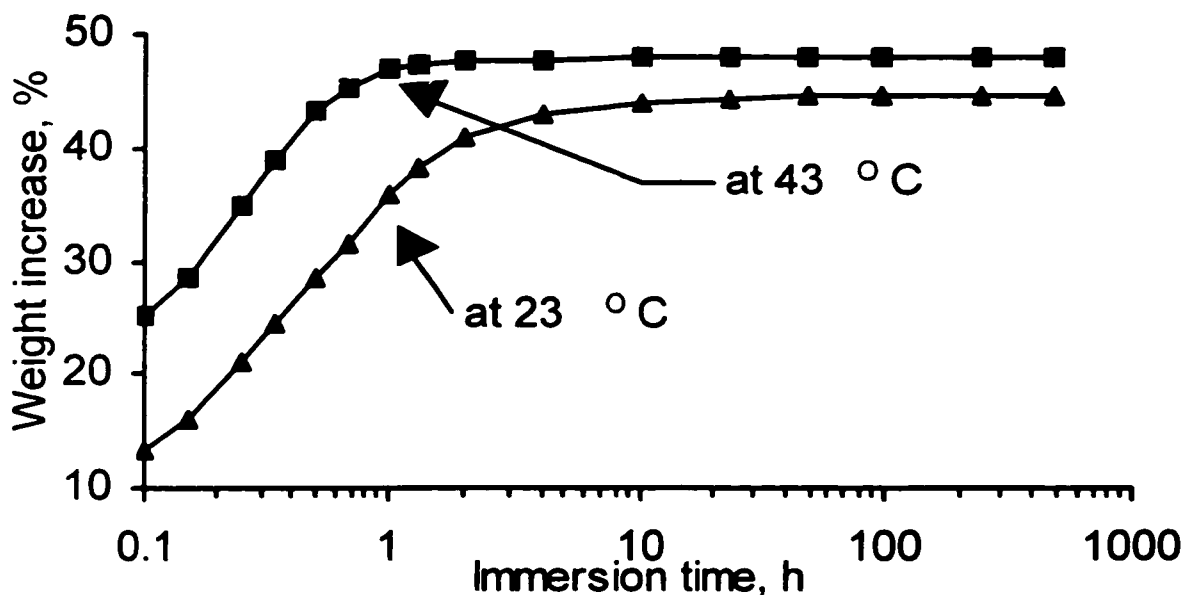


Figure 4.2 Percentage weight increase of the specimens vs. immersion time in hexane at 43 ± 2 and 23 ± 3 °C.

The specimens with thickness around 2 mm were then immersed in hexane at 43 °C for different time to find the appropriate immersion time for a complete extraction. Figure 4.3 shows the amount of the fluid extracted as a function of immersion time. In Figure 4.3, after 96 h immersion in hexane at 43 °C the total amount of the LMW fluid removed was found to be 1.51% of the specimen weight. One specimen with the same thickness was cut into pieces and immersed in hexane at 43 °C for 860h. Fluid of 1.51% was found removable. Therefore immersion of 96 h was enough for a complete extraction of fluid in the specimen with a thickness around 2.0 mm or less. Experiment on the specimens with thickness of 4 mm shows that longer immersion time is needed for a complete extraction of the LMW fluid. After 96h immersion at 43 °C the geometrical size of the specimen was increased by 33%.

According to the above optimization, a complete extraction-evaporation procedure to remove the mobile LMW fluid in the HTV silicone rubber was set as: immerse the specimen in hexane for 96 h at 43 °C and then take it out for evaporation of 24 h in air.

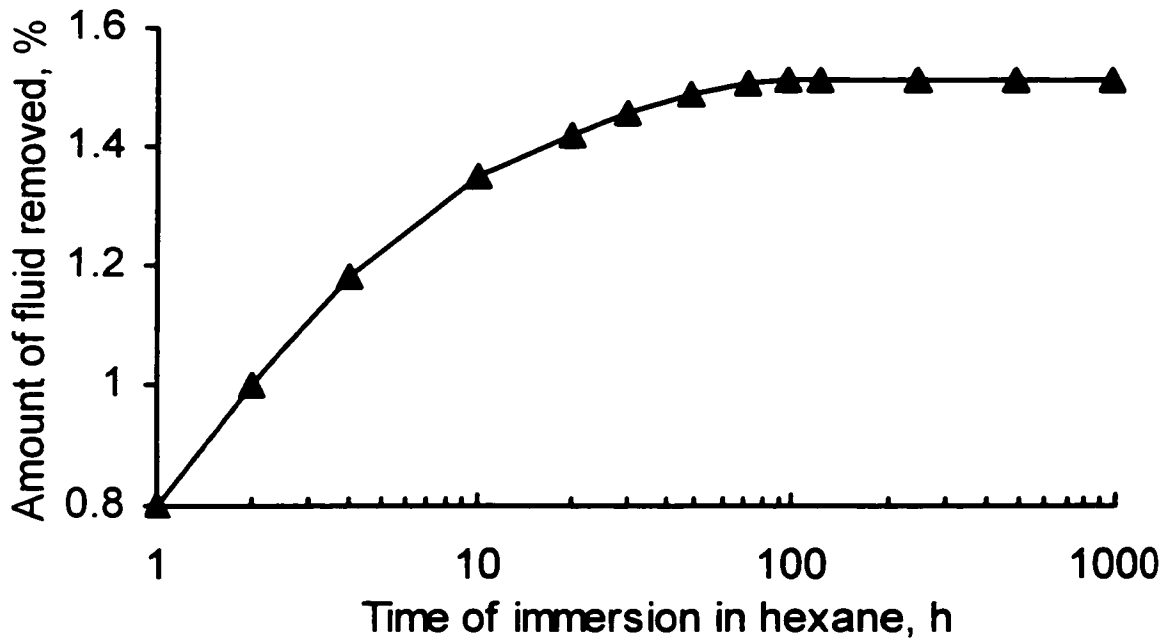


Figure 4.3 Amount of the LMW fluid extracted as a function of immersion time. Immersion temperature was 43 °C. Evaporation time was 24 h.

4.3 Results and Discussions

4.3.1 Weight Loss Due to Heating

The specimens were firstly devoid of the LMW fluid following the extraction-evaporation procedure described above and then were heated at the different temperatures for a continuous duration up to 20 h. After being heated for 2, 5, 10, 20 h, the specimens were taken out and weighted. Figure 4.4 shows the weight loss of the specimens as a function of heating duration at different heating temperatures. It is observed from Figure

4.4 that at 50, 150 and 250 °C, the weight loss increased with increasing time of heating. The loss of weight can be partly attributed to the decomposition of ATH filler. However, it is found from Figure 4.4 that at 375 °C, after 2, 5, 10, 20 h heating, the weight loss was 19.5, 36.7, 40.8, 41.6%, respectively. The weight losses after 5, 10, 20 h heating are much higher than 20.2%, the theoretical value of weight loss exclusively due to ATH decomposition. More loss besides the decomposition of ATH is caused by chemical reactions during heating. Because of the interactions between silicone rubber and the filler, between silicone rubber and the air, hydrolysis and oxidation may take place [38, 39]. The direct reason for the weight loss is that the both kinds of reactions produce volatile materials such as H_2 , CH_4 , H_2O .

Physical inspection on the specimen after being heated for 10 h at 375 °C found that the specimen was toughened and the color turned from originally gray to light yellow. Some parts on the surface were powdered. It seemed that being heated at 375 °C for more than 10 h could damage the material. The contact angle on the damaged specimen never recovered to the value more than 80°(virgin specimen has a contact angle ~108°).

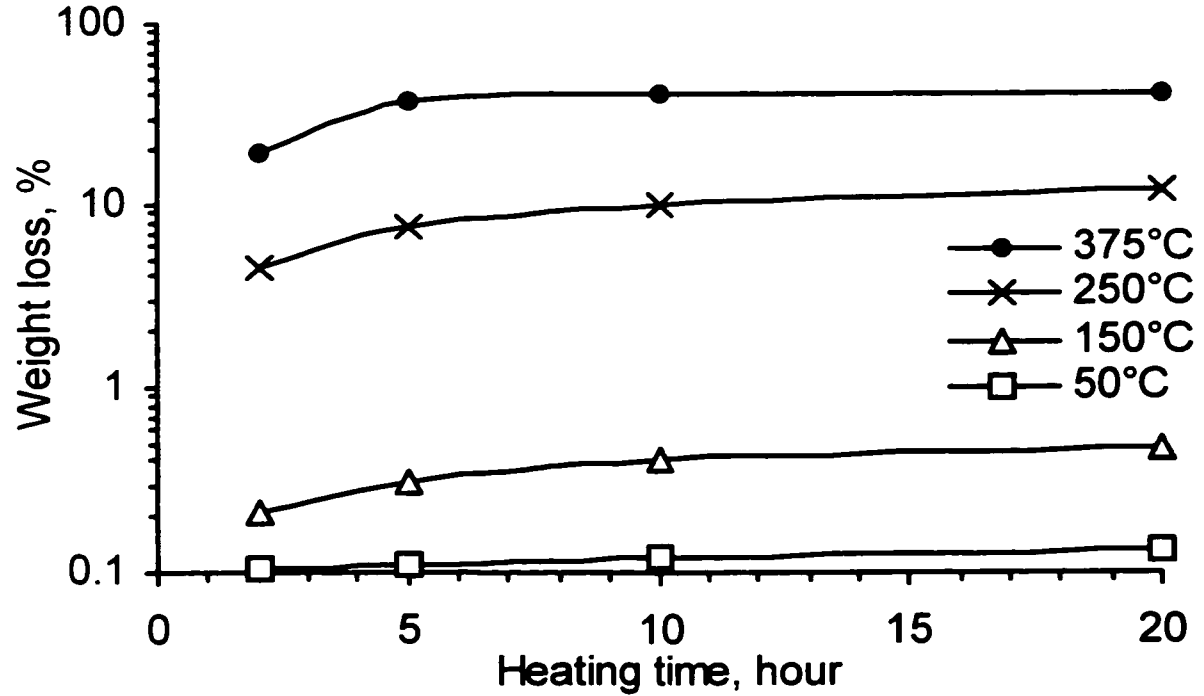


Figure 4.4 Weight loss of the HTV silicone rubber specimens as a function of heating time at different heating temperature. Specimens were devoid of fluid before the first heating of 2 h.

4.3.2 Loss of Fluid Due to Heating

In order to investigate the loss of fluid due to heating, virgin specimens with the fluid content of 1.51% were heated at different temperatures for 2 h. Figure 4.5 shows the variation of the fluid content after heating of 2 h with different temperatures. It will be observed from Figure 4.5 that the amount of the fluid decreased from 1.51% to 1.47, 1.41, 1.25, 0.68% after being heated for 2 h at 50, 150, 250, 375 °C, respectively. By

deducting the amount of fluid remained after heating from the original value in the virgin specimen the loss of fluid due to heating was found to be 0.04, 0.10, 0.26, 0.83% after being heated for 2h at 50, 150, 250, 375 °C, respectively.

It is known that in vacuum PDMS does not decompose to volatile oligomers until heating temperature beyond 343 °C [40]. Under the circumstance of heating in air, the reasons accounting for the observed loss of the LMW fluid at different temperatures in the range from 50 to 375°C (shown in Figure 4.5) are: (1) possible decomposition at temperatures lower than 343 °C because of the presence of air, (2) hydrolysis of siloxane bonds and hydrocarbon groups, and (3) oxidation of hydrocarbon groups and crosslinking of siloxane bonds.

While complete decomposition can not happen during heating of 2 h in air, intermediary decomposition may produce volatile materials which were evaporated during the heating and result in the loss of LMW fluid. It has been shown that a complete decomposition of PDMS can produce cyclic $[(CH_3)_2SiO]_n$ (with n mainly equal to 3 or 4) and shorter linear fractions with broad molar mass distribution [40].

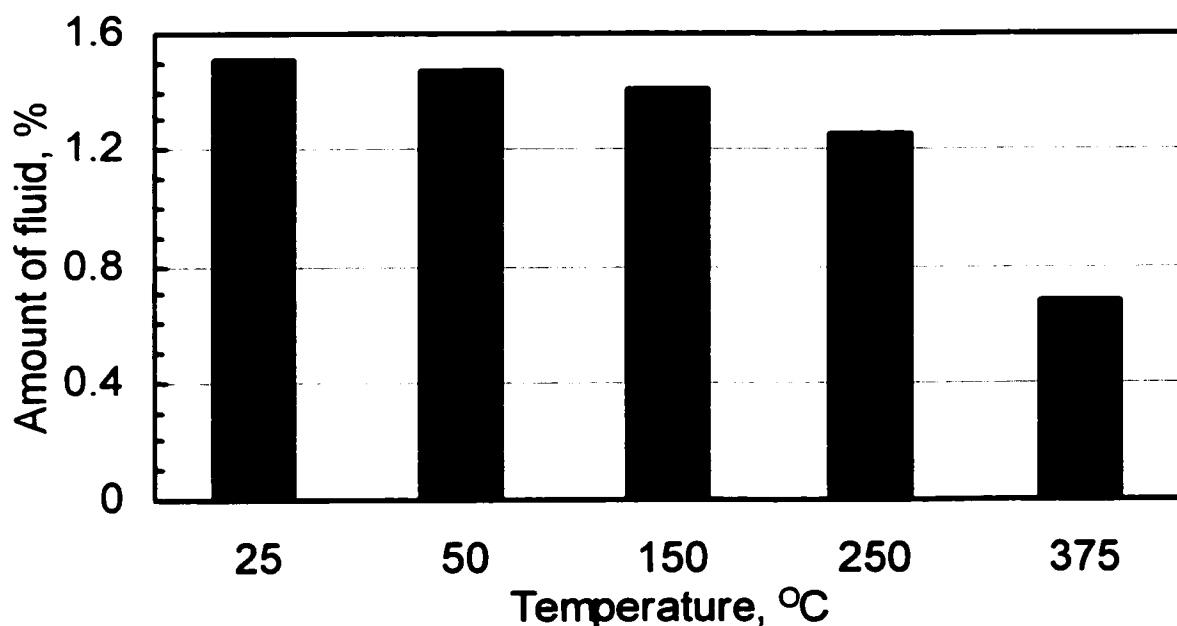


Figure 4.5 Amount of fluid after 2 h heating. All specimens were virgin.

4.3.3 LMW Fluid Content in Samples from Different Manufacturers

Five HTV silicone rubber samples (#1 to #5) were employed from different manufacturers. In this paper, sample #1 is intensively studied. Without additional statement, all HTV silicone rubber specimens were #1. Figure 4.6 shows the content level of LMW fluid in these five different samples. It is observed from Figure 4.6 that the content level of LMW fluid varies from 1.51% (sample #1) to 8.3 % by weight (sample #3). The aging characteristics for these five samples will be in another work. Since composite insulators from all five manufacturers meet relevant technical requirements and are dominating in the market, the results in Figure 4.6 indicate that the

content of LMW fluid in the virgin HTV silicone rubber could be much different from a product to another and may not be used as the only criteria for evaluating the products.

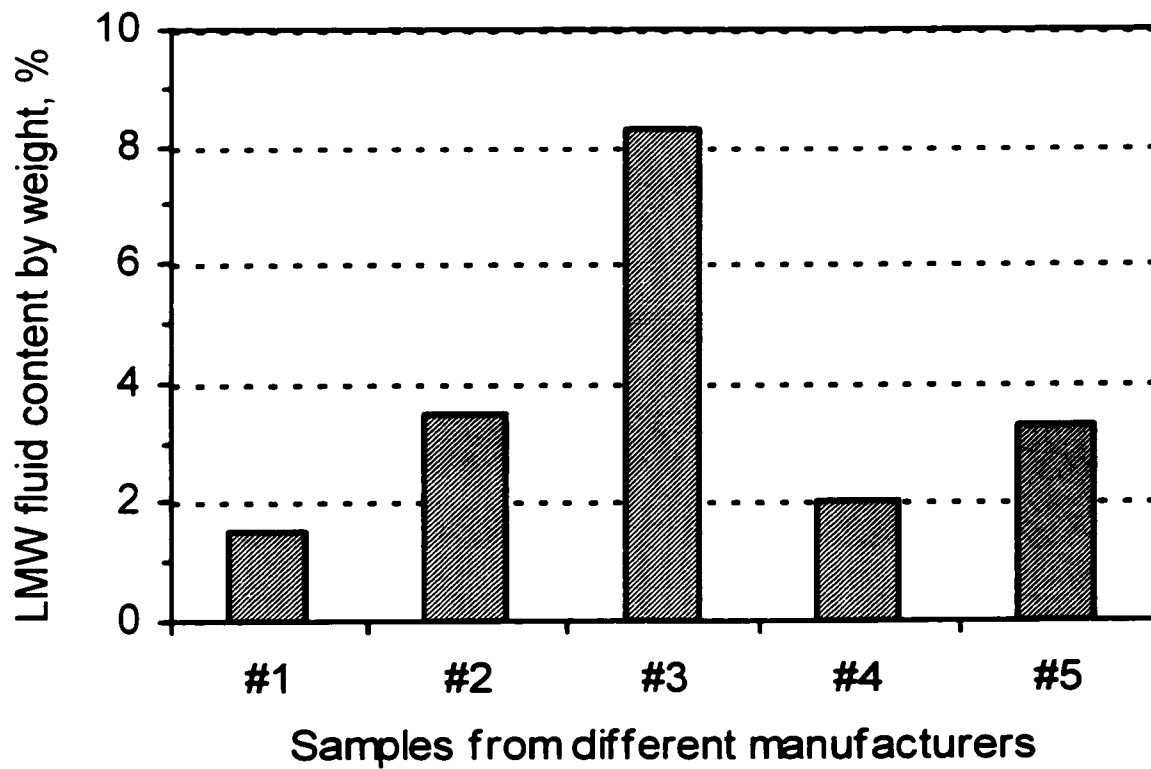


Figure 4.6 LMW fluid content by weight for samples from different manufacturers. All samples are in virgin status.

4.3.4 Regeneration of Fluid

Heating specimens devoid of fluid found that extractable fluid could be regenerated. Figure 4.7 shows the amount of fluid regenerated after heating of 2 h at different temperatures. Figure 4.7 illustrates that new fluid of 0.12, 0.19, 0.33, 0.65% was detected after being heated for 2 h at 50, 150, 250 and 375 °C, respectively. This regeneration of

fluid in a silicone rubber specimen devoid of fluid is due to the release of trapped fluid in the lattice of silicone rubber and a production of the fluid attributed to thermal activation [41]. What kinds of specific chemical reactions will produce LMW fluid in such conditions is not the purpose of this paper. It is known, however, at the present that most of reactions related with LMW generation are sensitive to temperature [36].

To study the accumulative effect of heating on the regeneration, seven cycles of heating-extraction-evaporation (HEE) were then repeated on the specimens of Figure 4.7. Figure 4.8 shows the production of the fluid after each cycle of HEE. It will be observed from Figure 4.8 that at 150 °C the specimen did regenerate the fluid every time while extractable fluid was not detected on the specimen heated at 250 °C after six times of HEE. For practical silicone rubber insulators, it is not clear whether or not there are any conditions under which the mobile LMW fluid may be depleted completely. The results shown in Figure 4.8 indicates that even the LMW fluid in the silicone rubber was lost completely, it can still recover to certain level. For example, at 150 °C after eight times of HEE, the amount of extractable fluid regenerated was still found to be 0.13% of the specimen's original weight.

Because the diffusion of the LMW fluid from the bulk to the surface will stop when equilibrium is reached, the thin polluted layer, whose weight is negligible compared with the bulk of the silicone rubber in a high voltage insulator, needs extremely small amount of mobile fluid to keep hydrophobicity. The regeneration of the fluid shown in Figure

4.8 may predicts a very long lifetime for composite insulators with silicone rubber as housing material from the viewpoint of keeping hydrophobicity and its transferability.

Figure 4.9 shows the accumulative amount of fluid regenerated as a function of heating time. For the specimen heated at 150°C, when heating time accumulated to 116 h, the total content of regenerated fluid was 2.29% while for the specimen at 250 °C the corresponding value is 5.45%.

For insulators in the field, being heated is possible under some running conditions. It is well known that surface discharge activities usually cause high temperature areas on the surface. In ac condition, periodical polarization causes the dielectric loss which is normally negligible because the factor of the dielectric loss, $\tan\delta$ is very small in good conditions. However, $\tan\delta$ depends on the property of the insulation material and the assemblage of the insulator. It may vary in large range during the lifetime of the insulator. Large $\tan\delta$ will cause high temperature points in the bulk of the silicone rubber. For example, $\tan\delta$ may be increased drastically when moisture is absorbed into the core of the insulator through defects such as small holes and slight crackles in the weather-shed.

For silicone rubber insulators in situ and with polluted layer, it is important to keep both hydrophobicity and its transferability. Due to the natural-cleaning effect from wind, rain etc., pollution accumulated on the surface of the insulator may be lost and brings away part of LMW fluid diffused from the bulk of the silicone rubber. The kind of

consumption of the LMW fluid, depending on the actual running conditions, would lower the content of LMW fluid in silicone rubber if the fluid can not be regenerated after the insulator has been put into service. It has been reported that no decrease of the fluid content was found in the silicone rubber insulators with service history of 6 to 12 years [33, 1]. The regeneration of fluid shown in this paper may be able to explain the constant content of fluid in HTV silicone rubber during the lifetime of insulators.

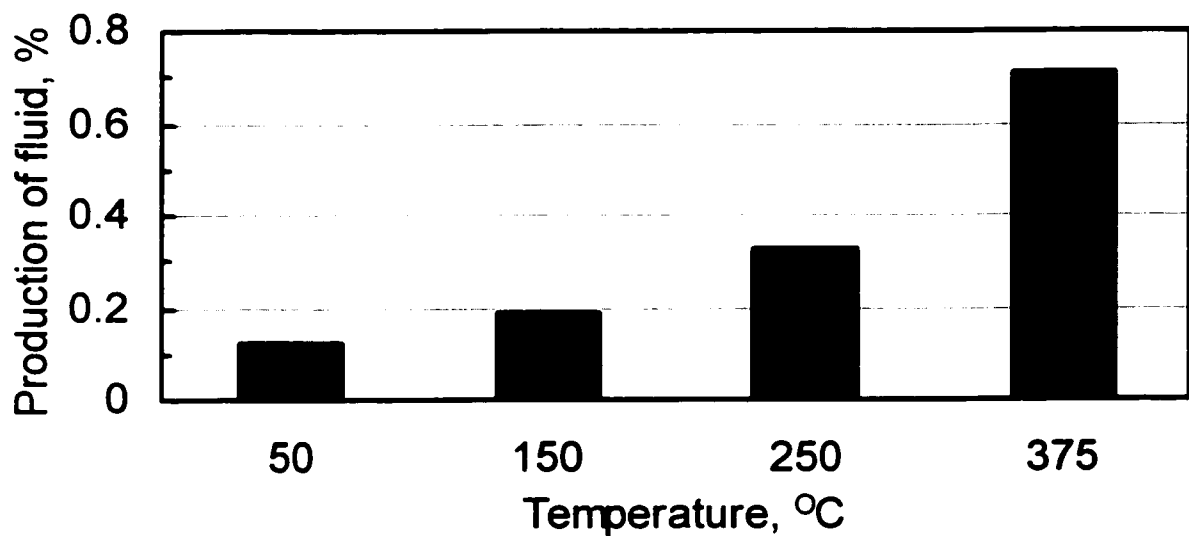


Figure 4.7 Amount of fluid regenerated with different heating temperature. The specimens were devoid of fluid before heating of 2 h.

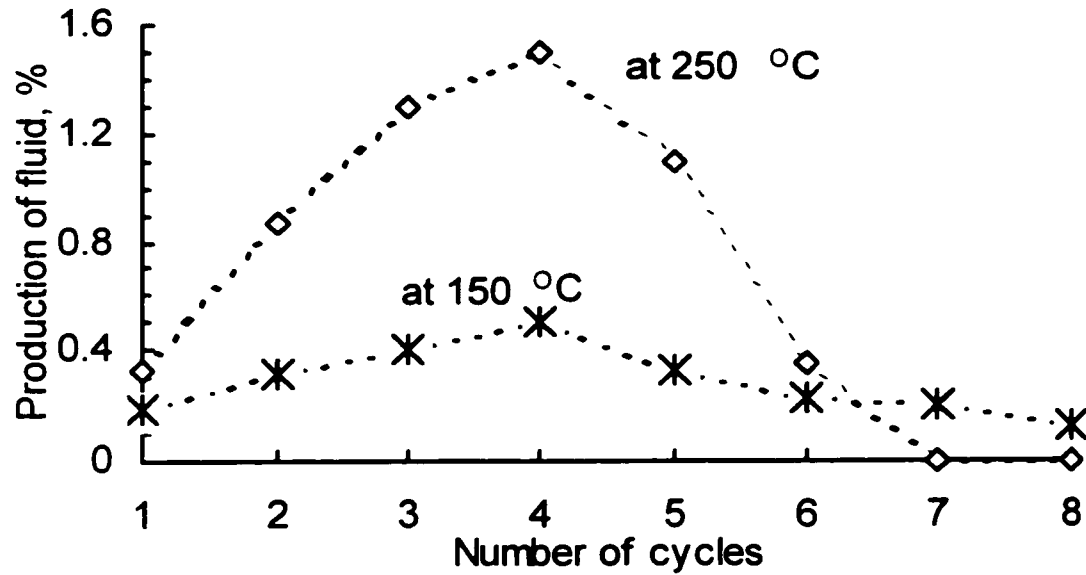


Figure 4.8 Production of fluid as a function of the number of heating-extraction-evaporation (HEE). The specimen was devoid of fluid before each time of heating. Heating time for the 1st to 8th HEE was 2, 3, 5, 10, 24, 24, 24, 24 h, respectively.

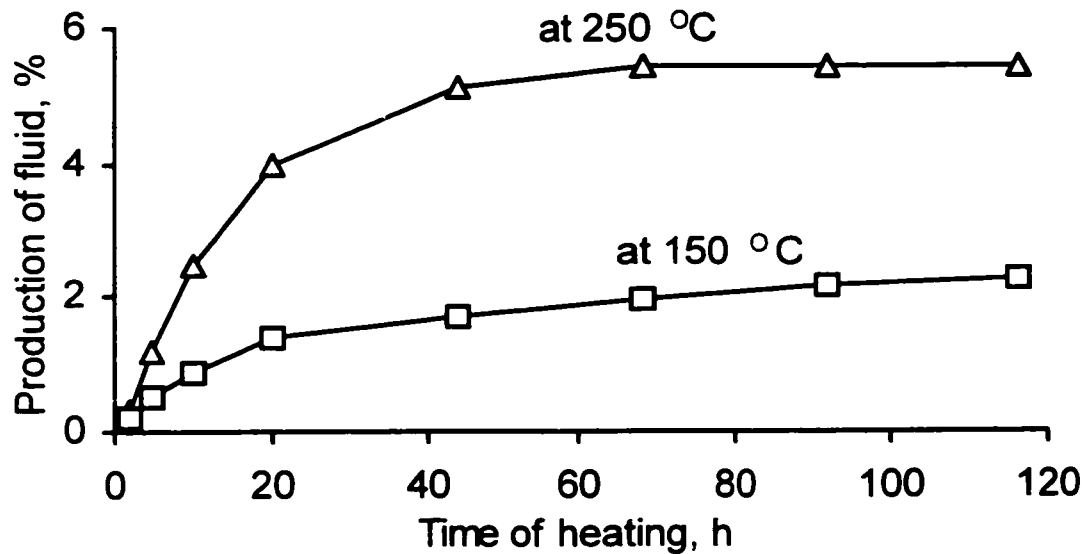


Figure 4.9 Production of fluid with accumulative time of heating. Fluid was depleted each time before heating.

4.3.5 GC-MS Analysis

GC-MS analysis was performed using a Kratos profile MS (mass spectrometer) with high resolution, magnetic sector and a Shimadzu 14 B GC (gas chromatography) equipped with a DB-5 capillary column. The GC initial settings were: injector temperature, 250 °C; oven temperature, 35 °C; interface temperature, 280 °C. A two-ramp GC temperature program was used. The initial temperature was increased to 180 °C (hold for 1 min) with a ramp rate of 20 °C/min. And then to 250 °C (hold for 20 min) with a ramp rate of 20 °C/min. The chemical components from GC were identified with an MS. The mass range for the MS is from 10 to 750 atomic mass units. The mass spectra were acquired in EI (electron inject) mode at an energy of 70 eV.

The specimen for the GC-MS analysis was a mix of removable low molecular weight fluid and the solvent, hexane. Since the HTV silicone rubber matrix is composed of PDMS (polydimethylsiloxane), $[\text{SiO}(\text{CH}_3)_2]_n$, analysis on GC spectra can indicate the distribution of homologous short-chain siloxane [42, 43]. Figure 4.10 shows GC spectra for the virgin HTV silicone rubber. Cyclic PDMS structures with $n^+ = 6, 7, \dots, 15$ are observed in Figure 4.10 (the + sign is used to represent the cyclic structure). All peaks in Figure 4.10 are obtained at the same conditions. So the area of each peak indicates the concentration of the correspondent components. Table 4.1 shows the area for some peaks in Figure 4.10. It is found from Table 4.1 that peaks for $n^+=7$ to 14 have higher concentration than $n^+=3$ or 15.

Figures 4.11 and 12 show GC spectra for HTV silicone rubber specimens with repeating depletion-heating treatment. The specimens for Figure 4.11 were treated with 4 cycles of heating-extraction-evaporation. The removable fluid was depleted before each time of heating. Heating time for the first 4 cycles was 2, 3, 5, 10 h, respectively. The specimens for Figure 4.12 were treated with one more cycle of heating and were heated for 24 h. Comparison of Figures 4.11 and 12 with Figure 4.10, it is observed that new polymers with short unit number, n , less than 6 appeared after 4 and 5 cycles of thermal treatment in Figures 4.11 and 12. Polymers with n larger than 6 do not appear in Figures 4.11 and 12. This means that PDMS with chain length longer than 6 had been removed in previous thermal treatment and did not regenerate. The above results of GC experiment indicates that the chain length of lower molecular weight fluid decreased with increasing number of thermal treatment cycles during experimental treatments.

Figure 4.13 shows mass spectra corresponding to peaks in Figure 4.12. The abscissas in Figure 4.13 are the ratio of the mean atomic mass (m) and the charge of the detected ion (z). The purpose of the mass spectroscopy is to identify the material corresponding to each peak in the GC spectra (Figure 4.12). Each peak in Figure 4.12 is a group of materials with lots of fragments passing the GC column at close time. To help the identification, the molecular weight for PDMS with n or $n+$ from 2 to 8 was calculated and shown in Table 4.2. The first scan marked with $n+=3$ in Figure 4.13 shows a highest mass peak at 207 and some small mass peaks including 133 and 162. The mass peaks at 207, 133 and 162 are considered as molecular weight for $n+=3$, $n+=2$ and $n=2$,

respectively. All the three mass peaks are corresponding to the short-chain PDMS with a methyl group missing. This is consistent with the founding in [42]. An observation on all four scans in Figure 4.13 shows that both linear and cyclic fragment can be found in the mass spectra. However, the abundance of linear structure is much smaller than that of cyclic structure. Actually, only a mass peak of 162, which is identified as $n=2$, is found in all four scans in Figure 4.13. And the height for the peak of 162 is very small. So the cyclic structure is dominating and the reason for this is unknown so far.

It is noted that most fragments found in the mass spectra (Figure 4.13) are short-chain PDMS with one methyl group missing. For example, 133 and 207 in the first scan, 133, 207 and 281 in the second scan, 73 and 355 in the third scan, 73, 133, 147, 429 in the fourth scan. The reason for the missing of methyl group is that the bond energy of Si-C (318 kJ/mol, see Table 4.3) is much less than that of Si-O (444 kJ/mol) and C-H (414 kJ/mol). So Si-C bond is the easiest to be broken in the short-chain PDMS.

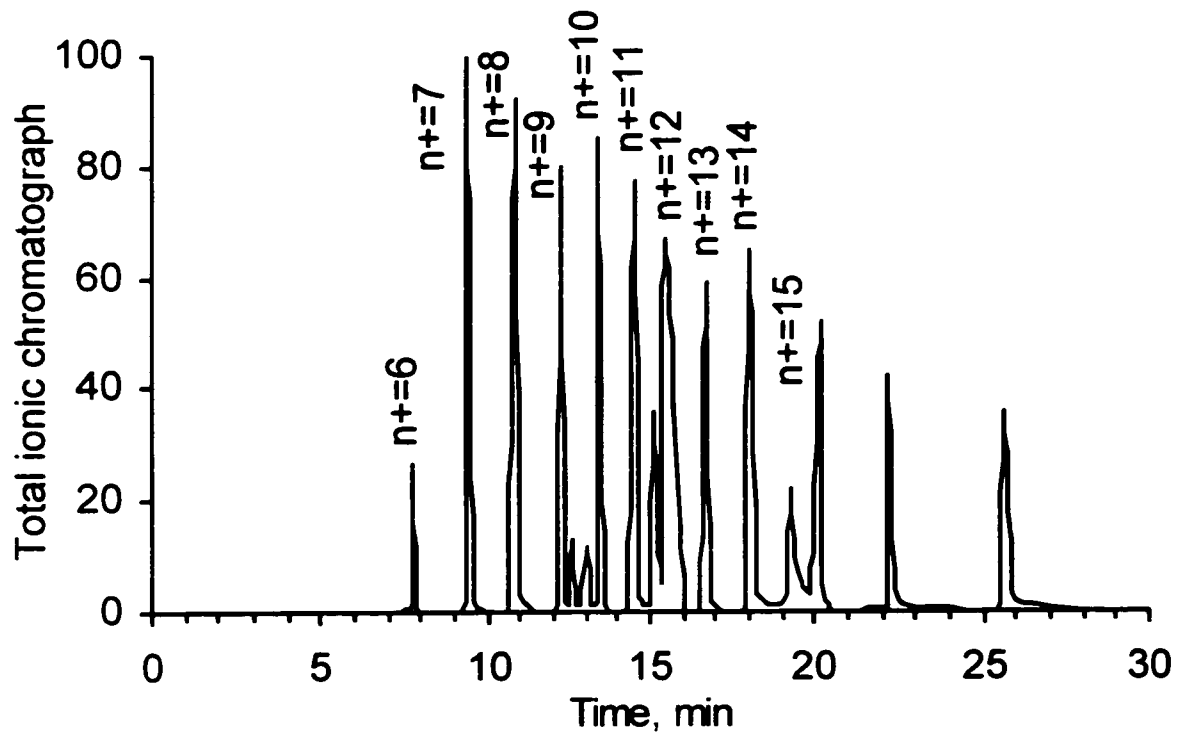


Figure 4.10 GC spectrum for HTV silicone rubber at the virgin status.

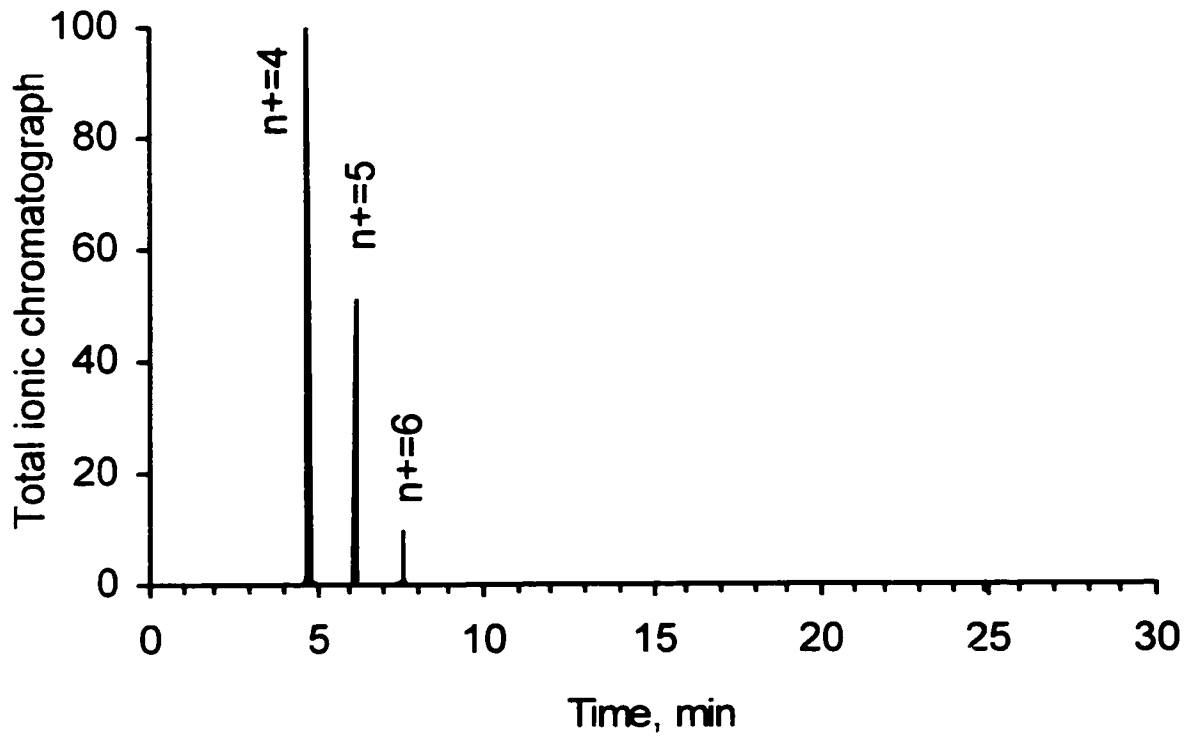


Figure 4.11 GC spectrum for HTV silicone rubber treated with 4 cycles of heating-extraction-evaporation (HEE). The specimen was devoid of fluid before each time of heating. Heating time for the 1st to 4th was 2, 3, 5, 10 h, respectively.

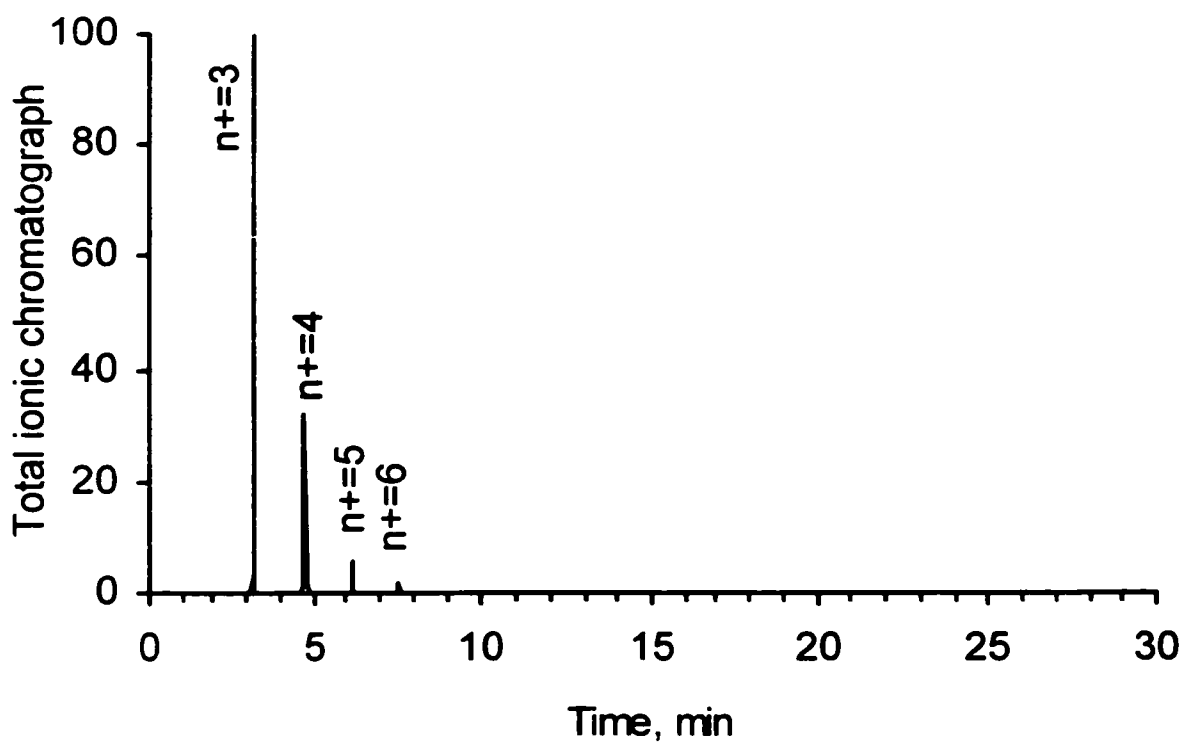


Figure 4.12 GC spectrum for HTV silicone rubber treated with 5 cycles of HEE. The specimen was devoid of fluid before each time of heating. Heating time for the 1st to 5th was 2, 3, 5, 10 and 24 h, respectively.

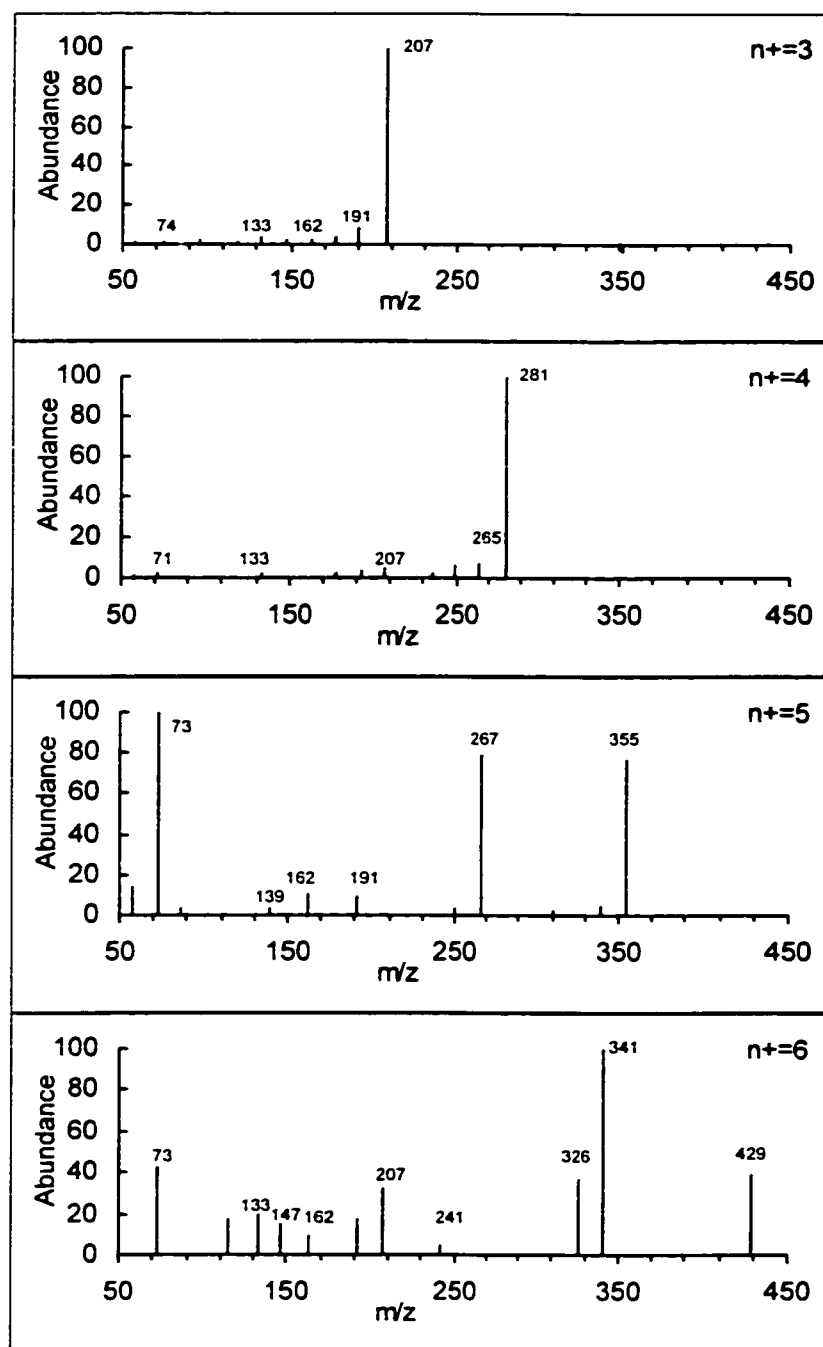


Figure 4.13 Mass spectra of peaks of GC spectrum shown in Figure 4.12. The four scans are corresponding to the peaks $n=3$, 4, 5 and 6, respectively.

Table 4.1: Area for some peaks in Figure 4.10

Peak	Area ($\times 10^8$, unit)
n+=6	2.23
n+=7	11.6
n+=8	12.8
n+=9	7.86
n+=10	7.81
n+=11	6.82
n+=12	7.71
n+=13	7.22
n+=14	7.96
n+=15	3.79

Table 4.2: Calculation of the molecular weight for PDMS with small n and n+

n or n+	Cyclic structure		Linear structure	
	Normal	Missing one methyl group	Normal	Missing one methyl group
2	148	133	162	147
3	222	207	236	221
4	296	281	310	295
5	370	355	384	369
6	444	429	458	443
7	518	503	532	517
8	592	577	606	591

Table 4.3: Bond energies of various carbon and silicone bonds [44]

Bond	Bond energy, (kJ/mol)
Si-O	444
C-H	414
Si-C	318

4.4 Conclusions

1. An extraction method has been developed to remove LMW fluid in the HTV silicone rubber.
2. The weight loss of the solid matrix of HTV silicone rubber increased with heating temperature and with increasing treatment time. At 375 °C, after 10 h of heating, the material damaged.
3. The loss of LMW fluid upon heating treatment increases with increasing heating time. The HTV silicone rubber specimen lost 0.04, 0.10, 0.26 and 0.83 % of LMW fluid after being heated for 2 h at 50, 150, 250 and 375 °C, respectively.
4. The LMW fluid content for samples from five different manufacturers range from 1.51 to 8.3 % by weight.
5. It is found that the LMW fluid can be regenerated by heating specimens. The amount of New extractable fluid is 0.12, 0.19, 0.33 and 0.65 % by weight for specimens being heated for 2 h at 50, 150, 250 and 375 °C, respectively.

6. Regeneration of the LMW fluid for specimens treated at 250 °C ceased after the seventh cycle of heating and depletion.
7. GC-MS is a useful tool for evaluating the surface degradation of HTV silicone rubber. The GC-MS analysis shows that PDMS with shorter chain was found after 4 thermal treatment cycles.

References

- [1] J. Kindersberger, A. Schutz, H. C. Karner and R. V. D. Huir, "Service performance, material design and application of composite insulators with silicone rubber housings", CIGRE, 33-303, session-1996.
- [2] J. Mackevich and M. Shah, "Polymer outdoor insulating materials, Part I: comparison of porcelain and polymer electrical insulation", IEEE Electrical Insulation Magazine, pp. 5-12, Vol. 13, 1997.
- [3] S. H. Kim, E. A. Cherney and R. Hackam, "Effect of dry band arcing on the surface of RTV silicone rubber coatings", Conference Record of IEEE International Symposium on Electrical Insulation, pp. 237-40, Baltimore, USA, June, 1992.
- [4] S. M. Gubanski, "Properties of silicone rubber housings and coatings", IEEE Trans. on Power Delivery, Vol. 27, pp. 374-82, 1992.
- [5] S. H. Kim, E. A. Cherney and R. Hackam, "Hydrophobicity behavior of insulators coated with RTV silicone rubber", IEEE Trans. on Electrical Insulation, Vol. 27, pp. 610-22, 1992.
- [6] M. Issi and M. Komatsubara, "Hydrophobicity of organic insulating materials", Annual report: CEIDP, Ottawa, pp. 134-39, 1988.

- [7] F. M. Clark, "Insulation materials for design and engineering practice", John Wiley & Sons, New York, 1962.
- [8] A. E. Vlastos and J. Hulten, "Insulator surface conduction and surface flashover voltage", Annual report: CEIDP, pp. 463-466, 1995.
- [9] W. J. Shugg, "Handbook of electrical and electronic insulating materials", 2nd Edition, IEEE press, 1995.
- [10] "IEEE standard techniques for high voltage testing", IEEE Std. 4-1978, pp. 31, 1978.
- [11] IEC Publication 507, "Artificial pollution tests on high voltage insulators to be used on ac systems", pp. 1-37, 1975.
- [12] S. H. Kim and R. Hackam, "Effects of saline water flow rate and air pressure on leakage current in RTV coatings", IEEE Trans. on PD, pp. 1956-1964, 1995.
- [13] S. H. Kim, E. A. Cherney and R. Hackam, "The loss and recovery of hydrophobicity of RTV silicone rubber insulator coatings", IEEE Trans. on Power Delivery, Vol. 5, pp. 1491-1500, 1990.

- [14] R. S. Gorur, E. A. Cherney and R. Hackam, "The ac and dc performance of polymeric insulating materials under accelerated aging in a fog chamber", IEEE Trans. PD, Vol. 3, pp. 1892-1902, 1988.
- [15] S. Wu, "Calculation of interfacial tension in polymer systems", J. Polymer Sci., Part C, Vol. 34, pp. 19-30, 1971.
- [16] S. Wu, "Polymer interface and adhesion", Marcel Dekker Inc., New York, Chapter 5, pp. 169-214, 1982.
- [17] J. Israelachvili, "Intermolecular and surface forces", Academic press, 1995.
- [18] H. Deng and R. Hackam, "Hydrophobic property of XLPE filled with calcium carbonate". IEEE Trans. on Dielectrics and Electrical Insulation, Vol. 3, No. 4, pp.577-86, 1996.
- [19] S. M. Gubanski and A. E. Vlastos, "Wettability of naturally aged silicone and EPDM composite insulators", IEEE Trans. on Power Delivery, Vol. 5, pp. 1527-35, 1990.
- [20] T. Tokoro and R. Hackam, "Recovery of hydrophobicity of nylon aged by heat and saline water", IEEE Int. Symps. on Electrical Insulation, Montreal, pp. 283-286, 1996.

- [21] S. H. Kim, E. A. Cherney and R. Hackam, "Artificial testing and evaluation of RTV coatings in a salt-fog chamber", IEEE Trans. EI, Vol. 26, pp. 797-805, 1991.
- [22] J. Crank, "Mathematics of diffusion", 2nd Edition. Claredon, Oxford, 1975.
- [23] U. Kaltenborn, J. Kindersberger, R. Barsch and H. Jahn, "On the electrical performance of different insulating materials in a rotating-wheel-dip-test", Annual report: CEIDP, pp. 398-401, 1997.
- [24] C. Hall, "Polymer materials - an introduction for technologists and scientists", Pub. McMillen, pp. 94, 1980.
- [25] D. K. Owens, "Estimation of the surface free energy of polymers", J. Appl. Polymer Science, Vol. 13, pp. 1741-1747, 1969.
- [26] S. H. Kim and R. Hackam, "Influence of multiple insulator rods on potential and electric field distributions at their surface", Annual report: CEIDP, pp. 749-54, 1994.
- [27] S. H. Kim and R. Hackam, "Effects of saline water flow rate and air speed on leakage current in RTV coatings", IEEE Trans. PD, Vol. 10, pp. 1956-1964, 1995.
- [28] K. L. Mittal (editor), "Contact angle, wettability and adhesion", VSP, the Netherlands, pp. 3-36, 1993.

- [29] H. R. Baker and R. N. Bolster, "Surface electrical leakage on insulators and coatings in the presence of moisture contamination", IEEE Trans. On Electrical Insulation, pp. 76-80, 1976.
- [30] T. Tokoro and R. Hackam, "Recovery of hydrophobicity of Nylon aged by heat and saline water", Conference record of the 1996 IEEE International Symposium on Electrical Insulation, Montreal, Quebec, Canada, June 1996.
- [31] J. C. Chan and Sim Jaczek, "The moisture absorption of XLPE cable insulation under simulated service conditions", IEEE Trans. EI, Vol. 13, pp. 194-197, 1978.
- [32] T. Tanaka, K. Naito and J. Kitagawa, "A basic study on outdoor insulator of organic materials", IEEE Trans. EI, Vol. 13, pp. 184-193, 1978.
- [33] J. Kindersberger, M. Kuhl, "Effect of hydrophobicity on insulator performance", 6th ISH, New Orleans, USA, 1989, paper 12.01.
- [34] H. Homma, T. Kuroyagi, C. L. Mirley, J. Ronzello, S. A. Boggs, "Diffusion of low molecular weight siloxane from bulk to surface", Conference record of the 1996 IEEE ISEI, Quebec, Canada, pp. 279-82, 1996.
- [35] R. S. Gorur, G. G. Karady, A. Jagota, M. Shah and A. M. Yates, "Aging in silicone rubber used for outdoor insulation", IEEE Trans. on Power Delivery, Vol. 7, pp. 525-538, 1992.

- [36] J. W. Chang and R. S. Gorur, "Surface recovery of silicone rubber used for HV outdoor insulation", IEEE Trans. on DEI, Vol. 1, No. 6, pp. 1039-46, 1994.
- [37] H. Deng, R. Hackam, E. A. Cherney, "Effects of addition of silicone fluid on electrical performance of RTV silicone rubber coatings", Proceedings of IEEE 5th International Conference on Conduction and Breakdown in Solid Dielectrics, pp. 616-20, 1995.
- [38] C. D. Doyle, "Logarithmic thermal degradation of a silicone resin in air", Journal of Polymer Science, Vol. 31, pp. 95-104, 1958.
- [39] D. K. Thomas, "Network scission processes in peroxide cured methylvinyl silicone rubber", Polymer, Vol. 7, pp. 99-105, 1966.
- [40] Stephen J. Clarson, J. Anthony Semlyen, "Siloxane polymers", PTR Prentice Hall press, pp. 121, 171, 230, New Jersey, 1993.
- [41] H. Deng, R. Hackam, "Electrical performance of RTV silicone rubber coating of different thickness on porcelain", IEEE Trans. on Power Delivery, Vol. 12, No. 2, pp. 857-866, 1997.
- [42] H. Homma, T. Kuroyagi, K. Izumi, C. L. Mirley, J. Ronzello and S. A. Boggs, "Evaluation on surface degradation of polymer insulating materials using GC/MS",

IEEE 5th International Conference on Conduction and Breakdown in Solid Dielectrics, pp. 575-579, 1995.

[43] Kevin Eldridge, James Xu, Weijun Yin, Anne-Marie Jeffery, JoAnne Ronzello and Steven A. Boggs, "Degradation of a silicone-based coating in a substation application", IEEE PES Winter Meeting 1995.

[44] K. J. Saunders, "Organic polymer chemistry", Second Edition, pp. 407, Chapman & Hall press, 1988.

Publications Supporting the Thesis

1. H. Zhang, R. Hackam, "Effect of low molecular weight fluid on aging performance of HTV silicone rubber", Conference Record of the 2000 IEEE International Symposium on Electrical Insulation, pp. 184-187, Anaheim, California, USA, April 2-5, 2000.
2. H. Zhang, R. Hackam, "Electrical surface resistance, hydrophobicity and diffusion phenomena in polyvinyl chloride", IEEE Transactions on Dielectrics and Electrical Insulation, pp. 73-83, Vol. 6, February, 1999.
3. H. Zhang, R. Hackam, "Identification of LMW fluid in HTV silicone rubber", 1999 IEEE Annual Report: Conference on Electrical Insulation and Dielectric Phenomena, pp. 739-742, Austin, Texas, USA, October 17-20, 1999.
4. H. Zhang and R. Hackam, "Influence of fog parameters on the aging of HTV silicone rubber", IEEE Transactions on Dielectrics and Electrical Insulation, pp. 835-844, Vol. 6, December, 1999.
5. H. Zhang and R. Hackam, "Loss and regeneration of the low molecular weight fluid in HTV silicone rubber", paper submitted to the IEEE Transactions on Dielectrics and Electrical Insulation. (in press)

6. H. Zhang, R. Hackam, "Influence of fog parameters on the surface resistance of HTV silicone rubber", 1998 IEEE Annual Report: Conference on Electrical Insulation and Dielectric Phenomena, pp. 43-47, Atlanta, Georgia, USA, October 25-28, 1998.
7. H. Zhang, R. Hackam, "Surface resistance and hydrophobicity of HTV silicone rubber in the presence of salt-fog", Conference Record of the 1998 IEEE International Symposium on Electrical Insulation, pp. 355-359, Washington DC, USA, June 7-10, 1998.
8. H. Zhang and R. Hackam, "Relationship between electrical surface resistance and hydrophobicity of polymer insulation", CAGE Club Conference, Univ. of Western Ontario, London, July 24, 1998.
9. Hui Zhang, Reuben Hackam, "Surface resistance of PVC in the presence of salt-fog", IEEE Annual Report - Conference on Electrical Insulation and Dielectric Phenomena, pp. 137-41, Minneapolis, Minnesota, USA, October 19-22, 1997.
10. H. Zhang, R. Hackam, "Electrical characteristics of PVC in the presence of fog", Canadian conference on High Voltage Engineering, CAGE Club, Toronto, Canada, August 26, 1997.

Vita Auctoris

NAME: Hui ZHANG

PLACE OF BIRTH: Jiangsu, China

YEAR OF BIRTH: 1971

EDUCATION: **Bachelor of Engineering (B. E.)**
Department of Electrical Engineering
Xi'an Jiaotong University
Xi'an, China
1991

Master of Engineering (M. E.)
Department of Electrical Engineering
Zhejiang University
Hangzhou, China
1994

Master of Applied Science (M. A. Sc.)
Department of Electrical and Computer Engineering
University of Windsor
Windsor, Ontario, Canada
2000